UNIVERSITY OF GENOVA

PHD PROGRAM IN BIOENGINEERING AND ROBOTICS

Conception, development and evaluation of polymer-based screen-printed textile electrodes for biopotential monitoring

by

Andrea Achilli

Thesis submitted for the degree of *Doctor of Philosophy* (31° cycle)

December 2018

Prof. A. Bonfiglio, Dr. D. Pani — Supervisors

Prof. G. Cannata — Head of the PhD program

Thesis Jury:

Prof. E. Ismailova, *Saint-Etienne School of Mines* — External examiner

Prof. A. Tognetti, *University of Pisa* — External examiner

Dibris

Department of Informatics, Bioengineering, Robotics and Systems Engineering

. . . to my past, my present, my future family . . .

Declaration

I hereby declare that except where specific reference is made to the work of others, the contents of this dissertation are original and have not been submitted in whole or in part for consideration for any other degree or qualification in this, or any other university. This dissertation is my own work and contains nothing which is the outcome of work done in collaboration with others, except as specified in the text and Acknowledgements. This dissertation contains fewer than 65,000 words including appendices, bibliography, footnotes, tables and equations and has fewer than 150 figures.

Andrea Achilli
April 2019

Abstract

Wearable technologies represent the new frontier of vital signs monitoring in different applications, from fitness to health. With the progressive miniaturization of the electronic components, enabling the implementation of portable and hand-held acquisition and recording devices, the research focus has shifted toward the development of effective and unobtrusive textile electrodes. This work deals with the study, development and characterization of organic-polymer-based electrodes for biopotentials.

After an overview of the main materials and fabrication technologies presented so far in the scientific literature, the possibility to use these electrodes as an alternative to the Ag/AgCl disposable gelled electrodes usually adopted in clinical practice was tested. For this purpose, several textile electrode realization techniques were studied and optimized, in order to create electrodes with adequate features to detect two fundamental physiological signals: the electrocardiogram (ECG) and the electromyogram (EMG). The electrodes were obtained by depositing on the fabric the organic bio-compatible polymer poly(3,4-ethylenedioxythiophene) doped with poly(4-styrenesulfonate) (PEDOT:PSS) with three deposition procedures: dip-coating, ink-jet printing and screen printing. The physical–chemical properties of the polymer solution were varied for each procedure to obtain an optimal and reproducible result. For what concerns the ECG signal, the research activity focused on screen-printed textile electrodes and their performance was first assessed by benchtop measurements and then by human trials. The first tests demonstrated that, by adding solid or liquid electrolytes the electrodes, the largest part of the characteristics required by the ANSI/AAMI EC12:2000 standard for gelled ECG electrodes can be achieved. Tests performed in different conditions showed that the skin contact impedance and the ECG morphological features are highly similar to those obtainable with disposable gelled Ag/AgCl electrodes ($\rho > 0.99$). A trial with ten subjects revealed also the capability of the proposed electrodes to accurately capture with clinical instruments an ECG morphology with performance comparable to off-the-shelf disposable electrodes. Furthermore, the proposed textile electrodes preserve their electrical properties and functionality even after several mild washing cycles, while they suffered physical stretching.

Similar tests were performed on screen-printed textile electrodes fabricated in two different sizes to test them as EMG sensors, with and without electrolytes. After a series of controlled acquisitions performed by electro-stimulating the muscles in order to analyze the waveform morphologu of the M-wave, the statistical analysis showed a high similarity in terms of rms of the noise and electrode-skin impedance between conventional and textile electrodes with the addition of solid hydrogel and saline solution. Furthermore, the M-wave recorded on the tibialis anterior muscle during the stimulation of the peroneal nerve was comparatively analyzed between conventional and textile electrodes. The comparison provided an R^2 value higher than 97% in all measurement conditions. These results opened their use in smart garments for real application scenarios and for this purpose were developed a couple of smart shirts able to detect the EGC and the EMG signal. The results indicated that this approach could be adopted in the future for the development of smart garments able to comfortably detect physiological signals.

Table of contents

List of figures

List of tables

Chapter 1

Introduction

The advancements in the area of wearable technologies are in a constant movement forward. Over the years, the use of smart textiles has expanded to several areas, including the medical field. Within this field, the aim to create smart clothes enabling diagnostics and monitoring from physiological signals has driven the innovation of products and equipment forward. Wearable health monitoring systems could represent a killer application for smart textiles, because of their peculiar properties such as low weight, comfort and unobtrusiveness.

Fabrics with knitted conductive elements include several interesting properties, such as good air permeability and humidity transport, which are crucial to ensure comfort, even though the presence of metal in contact with the skin is not the best solution to detect electrophysiological signals, with also some risks in terms of skin reaction. Many of today's projects focus on monitoring heart activity, breathing and movements by bringing the technology of textile sensors into specific applications. One type of sensor needed for enabling this type of measurement is represented by textile electrodes. These electrodes are an advancement in the textile field when used for the measurement of electrophysiological signals. They have the potentiality to solve problems related to conventionally used electrodes that cause discomfort in patients undergoing long-term recordings. Conventional electrodes require a hydrogel layer, or a liquid electrolyte, between the active part of the electrode and the skin in order to detect good-quality signals. Furthermore, they stay in place by means of mild glues, with the result that both this glue and the electrolyte could cause skin reactions in sensitive subjects. In principle, textile electrodes could be also used on the dry skin, without electrolytes, provided that the material and the fabrication process enable this kind of result. Nevertheless, the matter has not been fully investigated, especially taking into account different testing conditions and the appropriate measurements dictated by the standards for the disposable electrodes.

This work presents the research carried out at the Department of Electrical and Electronic Engineering of the University of Cagliari, Italy, during the three-year Ph.D. program in Bioengineering and Robotics of the University of Genoa, Italy. The research goal was to go further the standard textile electrodes composed of metallic elements embedded on the fabric, by using organic polymers and by studying effective and efficient approaches to apply them on the finished garment. Moreover, complete analysis tool-chains where deployed to quantitatively compare the developed electrodes with off-the-shelf disposable solutions, taking into account both the currently adopted ISO standards for the latter and adequate methods to analyze the accuracy of the measured biopotentials with respect to the specific biomedical application. In particular, electrocardiographic (ECG) and electromyographic (EMG) signal acquisition was pursued and studied, by using electro-conductive polymers to functionalize textile substrates, changing their chemo-physical properties without affecting those related to the soft touch and comfort. In this work, the basic component of the conductive ink was the poly(3,4-ethylenedioxythiophene) doped with poly(styrene sulfonate) (PEDOT:PSS).

Different procedures were tested to deposit the conductive ink in the fabric: dip coating, screen-printing and ink-jet printing. For each printing procedure, the polymer solution was modified to obtain an ink suited for it. Between the ink-jet and the screen-printing, the second one was established as the best one to create seamless textile electrodes with good electrical performances in a timely manner. This was justified by several tests performed in collaboration with SPES MEDICA Srl, an Italian company producing electrodes for the medical market. These results were the starting point to design and characterized several screen-printed textile electrode prototypes to detect the ECG and the EMG signal. In addition, this technique was used to develop an exemplary smart shirt able to unobtrusively detect electrophysiological signals by PEDOT:PSS-based screen-printed electrodes. The ECG signals validation was performed in collaboration with the Cardiology Department of the Cagliari University Hospital, whereas the EMG signals validation was performed in collaboration with the LISiN Lab of the Politecnico di Torino, Italy.

This work is structured in six chapters. In the next chapter, the rationale behind this research for the development of unobtrusive wearable sensing technologies is presented, along with the ECG and EMG electrodes currently used in clinical practice and in the academic research, highlighting their advantages and limitations. Then, the main obstacles to the introduction of textile electrodes are explained, together with the description of the first clinical studies which presented their potential benefits. In the third chapter, three different techniques to develop textile electrodes are presented with the description of the

procedure used to characterize the fabric substrate. All these techniques use an ink based on the PEDOT:PSS conductive polymer, optimized for each printing procedure. The first technique is the dip coating previously used by the research groups at the University of Cagliari for the detection of the ECG signal with textile electrodes. The second one is the screen-printing, the most studied and thoroughly used one in this work. Finally, ink-jet printing was only preliminarily studied, revealing soon the limits hampering their use for the final purpose. In the fourth chapter, were investigated all the possible implementation of the screen-printed textile electrodes included the main problems related to this type of sensors. This chapter includes, in addition, the evaluation of the performance with different skin treatments compared to commercial disposable electrodes. The performance was analyzed also with benchtop measurements to compare the results with the standards imposed by ANSI/AAMI for gelled ECG electrodes. The results obtained were compared with the one recorded with a clinical instrumentation. Then, in the fifth chapter, the results related to these tests were reported with a focus on the limitation imposed from the textile electrodes like the resistance to repeated washing cycles or stretching the textile substrate. The sixth chapter reports the discussion about all the results obtained in this work with textile electrodes. Then the conclusions are reported, highlighting all the advantages of a technology able to detect the ECG and the EMG in a completely non-invasive way with an affordability comparable to the one obtained with standard gelled electrodes and showing the current direction of the research.

Chapter 2

State of the art

The gold standard for surface biopotentials acquisition is represented by disposable gelled Ag/AgCl electrodes. These electrodes present several well-known advantages compared to reusable solutions, such as the signal quality and the robustness to movement perturbations due to their adhesion with the skin. In the last years, researchers started developing alternative solutions as smart textiles, able to replace gelled electrodes in the acquisition of electrophysiological signals (Searle and Kirkup (2000)). The interest in wearable devices and smart textiles is continuously growing, fostered by the growth of the research in the field and by the continuous introduction of novel products in the market. In 2016, IDTechEx, an agency specialized in market researches focused on emerging technologies, depicted the wearable technology sector as a market with great opportunities of expansion and expected to reach 51.6 billion USD by 2022. This compound annual growth rate of 15.5% is mainly due to the involvement of the big companies in the sector, such as Google, Apple, Adidas, Nike, Samsung and Intel (Hayward et al. (2017)). Considering an estimated number of 3 billion wearable sensors by 2025, the fast growth is associated with the introduction of consumer products on the market (e.g. smart wrist-wears for wellness, fitness, health and fashion applications) along with a growing popularity of the Internet-of-Things (IoT) and connected devices (Page (2015)). Wearable devices and smart textiles also represent target technologies in the military sector (Nayak et al. (2015)), even though healthcare remains the most interesting market, since this technology could potentially lead to the development of new healthcare system models ensuring significant cost reductions. Nevertheless, this market is also the most challenging one, with several barriers (Lewy (2015)), regulatory issues (Erdmier et al. (2016)) and blurred boundaries between consumer wearable devices and medical devices accepted in clinical practice, which leads the patients to make improper medical use of the data generated by their devices (Piwek et al. (2016)). Incontrovertibly,

different categories of subjects (from neonates to elderly), including patients with specific health conditions, could achieve substantial benefits using wearable devices (Park and Jayaraman (2003); Wieringa et al. (2017)). The market of wearable devices and smart textiles is research-driven, as demonstrated by the high number of projects in the field funded by the European Commission in the framework of the Horizon 2020 program compared to those in the 6th and 7th framework programs (Stoppa and Chiolerio (2014)). In the first part of this chapter, the characteristics of the current wearable and smart textile technologies developed for ECG signal monitoring will be described, with a special focus on electrodes, which currently represents the most critical aspect to deal with, and the approaches to their characterization. The research interest for this specific aspect is demonstrated by the exponentially growing number of publications on *textile electrodes, Wearable technology* and *smart textile* resulting from the Scopus database updated at October 2018, Figure 2.1.

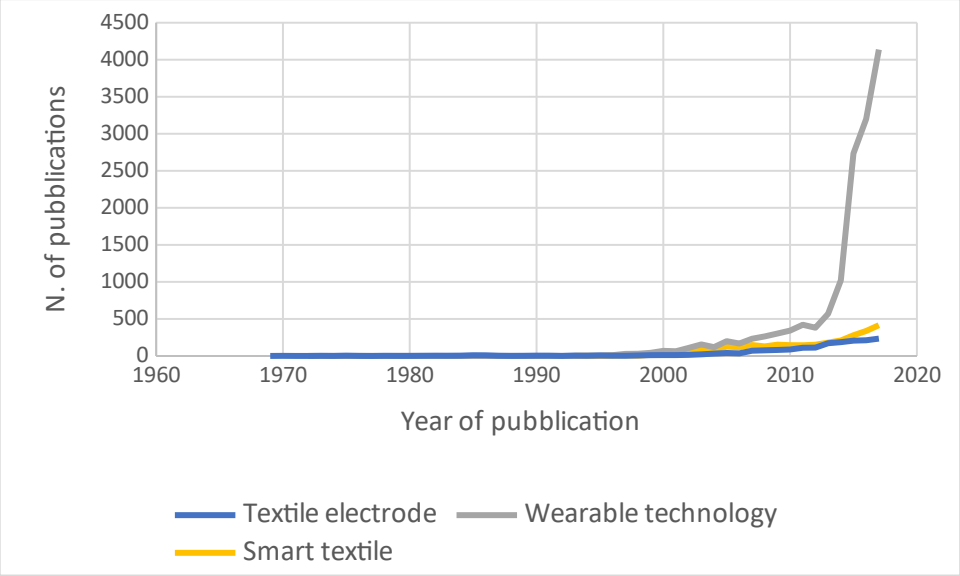

Figure 2.1 Number of publications indexed by Scopus at the end of 2018 reporting the keywords: textile electrode, wearable technology, smart textile.

Remarkably, the same trend can be observed for other keywords, such as *wearable*, *monitoring* and *human* (Scilingo and Valenza (2017)). A more detailed analysis of the research fields associated with these publications revealed that the largest part of these works belonged to engineering (22%), material science (15%) and chemistry or chemical engineering (22%) and related to the development of these devices. Meanwhile, only 7% of the publications were a medical journal, reflecting the current limitations of such technologies for clinical applications.

2.1 Wearable devices and smart textiles

The wearable revolution started in the 1990s for several fields, such as health care, battlefield management, entertainment, public safety, space exploration and sports and fitness, among others (Gopalsamy et al. (1999); Park and Jayaraman (2017)). A pioneering example of the vital sign recording through wearable sensors, which paved the way for *smart garments*, was represented by the Wearable Motherboard from Georgia Tech (Gopalsamy et al. (1999)). The motherboard was an interactive fabric-based wearable system composed of seamless sensors and electronic components. From then on, different approaches have been proposed, and different requirements have been identified. Even though such requirements change with the specific human monitoring application, some basic requirements are shared by all the devices, including textile sensors, and concur to define the specifications for their development (Kumari et al. (2017)):

- Aesthetics. The opportunity to wear and expose these devices requires them to be fashionable and with a design compatible with the final application.
- Size and weight. As for the previous point, these devices need to be comfortably worn, often with specific restrictions imposed by the human anatomy and/or physiology.
- Water and stress tolerance. The everyday use and maintenance dictate robustness to temperature, moisture and physical stress conditions expectable for the intended use.
- Power consumption. The system must be battery powered, and the duration of the charge should be adequate for the intended use.
- Wireless communication. Cable connections limit the comfort for the users and represent a pitfall for the system robustness.
- Security. Wearables are in contact with the subject for long periods; hence, they should guarantee electrical safety and biocompatibility.

Wearable devices have just recently started, including the innovative field of *smart materials* (i.e. materials able to detect a chemo/physical variation in the surrounding environment and react by changing their properties). Smart materials could be classified as passive, active or very smart depending on their response to external inputs (Ghahremani Honarvar and Latifi (2017)), which range from passive sensing to sensing and reaction, which could include self-adaptation for very smart materials.

A restricted category of wearable devices, including textile sensors and electronics, is represented by *e-textiles* or *smart textiles* (ST) (Berglin (2013)). This approach enables the development of *smart clothes* (e.g. smart T-shirts) for health monitoring. Even though a branch of the research on smart textiles aims at embedding sensors in finished garments, hereafter, we will expressly refer only to STs developed by treating fabrics to convert them into textile sensors as required for surface electrophysiological signals acquisition (e.g. ECG). Thanks to their physical properties, textiles typically present good flexibility and strength, making them both conformable and comfortable and, at the same time, able to resist harsh environmental conditions (either bio-hazards or climatic) and mechanical stress (Kirstein et al. (0)). These properties could be exploited to develop unobtrusive sensing devices embedded into garments by means of several manufacturing techniques (e.g. weaving, knitting, nonwovens and printing), with the option of changing the properties of single wires (Tsukada et al. (2012b)) or parts of the finished garment (Takamatsu et al. (2015)), thereby preserving the physical/mechanical properties of the fabric (Cochrane et al. (2007)).

Despite the focus of this thesis being on electrodes for biopotentials sensing, it is worth mentioning that the interconnection between the flexible textile sensors and the rigid hardware readout circuitry is a key aspect to consider (Park and Jayaraman (2010)). The optimal option could be a seamless connection embedded in the yarn or added externally with conductive textile wires. Compared to the adoption of metallic signal cables, this solution preserves the substrate flexibility and comfort along with an easier fabrication. However, conductive textile wires are less stress-resistant, more sensitive to motion artifacts, spurious contacts, cross-talk and electromagnetic coupling because of the difficulty in realizing shielding and insulation (Akşit et al. (2009)).

Hereafter, the ECG and EMG electrodes technologies and underlying problems will be presented, in order to introduce the rationale behind the development of the current research.

2.2 ECG electrodes

Diagnostic electrocardiography is a consolidated clinical procedure performed in adults and children, which allows discovering pathological conditions even before structural changes in the heart can be diagnosed by other methods (Stern (2006)). The non-invasive nature of the exam, low cost of the devices used to perform it and reduced data size caused by the data rate and the typical number of channels (Kligfield et al. (2007)) make exploitation possible in any scenario, including tele-cardiology (Al-Zaiti et al. (2013)) and, in general, tele-health.

These characteristics, along with the possibilities offered by the miniaturization of electronic devices, fostered the development of diagnostic and monitoring devices for long-term ECG recording, which opened the possibility of *wearing* ECG devices for personal or clinical use (Baig et al. (2013)). The achievement of this goal moved the target from the realization of lightweight ECG devices and efficient transmission protocols to the realization of unobtrusive electrodes, particularly the production of highly conductive textile materials according to the current industrial processes with solved cleaning and washing issues (Lymberis and Olsson (2003)).

The gold standard for the ECG signal acquisition is represented by gelled Ag/AgCl electrodes (either disposable or reusable). Adhesive disposable electrodes particularly combine well-known advantages in terms of the signal quality of this material to the reduced signal perturbation caused by skin-electrode movement artifacts. Their limited cost and the acceptable comfort for patients have led to their adoption for both short- (i.e. typically 10s rest ECG or stress tests) and long-term (24 h or more Holter recordings) applications. However, in the last decades, the research started developing alternative solutions to replace them (Searle and Kirkup (2000)) because of some important limitations. First, they need an electrolyte typically in a form of a solid hydrogel or a liquid gel applied on a sponge to properly operate (Webster (2009)). Its presence represents the main drawback because the electrolyte (along with the adhesive, if separately present), when applied for a long time, can stimulate the skin, causing a rash or a reaction (Crawford and Doherty (2012)) and, in rare cases, dermatitis (David and Portnoy (1972)). Furthermore, the electrolyte gets dry over time, worsening the quality of the ECG signal. The presence of the electrolytic adhesive layer also limits the possibility to integrate these electrodes in a garment, whereas reducing the need for the electrolyte through skin treatment does not represent a solution because this process also presents several issues (Taheri et al. (1994)).

Many types of ECG electrodes have been developed in the past few decades, which can be classified according to different criteria. The first, macroscopic aspect, is their shape and application method:

- Metal-plate electrodes. This is one of the most frequently used forms of electrode for biopotential sensing, which consists of a metallic conductor in contact with the skin. An electrolyte soaked pad or gel is used to establish and maintain the contact. Figure 2.2 shows one of these electrodes. This type of electrode is popular for ECG, EMG, or electroencephalography (EEG) recording. In order to fix the electrode onto the skin, soft glues or adhesive electrolytes can be used; moreover, rubber bands or

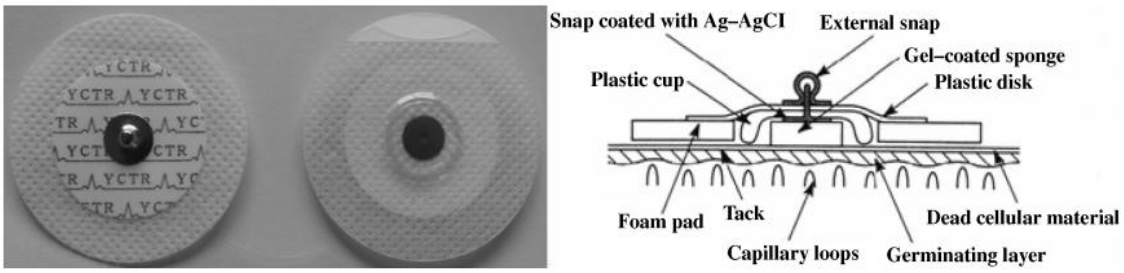

Figure 2.2 Metal-plate electrodes: top view (left), bottom view (middle) and cross-section view (right)

medical nets can be also adopted to ensure the mechanical contact and the electrode stability, when no adhesive is present.

- Suction electrodes. They are a modification of metal-plate electrodes, which require no straps or adhesives for holding them in place. An example of these electrodes is shown in Figure 2.3. It consists of a hollow metallic cylindrical electrode, which contacts the skin at its base. A terminal for the lead wire is attached to the metal cylinder, and a rubber suction bulb is fitted over its other base. Electrolyte gel is placed over the contacting surface of the electrode. The bulb is squeezed and the electrode is placed on the body surface. The electrode holds to the skin by suction after releasing the bulb. This electrode can be used only for a short period of time.

- Floating electrodes. These electrodes are developed to reduce motion artifact. The source of motion artifact is the double layer of charge at the electrode-electrolyte interface. Although the characteristics of the Ag/AgCl electrodes (discussed in the following sections) can greatly reduce this artifact, they cannot eliminate it. Floating electrodes try to reduce this instability at the interface by separating the metal plate from the skin, avoiding their direct contact, through a large layer of gelled electrolyte. The cross-section view of floating a electrode is shown in Figure 2.2, where the metal disk is surrounded by electrolyte in a cavity, which does not move with respect to the metal disk. The insulated cavity is filled with electrolyte gel and attached to the body by a double side adhesive ring tape. This electrode is used more for EEG recordings.

- Flexible electrodes. The body surface has its own topography that the electrodes described above cannot conform to, resulting in additional motion artifacts and skin effects (the pressure on the skin gives rise to baseline wandering artifacts). Flexible electrodes were developed to overcome problems due to the fixed curvature of plate

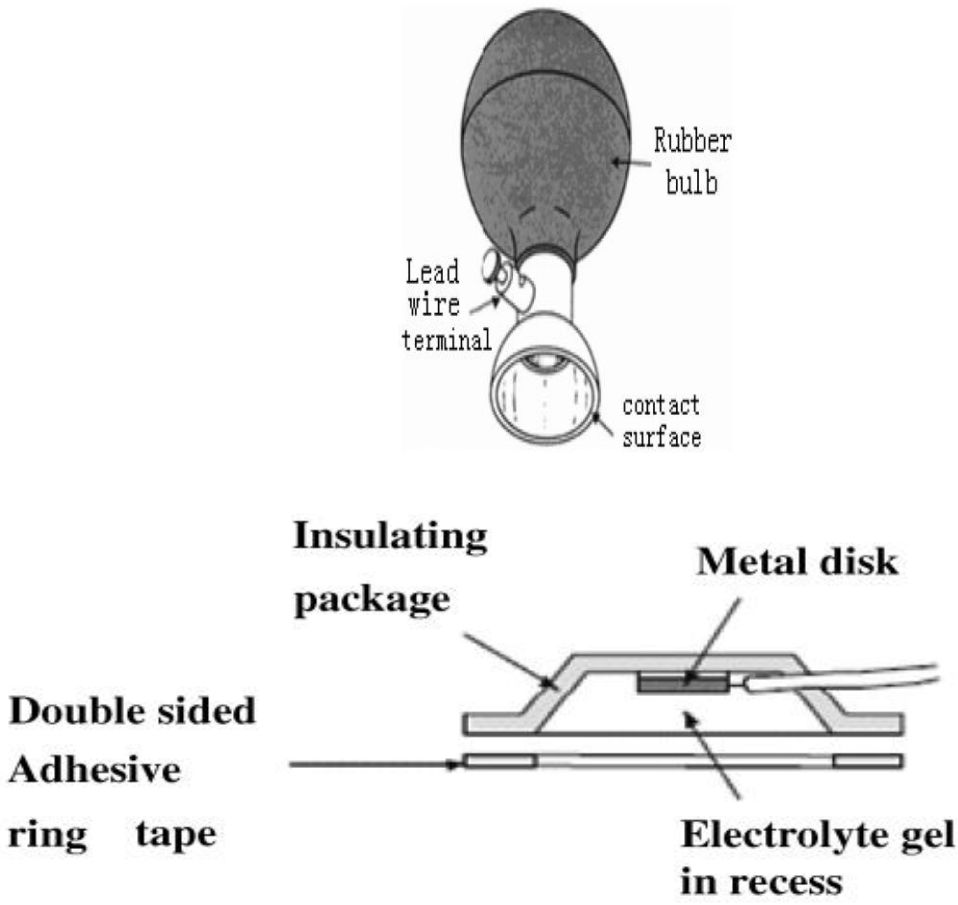

Figure 2.3 Suction electrode(top), Cross-section view of a floating electrode(Bottom)

electrodes. The most known flexible electrodes is composed of a carbon-filled silicone rubber compound in the form of a thin strip or disk. This kind of electrode is used in chest-bands measuring the heart rate, mainly for sport purposes, but also for electrostimulation. Another type of flexible electrode can be represented by a woven, stretchable, nylon fabric, coated with silver particles.

As touched above, electrodes can be also classified from a functional point of view, as recording electrodes and defibrillation/pacing electrodes (multi-function electrode) (Gadsby (2004)). Because of the complete different application, challenges and requirements are different (e.g. the active area has opposite requirements for the two) and only recording electrodes will be discussed in this thesis.

The electrodes are elements of transduction of electrical signals between an ion-conducting medium (electrolyte solution or biological tissue) and an electron-conducting medium (metal conductor). Based on the working principle, the electrodes can be classified as resistive and capacitive electrodes (Matthews et al. (2005)). Resistive and capacitive electrodes are made of conductive metals, directly in contact or not with the skin, respectively. For a resistive electrode, the most used material is Ag/AgCl, which is usually applied onto the skin by interposing a layer of an electrolyte to improve electrical contact with the skin and reduce skin-electrode contact impedance. This electrolyte layer serves as a promoter of the ionic-electronic current conversion happening at the interface. It creates an interface between the material of which it is made (usually metal) and the electrolytic gel. The interface can be schematized with a voltage generator (the electrode potential) in series with an impedance (contact impedance). An ideal electrode should behave like a non-polarizable interface (Lewy (2015)). Conversely, capacitive electrodes use a dielectric material to create a capacitive coupling with the skin. Both electrodes suffer the motion artifacts, due to the relative movement of the skin and the electrodes. However, capacitive ones are more sensitive to this kind of noise.

An important categorization is also made between *polarizable* and *non-polarizable* electrodes (Warren and Patel (2008)). The classical examples of these two types of electrodes are represented by the platinum electrodes and the Ag/AgCl ones, respectively. Even though the largest part of the electrodes does not really exactly belong to one of these categories, unlike the latter, the former does not present an electrical current flow between the electrode and the skin, being rather characterized by the presence of a displacement current generated by a change in the ionic concentration at the electrode–skin interface. An example of non-polarizable electrode is represented by gelled Ag/AgCl electrodes normally used for clinical recordings because an electrochemical process between the gel and the skin surface occurs

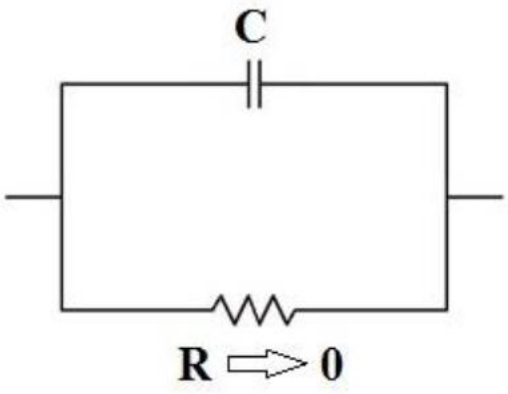

Figure 2.4 Non-polarizable interface

creating a conductive path (Taji et al. (2014)). This process is usually facilitated by the presence of an electrolytic layer and for this reason the most common electrodes for clinical use, which encompass almost all the electrophysiological signals, are gelled electrodes (Searle and Kirkup (2000)).

In Figure 2.4 it is possible to see the schematic representation of an ideal non-polarizable interface: whatever the potential difference of the generator, this causes a charge passage through the resistance and the impossibility to charge the capacitor. Any variation in tension on the generator does not translate into a variation of potential at the ends of the parallel capacitor-resistor. This means that the electrode potential does not change from its equilibrium value upon a current is applied and, in any case, the reaction at the skin-electrode interface is extremely fast. Even though the electrolyte presence is beneficial for this kind of electrodes, for long-term monitoring this gel could create skin irritations. Moreover, gel drying leads to the temporal signal degradation. For this reason, these electrodes work better as disposable electrodes for short-term use. Despite these restrictions, they show high performance as ECG electrodes. Typically, in order to ensure a good contact and reduce the skin impedance due to the *stratum corneum*, it is necessary to perform a preliminary skin treatment, including shaving and/or application of abrasive skin gel.

Conversely, polarizable electrodes do not present an electrical current flowing between the electrode and the skin but they are characterized by the presence of a displacement current generated by a change in ionic concentration in the electrode–skin interface. For this reason, they do not require an electrolyte or a gel because their working principle is based on the capacitive coupling between the electrode conductive surface and skin. For this reason dry electrodes as simple stainless steel plates or flexible textile electrodes with an high conductivity do not require any conductive gel. For this reason, textile electrodes are

sometimes studied to be used as dry electrodes with acceptable skin-contact impedance and noise (Webster (2009)), since this could unleash their massive use for unobtrusive monitoring.

Based on Figure 2.4, for a polarizable electrode the resistance will tend to infinity and the system will behave like a pure capacitor.

2.3 Textile electrode technologies for ECG acquisition

In the last years, textile electrodes for ECG have been produced using different conductive materials (Lee et al. (2017)), such as stainless steel/viscose yarns (Scilingo et al. (2005)), silver yarns (Marozas et al. (2011); Pola and Vanhala (2007)), silver/polyester covered yarns (Hakyung (2016)) carbon nanotubes, graphene, polypyrrole (PPy) (Alkhidir et al. (2015); Jung et al. (2012); Zhou et al. (2014)), PEDOT:PSS (Bihar et al. (2017); Pani et al. (2015)) and so on. In this section the main materials and fabrication processes will be described.

2.3.1 Conductive metallic wires or metal-coated yarns

Fabrics composed of natural fibres (as cotton or wool) or synthetic ones (as nylon or polyester) are electrical insulators with an electrical resistance greater than 10^8 Ω (Akşit et al. (2009)). In obtaining textile substrates with conductive properties, the first option consists of the integration of conductive filaments in the wire structure, woven or stitched with conventional textile fibres. These filaments could be made up of either pure metal or alloys (metallic monofil) or textile fibres treated with conductive inks able to provide conductivity (e.g. polyamide monofil or polyethylene (PET) or polyurethane (PU) yarns coated by a metallic layer) (Ghahremani Honarvar and Latifi (2017); Mattila (2006)). Hybrid threads based on a mix of insulating yarns and metallic micro-wires have also been developed according to specific ratios (Bystricky et al. (2016)). In the same manner, sensors can be integrated, rather than sewn, into garments for ECG signal monitoring (Bouwstra et al. (2011); Bystricky et al. (2016)) or for other biopotentials (Bouwstra et al. (2011)) by opportunely integrating these conductive yarns during fabric production. Different electrical performances can be achieved depending on the material as shown in Table 2.1 where are compared metal monofilaments produced by Elektrisola Feindraht AG (Escholzmatt, Switzerland). The products range from copper (Cu) and silver-plated copper (Cu/Ag) filaments, brass (Ms) and silver-plated brass (Ms/Ag) filaments, aluminum (Al) filaments to copper-clad aluminum (CCA) filaments. In

German Milbe denomination "Ms" is accompanied by a number stating the composition in % of Cu with respect to a Zn complement to 100 %.

Metal	**Conductivity [S·m/mm^2]**	**Resistivity [Ω·mm^2/m]**	**Thermal coefficient resistance**
Cu	58.5	0.0171	3930
Cu/Ag	58.5	0.0171	4100
Ag 99%	62.5	0.0160	3950
Ms*70	16.0	0.0625	1500
Ms/Ag	16.0	0.0625	1500
AgCu	57.5	0.0174	3950
Bronze	7.5	0.1333	650
Steele 304	1.4	0.7300	1020
Steel 316L	1.3	0.7500	1020

Table 2.1 Electrical properties of the metal monofilament fibers

Among the different materials used to develop textile electrodes, silver and Ag/AgCl are the same materials present in clinical electrodes. The sensor area is typically composed of a silver-coated nylon thread knitted to build up the sensor (Deignan et al. (2015); Ottenbacher et al. (2004); Puurtinen et al. (2006); Rattfalt et al. (2007)). Several off-the-shelf textile conductive wires are available, and in prevalence they are composed of silver filaments, which have been used for the development of stand-alone ECG electrodes (Bouwstra et al. (2009); Chen et al. (2010); Zhu et al. (2015)). These yarns are also widely used in wearable devices to connect textile sensors with readout electronics (Ghahremani Honarvar and Latifi (2017)). In (Kim et al. (2017)), DEV-10055 (SparkFun Electronics), which is no longer available in the market, is composed of 78% nylon and 22% elastomer, and has elastic properties in one direction only, was adopted. The material, which targeted wound care, antimicrobial products and garments, was conductive because of the presence of a plating layer characterized by a high ionic silver release (pure 99.9% Ag), which exhibited a surface resistance lower than 5 Ω and a surface resistivity lower than 1 Ω/sq. In (Yokus and Jur (2016)), the following three different conductive yarns were compared: Bekitex (by Bekaert, Belgium), which was also used in (Van der Pauw (1958)), is a one-ply 80% polyester plus 20% stainless steel staple fibre yarn; and Elitex (by TITV Greiz, Germany) and Shieldex (by Statex, Germany), which are polyamide silver-plated yarns. The last one was used to

unobtrusively acquire signals from neonates (Bouwstra et al. (2011)). The silver-plated-based yarns present a high conductivity, whereas the stainless steel-based one had a nominal resistance of approximately 100 Ω/cm. Aside from commercial yarns, custom processes were also presented for the same aim, for instance by coating a polyurethane-based fabric with silver through a process using an aqueous solution containing silver metal ions and $AgNO_3$ as a reducing agent (Alzaidi et al. (2013)). A similar fabrication process was applied to develop other kinds of sensors for biomedical applications, such as strain sensors in the form of stretchable e-textiles for human movement analysis (Li et al. (2017c)). In this case, the textile sensor in silver/polyester was obtained via the electronic dyeing method using a low-temperature *in situ* reduction of a silver precursor into silver nanocrystals. This result highlighted a characteristic of these substrates to be sensible to stretch, which was a drawback for biopotential electrodes that should not change their electrical properties as a function of the stretch level. For this reason, non-stretchable substrates were often adopted to control this phenomenon even with different conductive materials (Pani et al. (2015)). An alternative method to uniformly coat the fabric is represented by sputtering. This technique exploits a vacuum chamber to collect from the fabrics all the atoms thrown out and create a uniform thin coating characterized by high adhesion. This method was used to develop ECG textile electrodes from Cu-sputtered polyester fabrics (Jayoung et al. (2005)). In (Puurtinen et al. (2006)), sputtering was performed on water-resistant nylon fabrics by applying a high voltage across a low-pressure Ar gas. A similar method was used in (Lee et al. (2017)) to develop a stable and durable non-contact textile ECG electrode by coating a PU layer with silver (Ghahremani Honarvar and Latifi (2017)).

Textile sensors are flexible, lightweight, non-irritating, and convenient to be integrated for instance into a neonatal jacket for ECG and respiration monitoring. Two different textile electrodes were tested for the integration into the jacket: the silver coated Medtex 130+B textile electrodes by Shieldex® and the gold printed textile electrodes from TNO Science and Industry. Figure 2.6 shows the test patches of different versions, made up of silver and gold textile electrodes and a blanket with large silver electrodes. The silver textile electrodes have a knitted structure of a nylon coated yarn with 99.9% silver metal. The nylon consists of 71% polyamide and 29% elastomeric fiber (Chen et al. (2010)).

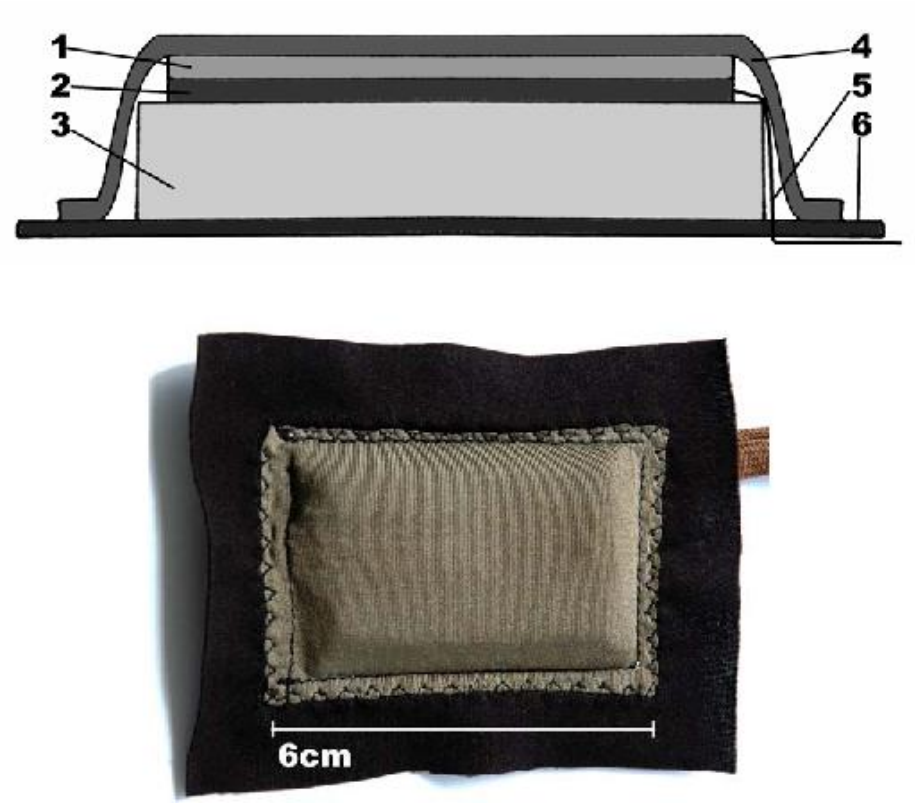

Figure 2.5 Textile electrode: cross section and photo

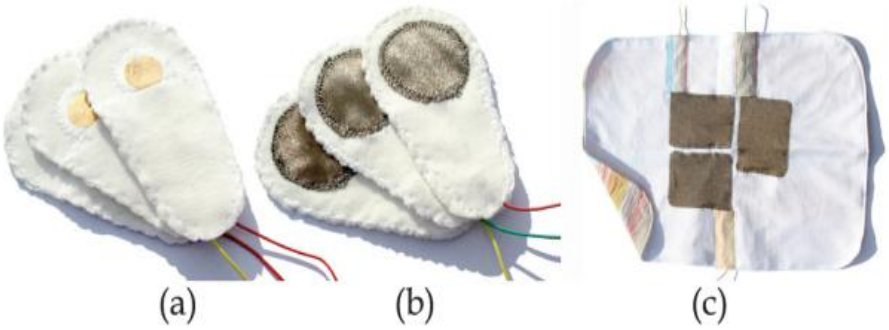

Figure 2.6 Test patches with different versions of silver and gold textile electrodes (a and b), and a blanket with large silver electrodes (c).

2.3.2 Graphene

Textile ECG electrodes can be developed using graphene films available on the market or by treating a textile substrate with graphene oxide (GO). In (Cho et al. (2011)) and (Alzaidi et al. (2012)), finished graphene paper (XFNano Materials Tech., Nanjing, China) and graphene films (Six Carbon Tech., Shenzhen, China; Vigon Materials Tech., Hefei, China) were used. In addition, a flexible graphene-based textile electrode reducing GO (XFNano Materials Tech., Nanjing, China) with hydrazine hydrate (Alfa Aesar, Massachusetts, USA) was synthesized. The GO deposition in the polyester fibres was executed by vacuum filtration to improve the conductivity and the absorption effect (Lou et al. (2016)).

Another possible deposition method to treat insulating fibres with graphene was based on an etching process on a metal substrate, Cu for monolayer graphene or Ni for a few-layer graphene, followed by chemical vapour deposition of graphene and by the transfer onto textile fibres fixed on a rigid support (Neves et al. (2017)).

2.3.3 Carbon nanotubes

The metallic element replacement can be achieved not only by graphene, but also by carbon nanotubes (CNT) that, similarly to graphene, present interesting electrical, mechanical and thermal properties (Alvarez et al. (2014); Ghahremani Honarvar and Latifi (2017)). Nanotubes could be divided into single-walled nanotubes and multi-walled nanotubes. Their electrical resistivity strictly depends on their molecular orientation and the number of walls (Burnham and Anderson (2002)), and could reach 10^2 Ω cm. As for graphene, CNTs have been used to change the electrical properties of yarns and filaments to obtain highly conductive fibres (Sun et al. (2003)).

CNT-based textiles have been successfully used as ECG electrodes, e.g. by applying on a textile substrate five layers of Multi-walled CNT (MWNT) conductive paste and a metallic snap button for an easy connection to readout electronics (Lam et al. (2013)).

An innovative method to fabricate high-performance polymer–composite electrodes for ambulatory ECG measurements was presented in (Hertleer et al. (2004)). These electrodes were fabricated mixing a high content of CNT and silver nanoparticles with polydimethylsiloxane (PDMS) and depositing the final solution using the doctor blade technique to obtain a highly conformable surface with the procedure schematized in Figure 2.9. CNT-based electrodes are washable and suitable for long-term monitoring and clinical use.

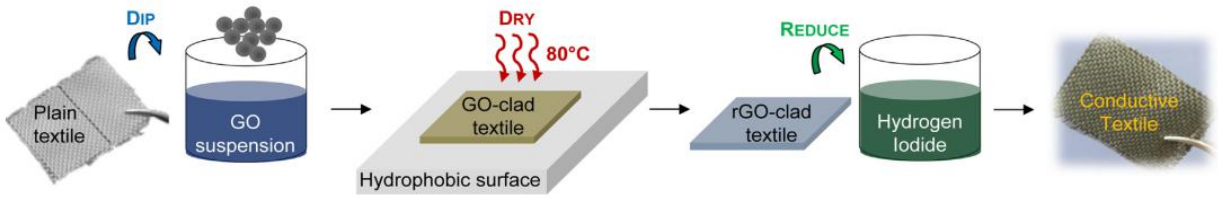

Figure 2.7 Diagram showing the three-step experimental procedure for synthesizing graphene-coated textiles.

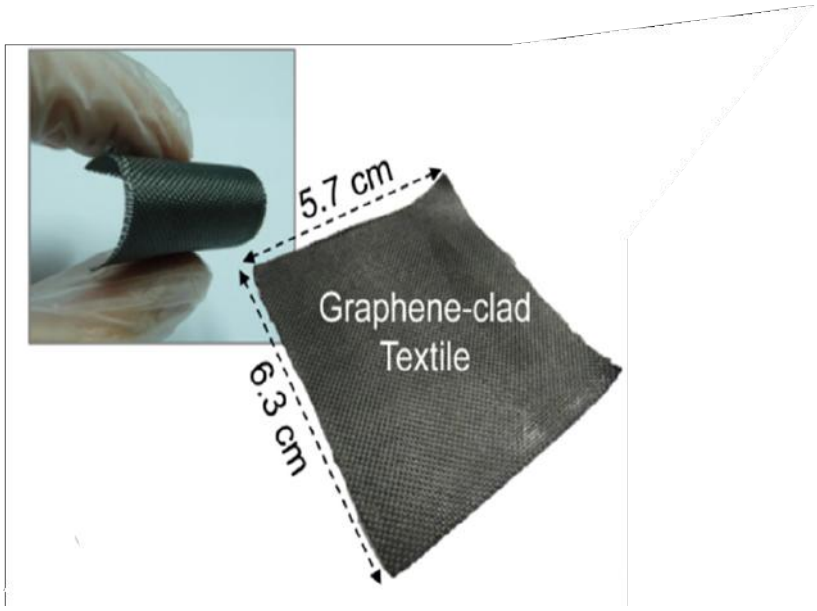

Figure 2.8 photograph of a sample of flexible nylon textile with rGO coating

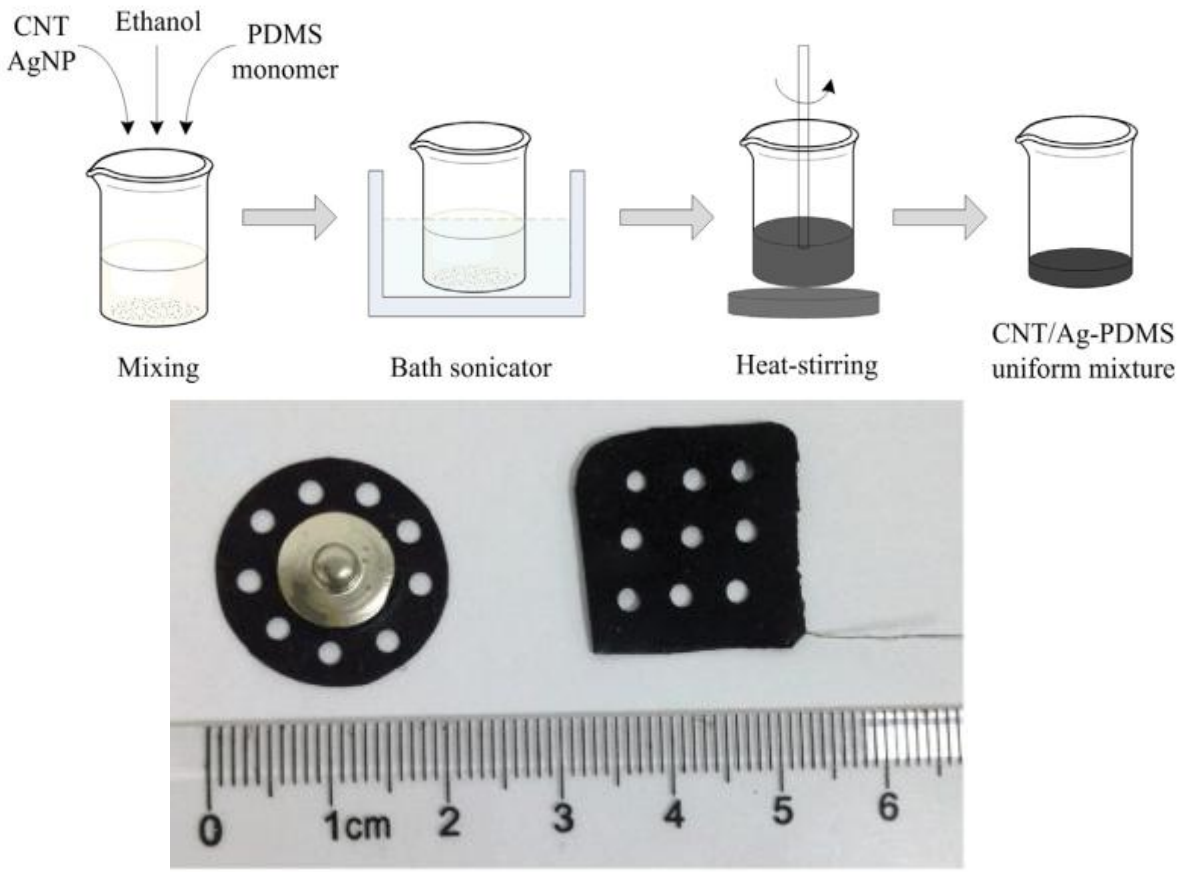

Figure 2.9 Top)The fabrication process of the conductive polymer mixture, Bottom) CNT/Ag-PDMS electrodes with different shape

2.3.4 Conductive polymers

The main properties behind the possibility to exploit conductive polymers for the development of textile electrodes are field emission effect, percolation and tunnelling effect (Liu and Liu (2015). The first property helps when non-contact sensing is pursued. Charge percolation is fostered by an increase in the applied current, whilst the tunnelling effect, with distances lower than 10 nm, could produce electron flows. Conductive polymers were proposed for the fabrication of conductive textile electrodes according to this theory.

The most adopted conductive polymer is PEDOT:PSS (Wen and Xu (2017)), which is used to coat single wires to create personalized garments (Tsukada et al. (2012a)) or electrochemical wearable sensors (Müller et al. (2011); Stoppa and Chiolerio (2014)).

A process for the development of textile ECG electrodes with a high surface conductivity from finished fabrics was presented in (Zhu et al. (2015)) and (Müller et al. (2011)). This process involved the immersion of non-conductive fabric in a solution composed of PEDOT:PSS and other organic solvents for 48 hours, followed by drying in an oven after a passage between squeezing rolls to remove the excess polymer.

A process inspired by the Japanese kimono dying method was presented to fabricate textile electrodes and treat only specific parts of a finished garment (Takamatsu et al. (2015)). In this case, PDMS was deposited on a polyimide master to define the pattern. After transferring it on the bulk of the textile, the PEDOT:PSS solution was brush-coated on the untreated area and dried.

Screen printing and ink-jet printing techniques, which are widely used on flexible substrates to create electrodes with silver ink characterized by high electrical conductivity, can also be used with polymers. This technique has been successfully adopted in different fields to produce electrochemical biosensors with good reproducibility, stability and low production cost (Li et al. (2012); Renedo et al. (2007); Taleat et al. (2014); Yamanaka et al. (2016)). The technique has also been used to produce passive electrodes composed of Ag/AgCl ink screen-printed on a nonwoven fabric (Yokus and Jur (2016)) and develop fully textile PEDOT:PSS electrodes for ECG acquisition, with adequate performance for clinical use (Pani et al. (2016a)). Moreover, screen printing was effectively exploited to produce conductive paths to connect electrodes and readout electronics on the garments, particularly exploiting the more conductive and stable silver ink rather than a conductive polymer (Gordon Paul and Tudor (2017)).

Screen printing is not the only technique able to control the exact amount of conductive polymer deposited on a textile substrate. Other printing processes, such as ink-jet printing,

flexography and 3D printing can also be adopted. Each printing technique presents pros and cons, and must be chosen according to the textile substrate and the desired electrical properties. With this aim, customized ink formulations, including conductive fillers, additives, solvents and binders, are required (Kim et al. (2017)).

As an alternative to screen printing, ink-jet printing represents a new frontier for the development of polymer-based textile electrodes for the acquisition of physiological signals. For instance, examples of ECG electrodes fabricated by ink-jet printing over a 100 wt.% polyamide substrate exist (Bihar et al. (2017)).

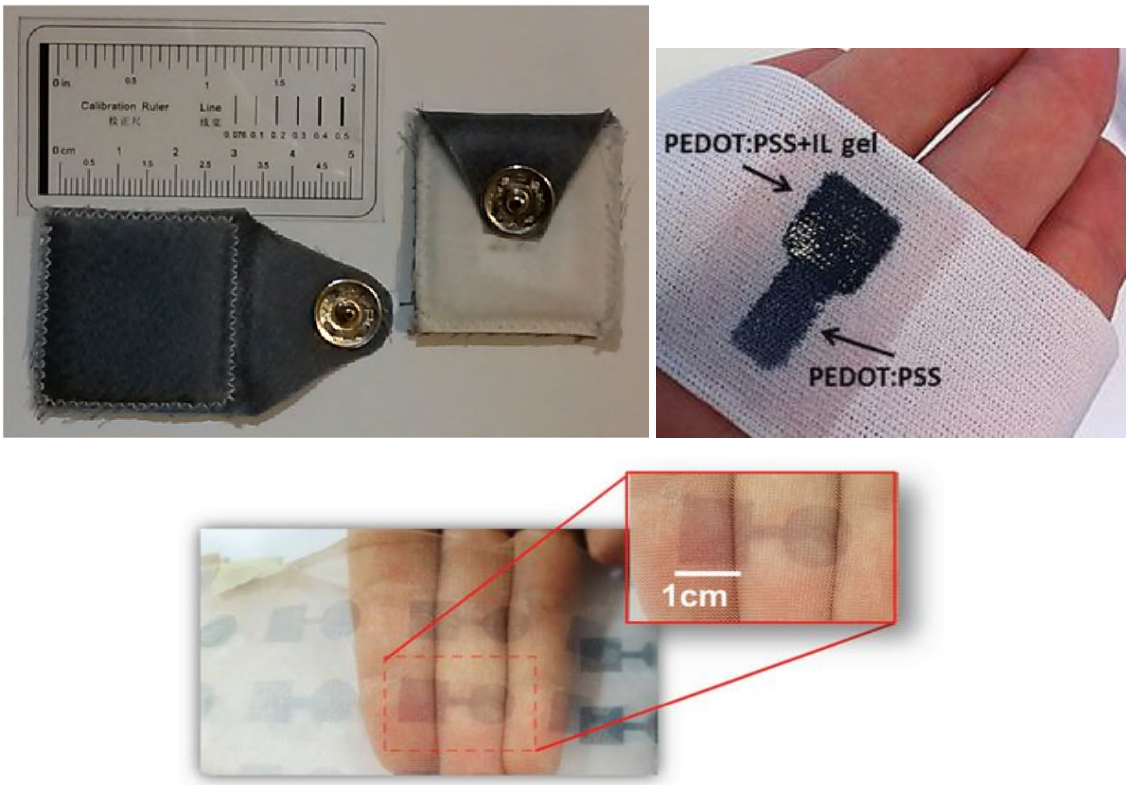

Figure 2.10 Prototypical PEDOT:PSS textile electrode developed with different techniques.

2.4 Relevant features and characteristics of textile electrodes

A characteristic that is often discussed in the literature about textile electrodes for biopotentials is the surface conductivity. A four-probe impedance measurement is usually performed on an isolated electrode (i.e. not in contact with the skin) to quantify this parameter (Van der

Pauw (1958)). Many textile electrodes have been created with metallic elements by looking at materials with good surface conductivity (Stoppa and Chiolerio (2014)). However, surface conductivity is not the most important feature for smart textiles. With the progress of knowledge about smart materials, the solutions exploiting metal wires have been progressively abandoned to be replaced by materials with other more important properties as skin contact impedance (Fernandez and Pallas-Areny (1996)). This parameter can only be measured by applying the electrodes on human subjects and by using an impedance meter. Remarkably, the largest part of mainstream measurement instruments certified for human use only provides the magnitude of the complex impedance value measured at a given frequency (e.g. 25 Hz for the EL-Check by Biopac Inc., 10 Hz or 30 Hz for the EIM-105 Prep-Check by General Devices, etc.) to quantify the quality of the contact. More complex devices and signal analysis techniques are required to investigate the impedance spectroscopy (Rosell et al. (1988)). These studies are typically aimed at the identification of the electrode model represented as a lumped element model fitting the actually recorded behavior (Beckmann et al. (2010)).

Other relevant characteristics, which are not independent from the skin contact impedance, are related to the ability of the electrode to capture the signal of interest, and are associated to a morphological analysis of the signal acquired with the electrodes, both in the time and frequency domains (Clifford et al. (2006)), including the noise level proper of the electrode and the DC level, somehow reflecting the behaviour of the electrodes at the high and low frequencies (the amount of baseline wander expectable in a real measurement), respectively (Puurtinen et al. (2006).

Moreover, the analysis of the typical morphological features of clinical interest extracted from the biopotentials acquired with the electrodes can provide other important information for the assessment of the textile electrode performance (Pani et al. (2016b)). These characteristics are often overlooked or improperly used because of the intrinsic complexity and the skills required for the result interpretation. For instance, the morphological analysis of the ECG signal could rely on the accuracy of identifying the fiducial points (typically the position of the QRS complexes, i.e. the epochs of the signal associated to the ventricular depolarization event) on the measurements of the main ECG waves (e.g. QRS complex, P wave associated to atrial depolarization and T wave associated to ventricular repolarization) after a proper ECG delineation (Martinez et al. (2004)) or on the ability to preserve the morphology of the signal when pathognomonic aspects are present (as the ST segment changes for ischemia) (MacLeod et al. (2005)). Frequency-domain features are typically analyzed by means of the power spectral density (PSD), which could provide further information on

the ability of the electrode to capture the meaningful aspects of the signal. The ECG PSD can be divided in several frequency bands representing specific aspects of the cardiovascular activity (Clifford et al. (2006), Murnaghan (1949)).

Compared to the disposable gelled electrodes, application-specific parameters, such as defibrillator overload recovery for ECG, are less important because of the different target application domain, where cardio-pulmonary resuscitation is also foreseen (Shyamkumar et al. (2014)). Conversely, some features are peculiar of textile ECG electrodes because they are correlated to the intended use.

The first one is biocompatibility, which is assumed for clinical electrodes because they are medical devices. The materials used should meet the appropriate regulations in terms of heavy metal release, toxicity, irritability etc. (Xu et al. (2008)). Comfort for long-term recordings is also important. The flexibility and stretch ensured by the substrate, which allows the reciprocal rotation and expansion of the fibres, lead to a smaller bending modulus compared to disposable electrodes (Xu et al. (2008).) However, such properties could influence other electrode parameters, such as the skin contact impedance, as discussed later on. Comfort is also ensured by breathability, which is largely reduced in commercial disposable electrodes and achievable with a textile support.

Lastly, washability is important because the electrodes are meant to be embedded into smart garments, which typically undergo normal maintenance cycles, including washing and drying. Some materials adopted for the textile electrode fabrication are intrinsically washing-proof because they are based on metallic elements or wires with properties that are preserved even after mild washing (Hertleer et al. (2004); Paradiso et al. (2005); Weber et al. (2003)). However, in spite of some washing cycles being tolerable without special production processes, other materials, such as conductive polymers, are less tolerant to washing because of the limited endurance of the polymer on the fibres (Pani et al. (2016a)). Another important safety requirement that should be considered is the biological response because the device shall be biocompatible. For this application (i.e. an electrode in contact with the skin) biocompatibility requires evaluation of cytotoxicity, skin irritation, and either skin sensitization or intracutaneous reactivity. This is deeply related with the electrode's adhesive performance and even in this case should meet certain specifications for the impacts on the using duration. For example, for a short-term resting ECG an adhesive should be able to maintain its contact to the body for a period of time, normally from 5 min to 30 min. On the other hand, long-term monitoring may require the electrode to be on the patient for a period depending upon the hospital protocol. Therefore, an adhesive that is to be utilized in

an ECG electrode should have performance characteristics that meet the intended use of the device.

2.4.1 Wet and Dry Textile Electrodes

The most common electrodes are those in Ag/AgCl that are widely used in medical applications. They are called wet electrodes because they are characterized by the presence of such a conductive liquid electrolyte interposed between the skin and the sensitive area of the electrode, Figure 2.11 (Chan (1996)). This electrolyte is composed of a water solution of chlorine salt (usually 4%) to improve the signal quality in the short term. Typical electrolytes are based on KCl or, less frequently, NaCl. However, other chlorine-free electrolytic solutions have recently been proposed to reduce the adverse effects on skin. Even though the term 'wet' should expressly refer to a liquid electrolyte, solid hydrogel is also adopted (Clifford J. Anderson (1976)). Solid hydrogel still presents a water component, and is subjected to drying. However, a cross-linked water-soluble polymer can keep the electrolyte compact (Cisterna (2000)). The solid hydrogel-based electrodes take benefit from the skin preparation by means of abrasive pads or creams because of the impossibility to wet the skin with solid hydrogel. Solid hydrogel is usually studied to provide *adhesion* on the skin, improve the electrode stability and reduce artifacts.

In the case of long-term use of the electrodes, the gel is uncomfortable and not very performing. As said before, in fact, the gel dehydrates over time reducing the quality of the signal and requires its reapplication, which it is not always possible. Furthermore, the electrolyte solution on the skin, especially if held for a long time, can give rise to dermatitis or irritation. In some cases, however, registration may have to be carried out in a sensitive area (near the eyes, for example) and the use of gel could be inappropriate. The alternative is represented by gel-free electrodes named also dry electrodes (Chi et al. (2010)). Dry electrodes do not require an electrolyte to enable a correct coupling with the skin to acquire physiological signals. However, the electrolyte absence affects the skin contact impedance, increasing its value up to three orders of magnitude, which in turn means more noise and sensitivity to motion artifacts. The former aspect could be solved by the adoption of a buffer amplifier in the close proximity of the electrode to transform the signal from high- to low-impedance (Searle and Kirkup (2000)). This is the working principle of active electrodes (Kang et al. (2008)). Aside from reducing the possibility of irritating the skin, the absence of electrolytes also provides substantial advantages in long-term monitoring applications because no signal degradation can be experienced. This is the reason why several research

works aim at the development of dry textile electrodes for smart garments (Liu and Liu (2015); Webster (2009)).

Taking to the extremes, this approach leads to contactless electrodes operating detached from the skin with a non-conductive textile layer (or air) in between (Chi et al. (2010); Li et al. (2017b)). Ideally, this is the perfect working condition for smart garments able to monitor ECG signals in the long term (e.g. for detecting arrhythmia or obtaining chest body surface potential maps) (Clippingdale et al. (1994)) or for patients with high skin sensitivity like patients with burns (Griffith et al. (1979)) or in neonatal units (Bouwstra et al. (2009); Kato et al. (2006)), being also possible the integration of the sensors in beds (Ueno et al. (2007)) or chairs (Aleksandrowicz and Leonhardt (2007)). For this reason, several works developed dry textile electrodes or smart garments able to acquired physiological signal without electrolytes or adhesive components that could reduce the comfort (Liao et al. (2011); Liu and Liu (2015); Webster (2009)). However, contactless electrodes require special readout electronics, and are more sensitive to motion artifacts, noise and interference, making them hardly usable in uncontrolled conditions or during movements (Chi et al. (2010)).

2.4.2 Contact impedance

The contact impedance between the electrode and the skin could change over time during the recording session for the environment variations but the skin condition could change for every subject even with a similar external condition, or from hour to hour. In (Beckmann et al. (2010)), an important variation in terms on impedance, especially at low frequencies, corresponding to a variation around 35% as shown in Figure 2.12, is reported during the day. In addition, the change of the dielectric properties of skin tissue was measured and showed a difference higher than 20% (Sunaga et al. (2002).

It is well known from the theory the relation between the electrodes size and their impedance but in (Takagahara et al. (2013)) was demonstrated also the correlation with amount of conductive fabric in contact with the skin. In fact, in case of textile electrodes in addition to the active area is important the effective amount of polymer and conductive fibers in contact with the skin as schematized in Figure 2.13. In another work is clearly exhibited that textile electrodes composed of different yarn and the manufacturing process present an evident variation in the skin contact impedance (Beckmann et al. (2010)).

This variation in terms of impedance largely affects textile electrodes with yarns covered by conductive elements such as PEDOT:PSS, but the same applies also in case of electrodes

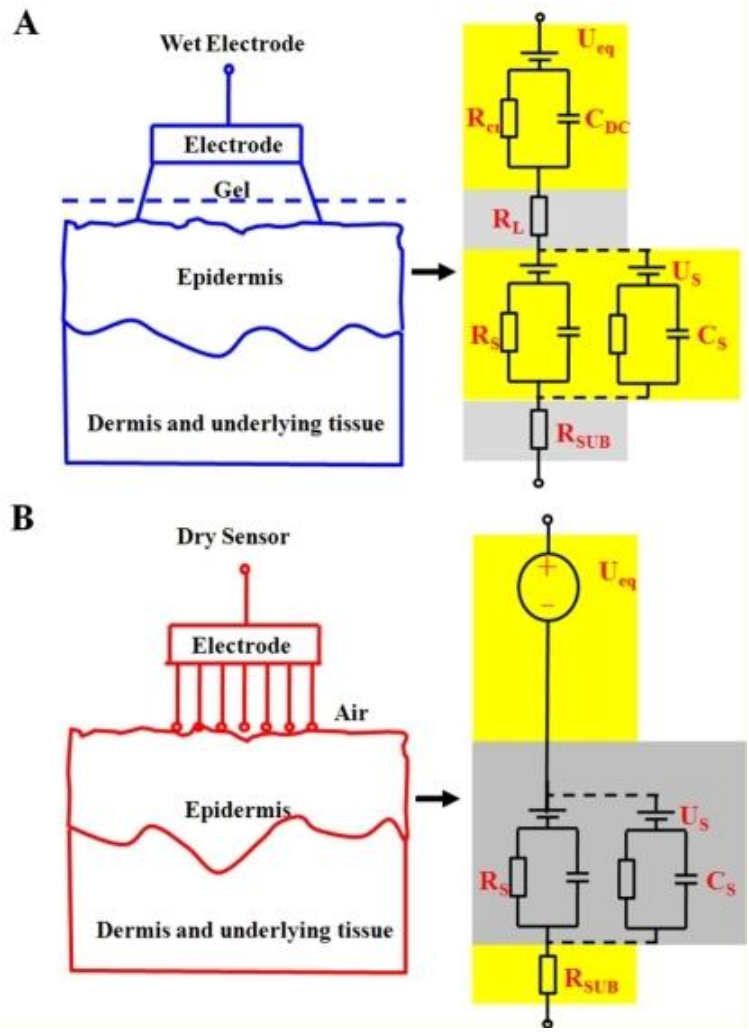

Figure 2.11 The equivalent circuits of a wet electrode-skin interface(A) and a dry skin-sensor interface (B).

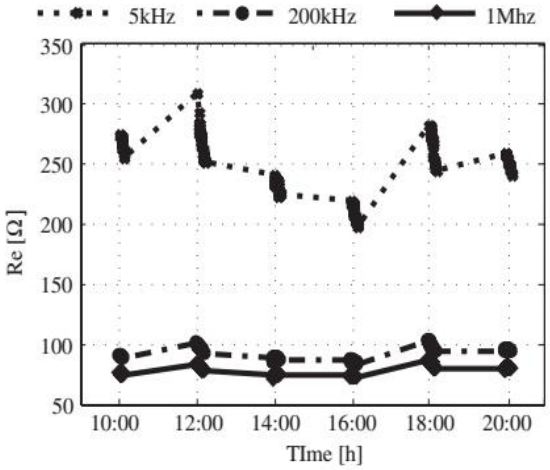

Figure 2.12 Skin contact impedance during a whole day measured with standard electrodes on the arm (Beckmann, 2010)

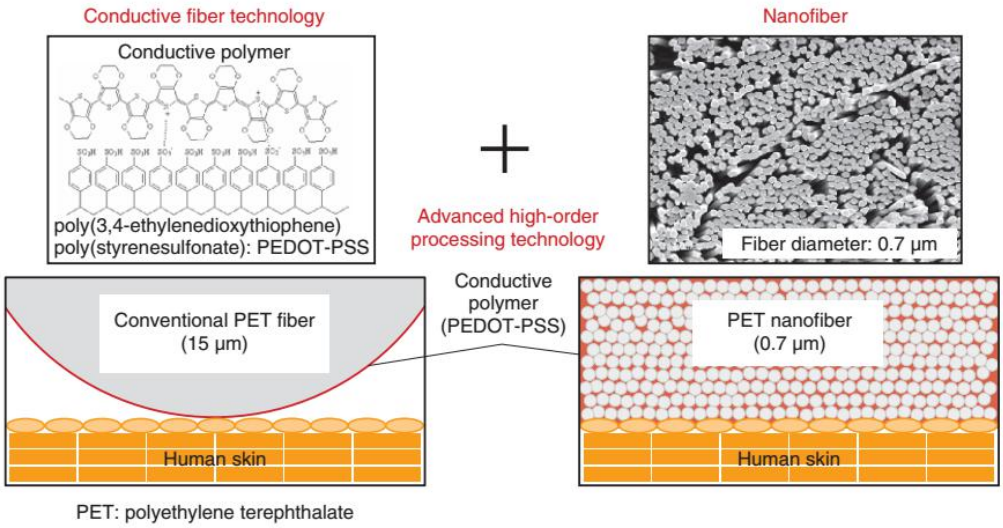

Figure 2.13 Differences between conductive fibers and nanofibers (Takagahara, 2013)

composed of metallic elements as represented in Table 2.2. In (Puurtinen et al. (2006)) the relationship between the impedance and silver textile electrodes developed in five different diameters (7 mm, 10 mm, 15 mm, 20 mm, and 30 mm) is highlighted.

	Electrode size (diameter)				
	30 mm	**20 mm**	**15 mm**	**10 mm**	**7 mm**
Dry	>100kΩ	>100kΩ	>100kΩ	>100kΩ	>100kΩ
Wet	∼25kΩ	∼50kΩ	∼50kΩ	∼70kΩ	∼40kΩ
Gel	∼35kΩ	∼80kΩ	>100kΩ	>100kΩ	>100kΩ

Table 2.2 Impedance with different electrode preparation and size

In (Sunaga et al. (2002)) and (Mihajlovi and Grundlehner (2012)) is described how an external agent, as the application of a force pressing the electrode against the skin, could decrease the skin contact impedance and increase the adhesion with the skin (Beckmann et al. (2010); M. Inoue and Tada (2017)). This behavior was demonstrated for graphene electrodes too, also at different frequencies as shown in Figure 2.14 (Lou et al. (2016)).

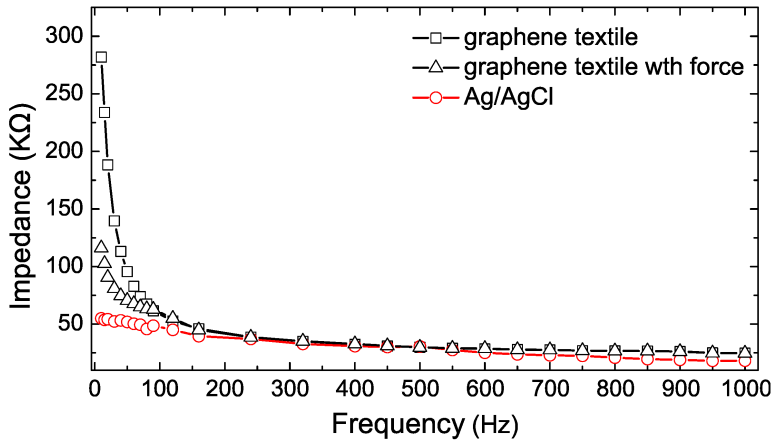

Figure 2.14 The skin–electrode contact impedance of Ag/AgCl and graphene textile (Lou, 2016)

The quality of the signal acquired with textile electrodes could drastically change with the contact impedance. In the literature, there are textile electrodes designed to work in dry condition and others that require electrolytes addition. In the following, some studies related to physiological signals acquired with textile electrodes developed with different techniques are presented, highlighting how the change of several parameters as noise and impedance is associated to the addition of a gel or a saline solution between the skin and the electrode.

In (Puurtinen et al. (2006)), the relation between the electrode area and the contact impedance was demonstrated but, at the same time, it highlighted how electrodes composed of conductive yarns change their skin contact impedance when electrolytes are added on their surface. These elements do not increase the already high sheet conductivity but influence the skin-contact impedance by moisturizing the *stratum corneum*. Also (Zhou et al. (2015) presents textile electrodes composed of silvered polyamide; because of this material, the superficial conductivity presents a similar behavior. Additionally, a sponge enwrapped into the conductive textile was inserted to enhance the electrode adherence and contact with the skin. In this case the impedance, measured on the leg, was evaluated at different frequencies. Such an approach was found in several other works related to textile electrodes because the impedance spectroscopy allows describing in a detailed way the response of the electrode at the low and high frequencies typical of specific physiological signals. In Figure 2.15 is evident the similarity of the trends in different measurement conditions, allowing to conclude that the electrolyte addition produces a shift in the impedance without significant further distortions at the different frequencies typical for the ECG signal.

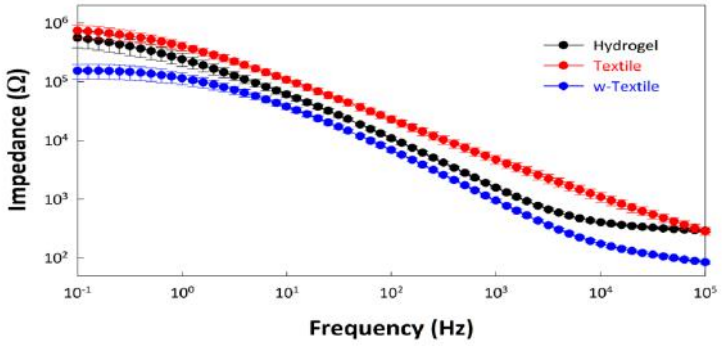

Figure 2.15 Impedance of the hydrogel electrode, textile electrode (w-textile electrode) tested on TA muscle of human legs (Zhou, 2015).

This skin contact impedance relation with the frequency is studied since 1988, when Rosell et al. tested this parameter from 1 Hz to 1 MHz and the results represented in Figure 2.16 are the demonstration that the skin impedance could be represented as a combination of resistive and capacitive components (Rosell et al. (1988). The principal reason for this behavior is related to the contact interface between the electrodes and the epidermis, the outer layer that compose the skin with the subcutaneous layer and the dermis layer (Xu et al. (2008)).

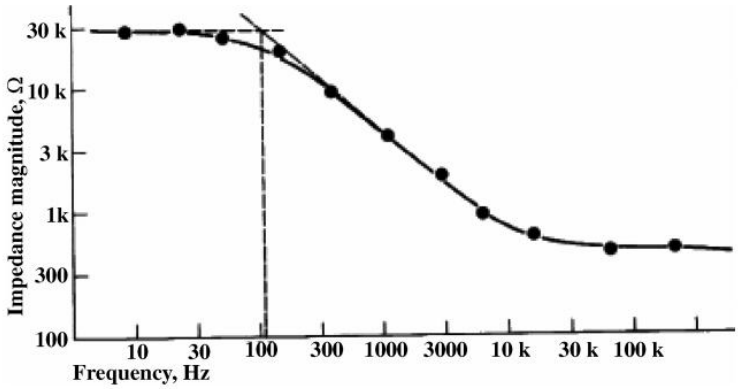

Figure 2.16 Relation between skin-electrode impedance and frequency (Rosell, 1988)

The same impedance analysis was performed on textile electrodes made up of PEDOT:PSS, by comparing their performance in dry and wet condition. In Figure 2.17, the results for dip coated electrodes in dry and wet condition are shown, whereas Figure 2.18 shows the impedance in different conditions for ink-jet printed electrodes (Bihar et al. (2017); Pani et al. (2016b)). In the first case, it is evident not only the well-known relation between the measurements in dry and wet condition but also the high impedance variability observable between different subjects without any electrolyte on the skin. Moreover, in Figure 2.18, skin moisture level, regulated by the amount of added electrolyte, is clearly related to the impedance level at different frequencies.

A similar trend in this parameter is present also for textile electrodes composed by a screen-printed silver layer with different active areas (Yokus and Jur (2016). To facilitate the comparison between textile electrodes and the gold standard represented by the Ag/AgCl gelled electrodes, a solution could be to follow the EC12:2000 standard imposed by ANSI/AAMI (American National Standard Institute and Association for the Advancement of Medical Instrument), established for disposable electrodes used for clinical ECG monitoring. This standard sets as limit for AC impedance at 10 Hz for two coupled gelled electrodes the maximum value of 2k Ω (ANSI/AAMi (2000). Remarkably, this value refers to the coupling between two electrodes without the human skin, in order to provide a stable reference. This means that the actual value of the skin contact impedance cannot be inferred from that obtained during such a test.

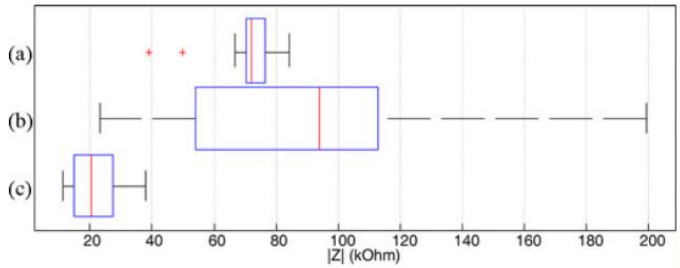

Figure 2.17 Boxplot of the electrode–skin contact impedance @10 Hz: a) dry textile electrodes on a single subject, b) dry textile electrodes and c) wet textile electrodes on ten subjects (Pani, 2016).

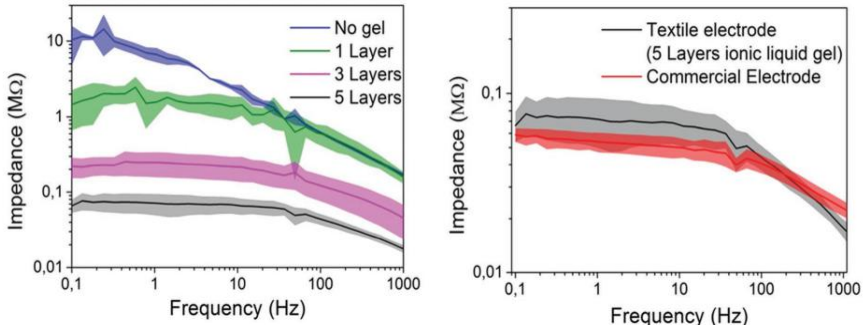

Figure 2.18 Left: Impedance spectra measured from PEDOT:PSS printed electrodes with various layers of ionic liquid gel, Right: Impedance spectra of a commercial electrode and a printed electrode with 5 layers of ionic liquid gel (Bihar, 2017).

2.4.3 Noise and artifacts

The ANSI/AAMI EC12:2000 standard set the limits also for another parameter to be taken into account for textile electrodes: the noise. The limit is equal to 150 μV for paired gelled electrodes. Similarly, to the impedance, there are several works demonstrating that textile electrodes can respect these limits but also in this case it depends strongly from several aspects, first of all the electrolyte addition. In (Searle and Kirkup (2000)) is clearly shown the noise variation for textile electrode between these three measurement conditions: dry, insulating and wet, Figure 2.19.

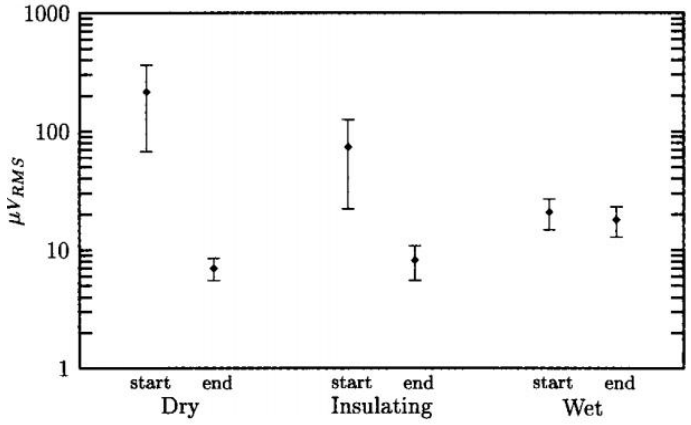

Figure 2.19 5 Hz RMS artifacts of three electrodes types: wet, dry and insulating (Searle, 2000).

As for the impedance, the explanation is again in the skin conditions and its interface with the electrode. The noise, in fact, is the expression of the electrical coupling quality between the skin and the electrode. When these two elements are in contact, they produce a half-cell potential with the electrolyte that contributes in the separation between the two plates of a capacitor: movements between them create a voltage change representing a noise for the ECG signal. Moreover, high impedance means higher imbalance between the two skin-contact impedances in a differential measurement, letting the system less robust to external power-line interference.

As seen also for the impedance, in the characterization of textile electrodes there is an important relation between the noise level and the active area of the electrode, Figure 2.20 (Puurtinen et al. (2006).

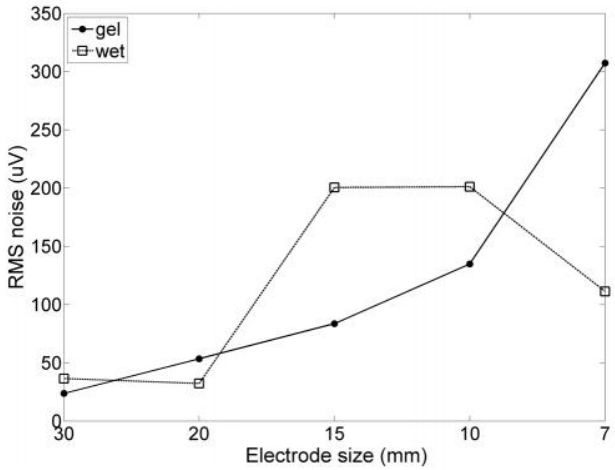

Figure 2.20 RMS noise in relation to electrode size in textile electrodes with saline solution and hydrogel (Puurtinen, 2006)

This is not the only similarity between noise and impedance, since there are other two parameters that influence the noise and are respectively the contact pressure and the skin moisture level. This is well demonstrated in (M. Inoue and Tada (2017)) for textile electrodes composed of Ag flakes.

2.5 Smart clothes for ECG signals

Textile ECG electrodes are developed to acquire the electrophysiological signal unobtrusively. Their performance as sensors has been mainly evaluated by applying them on the body with adhesive tape or by elastic bands, with or without electrolytes.

To test how textile electrodes can provide a valuable support to monitor biopotentials in long-term measurements, e.g. during athletic performance or home health care or telemedicine, the electrodes have been embedded in wearable devices (Baig et al. (2013); Liu and Liu (2015); Scilingo and Valenza (2017); Wang et al. (2017)), as exemplified in Figure 2.21.

In the last years several research groups developed wearable monitoring systems able to show in real time the physiological condition (some of them are reported in Table 2.22). These wearable devices according with telemedicine systems could represent a solution to several problems associated to population aging, chronic diseases management, and so on,

Figure 2.21 Examples of smart shirts for man and woman, respectively composed of textile and polymeric electrodes

Project title	Basic component	Communication mode	Measurement object	Medical applications
MagIC	Vest with sensors embedded/portable circuit board	Bluetooth technology	ECG/breathing/ temperature	Record the signal of cardiopulmonary function and daily activities
WEALTHY	Vest with sensors embedded	Conductive yarn/ Bluetooth technology/GPRS	ECG /breathing/ Temperature/EMG signals/ mechanical activity	Monitoring the recovery of elderly chronic disease
MyHeart	Chest belt with sensors embedded/PDA	Conductive yarn/ Bluetooth technology/ GPRS	ECG/other important signals/mechanical activity	Prevention of cardiovascular disease in elderly
Vital Jacket	Vest with sensors embedded/PDA/PC	Conductive yarn/ Bluetooth technology/ GPRS	ECG/breathing/temperature/ mechanical activity /oxygen saturation	The elderly physiological signs monitoring
CHRONIOUS	T-shirt with sensors embedded/PDA/PC	Conductive yarn/ Bluetooth technology/ GPRS	ECG/other important signals/mechanical activity	Elderly chronic disease prevention

Figure 2.22 Examples of smart shirts for man and woman respectively composed by textile and polymeric electrodes

enabling the reduction of the hospitalization costs and the risk of medical errors (Baig et al. (2013, 2017)).

The electrodes described in (Chen et al. (2010)) were integrated in a wearable system able to monitor physiological signals from neonates that, compared with elderly patients, require additional care when the electrodes are placed on the skin. The specific requirements includes the ability to acquire with adequate stability continuous vital parameters in daily use, considering the interference introduced by neonates and the part in contact with the sterilized skin (Bouwstra et al. (2009). For younger and elderly patients, the coupling with the skin is a crucial aspect because the skin is more sensitive and skin irritations could appear easily. The majority of textile electrodes embedded in smart clothes are composed of metallic yarns to obtain stable signals also with a bad coupling with the skin due to the reduced pressure required to increase the comfort (Boehm et al. (2016); M. Inoue and Tada (2017); Tuohimäki et al. (2017); Yapici and Alkhidir (2017)). However, the amount of metallic elements in the electrodes and their superficial conductivity, strictly correlated with the quality of the signal, are also associated to the increased probability of skin irritation.

Another important feature for wearable devices, especially in telemedicine field, is the connectivity. The signal acquired could be saved or visualized in real time with the electronics readout or could be sent wireless via Bluetooth or via Wi-Fi to the electronic system (Baig et al. (2017); Cheng et al. (2008); Gaikwad and Dekate (2017); Ottenbacher et al. (2004); Tuohimäki et al. (2017); Wang et al. (2017)).

2.6 EMG electrodes

The EMG signal can be gathered either on the surface of the body (suface EMG or sEMG) or invasively by needles (an example of this type of electrodes is shown in Figure 2.23). EMG is used to diagnose conditions of the lower motor neurons, to distinguish neuronal or muscular damage, myopathies or even muscular dystrophies. In addition to being functional to diagnosis, electromyographic signals are widely used in the prosthetic field and in sports.

For invasive EMG, both single and concentric needles can be used. A single needle is simply a sharp needle in metallic surgical material (stainless steel is widely used) fixed to a single cable to connect it with the instrumentation. They could be made of thin, resistant and flexible wires, created in nickel, platinum, silver and chrome metal alloys. The length of the needle is functional to the position of the muscle, in fact the more it is placed in depth the greater the length. This is a solution that obviously does not allow a long-term measurement due to the rigidity introduces from the metallic nature of the electrode. Percutaneous wire electrode, with a variable diameter from 25 to 125μm, insulated by a thin dielectric film, can be used for invasive long-term measurements. Coaxial needles, composed of a hollow needle where a conductive thread insulated from the needle passes through it without any electrical contact. This can be useful to guarantee an effective shielding of the cable or to provide a possibility to perform a differential measurement between the inner thread and the conductive external needle.

For what concerns surface electrodes there are different types depending on the specific application. As in the case of the ECG, there are electrodes requiring the use of a suitable conductive gel, pre-gelled or dry electrodes, whose shape and size could change depending on the application. In general, the electrodes are made up of Ag/AgCl as those for ECG, because of the good performance and important features of this material.

In unipolar EMG measurements, electrodes similar to those for the ECG are placed on the skin surface on the muscle to be examined. A second electrode, called neutral, is placed in a position far from the other one, as represented in Figure 2.24, so that the potential between these two electrodes could be amplified and recorded. The monopolar electrodes are those that allow to obtain the EMG in the simplest way but are not recommended for an accurate acquisition because they also detect electrical signals near the area of interest. In some systems, when multiple leads are used, a unipolar recording could be performed between a single electrode and the average of all the connected electrodes.

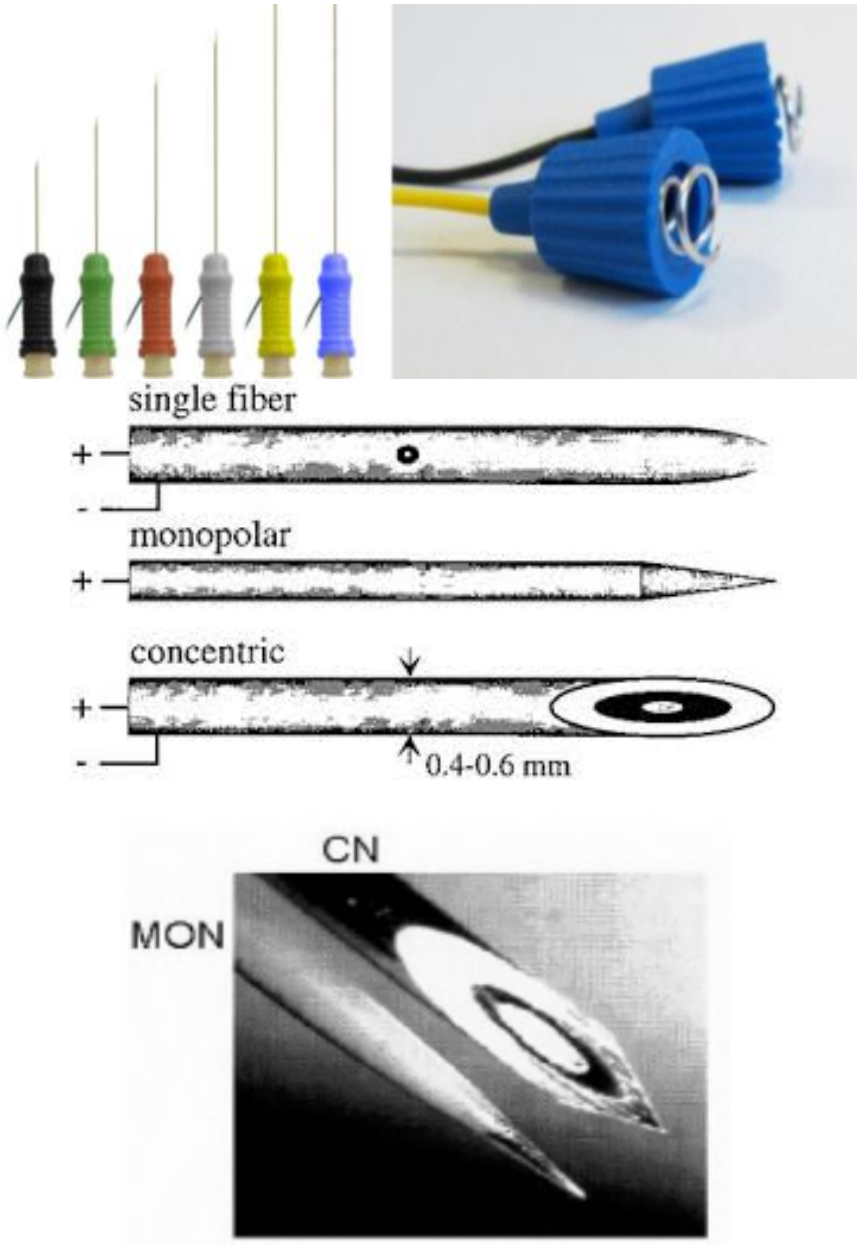

Figure 2.23 Different type of needle electrodes for deep EMG.

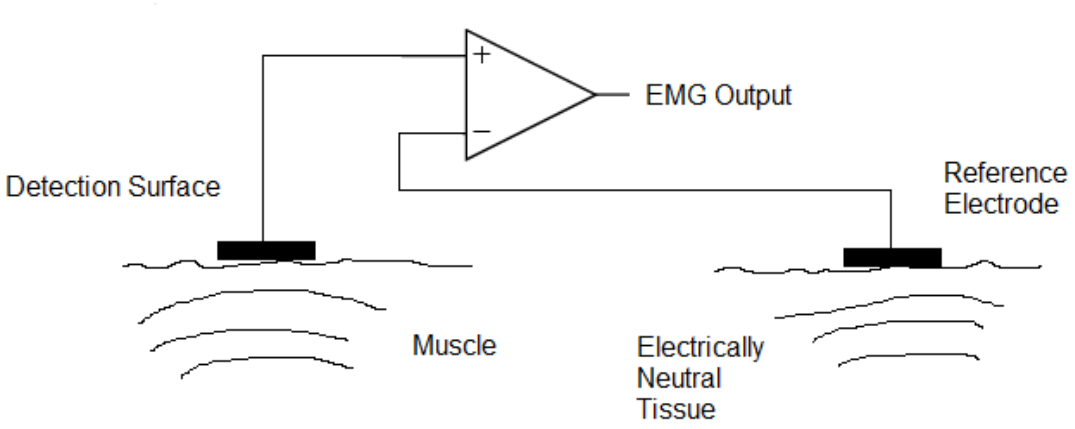

Figure 2.24 Monopolar configuration for EMG recording

In bipolar configurations, the signal is acquired between two electrodes placed one next to the other (typically at a distance of 1-2cm) and the ground of the instrument is applied away from the active area as sketched in Figure 2.25. In order to have a better performance it is preferable that the two electrodes have the same size and are composed of the same material to maintain balanced the skin-contact impedance between the electrodes. This configuration is the one used most frequently because of its spatial selectivity and the increased signal-to-noise ratio (SNR). It is also possible to use amplified electrodes to limit external interference, then increasing the SNR. By adding a local conversion stage and a radio module, it is possible to use these electrodes in conditions of significant mobility (for example during physical exercise, gait, etc.). There are typically two placements allowed for bipolar recordings: longitudinally with respect to the major axis of the muscle (therefore in the direction of the fibers) or transversely. In both cases, the electrodes must be placed on the specific muscle but far from the tendon and the central part (i.e. on the first or the third quarter from one of the tendons, approximately), as much as possible above the active zone of interest and away from other muscles and tendons.

Beyond monopolar electrodes, for the EMG recording the are also multipolar electrodes (Figure 2.26 and 2.27), either concentric, or composed of equally spaced monopolar electrodes. Long multipolar electrodes are principally used in the study of electrical conduction through muscular fibers on large muscles. Such electrodes allow the execution of topological analyses in two dimensions of the EMG signal and the determination of important parameters such as the orientation of the muscle fibers, the speed of the conduction and the localization of the motor areas.

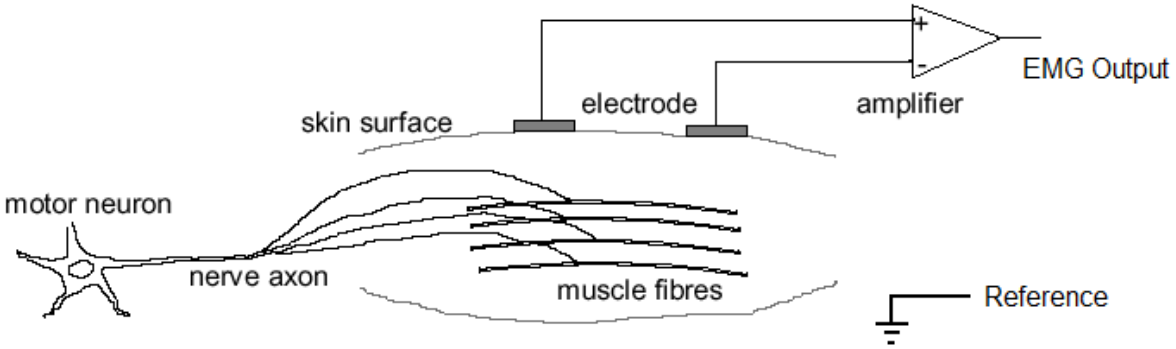

Figure 2.25 Bipolar configuration for EMG recording

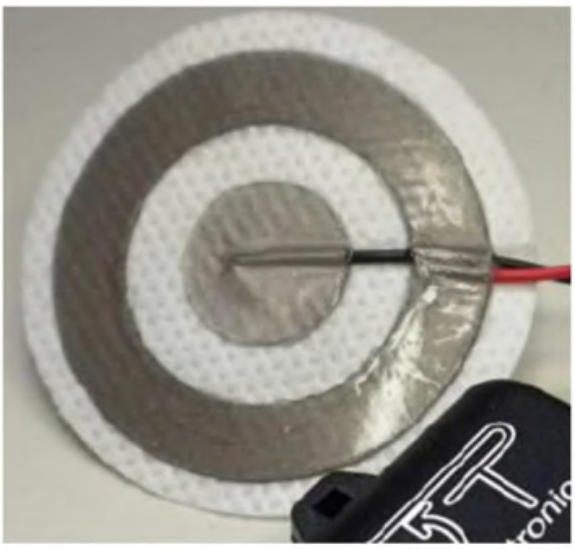

Figure 2.26 Concentric ring electrode used for the recording of the EMG signal

Figure 2.27 Multipolar EMG electrodes.

Several aspects already seen for ECG measurements also apply to the acquisition with EMG electrodes, in particular for what concerns the noise reduction. For instance, a fundamental aspect is the reduction of the skin electrode impedance, which could be reached with special creams or with a scrub with fine sandpaper with consecutive deep cleaning with ethyl alcohol solution. It is important to:

1. adapt the impedance to the amplifier input stage,
2. reduce the imbalance of the skin contact impedance in order to minimize the common mode noise,
3. reduce the DC component and baseline drifts generated from movement artifacts,
4. reduce the signal attenuation.

2.7 Textile EMG electrodes

The advent of smart textiles, with the possibility to integrate sensing/actuation features and electronic components into the garments, opened new approaches also in the detection of the

electromyographic signal. Moving from the first steps in the field, represented by metallic wires embroidered or knitted with non-conductive fibers to give rise to conductive pads (Gonçalves et al. (2018); Stoppa and Chiolerio (2014)), the industry proposed smart garments for several applications. This led to the introduction on the market of smart clothes for personal health and wellness with a particular focus in the detection of the electrocardiogram (ECG) (Park et al. (2017); Wang et al. (2015)) or the surface electromyogram (sEMG) (Colyer and McGuigan (2018); Pylatiuk et al. (2009)), or even to provide electrical stimulation for workout improvement (Zhou et al. (2015)). As said, these smart clothes use integrated textile electrodes obtained by embedding metallic wires into the fabric. Even though such a solution is robust, in order to avoid the introduction of seamed electrodes, their production must be integrated into the main garment weaving process. The main goal of the research in the field is to identify valid alternatives to metal wires for the production of this kind of electrodes, possibly with a limited impact on the garment fabrication processes and characterized by better performances (Pani et al. (2018)). Beyond an improved technological process, avoiding metallic electrodes improves comfort, especially in long-term measurements (Li et al. (2011); Mangezi et al. (2017)). This could be crucial for specific sEMG applications such as for the production of electrodes for sEMG-controlled prostheses (Zhang et al. (2013)). A variety of sEMG electrodes integrated into clothes have been proposed in the last few years. They were designed to acquire sEMG signals from several body regions: frontalis, temporalis and lateral rectus (Paul et al. (2014b)), vastus lateralis, rectus femoris and vastus medialis (Finni et al. (2007)), gluteals, vasti, hamstrings (Bifulco et al. (2011)), masticatory muscles (Niijima et al. (2017)), trapezius muscle to monitor the stress load (Taelman et al. (2007)), flexor and extensor forearm muscles (Shafti et al. (2016)). A limitation introduced by textile electrodes used to detect physiological signals is the capacitive coupling that, especially with dry or contactless electrodes, increases the impedance reaching extremely high values. The result is that environmental noise is easily picked up. This problem can be solved by placing an impedance converter directly on top of the textile electrode, as shown in Figure 2.28, transforming it in an active textile electrode (Linz et al. (2007)). The electrode is actively shielded by feeding back the output signal of the local amplifier to a metal cap over the electrode. The individual sensor output signals are fed into an analog-to-digital converter after anti-alias filtering. In (Linz et al. (2007)), the active EMG sensor embroidered into the fabric was placed on human biceps and compared with commercial active sEMG electrode (B & L Engineering type BL-AE-N).

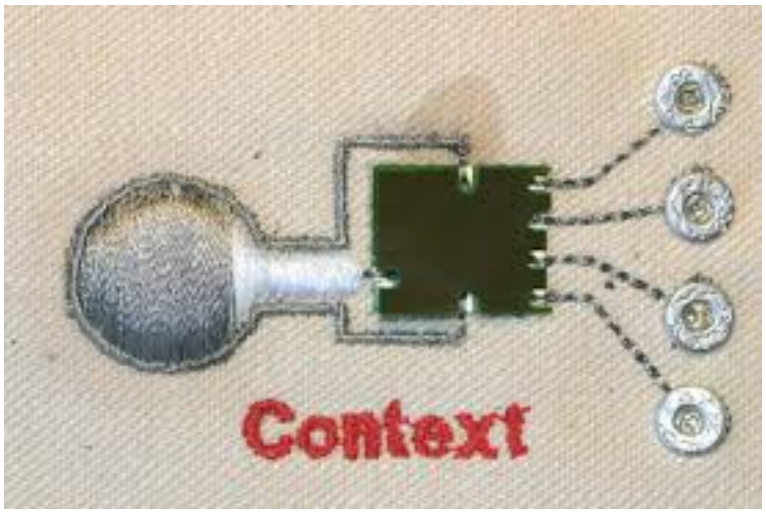

Figure 2.28 Amplified textile EMG electrode

In all these works, the electrodes were realized adding, onto finished clothes, conductive patches or wires, composed of metallic elements, or integrating screen-printed electrodes deposited on a plastic substrate. Both solutions affect the roughness of the garment surface and, finally, the comfort for the subject.

Chapter 3

Textile electrodes fabrication

3.1 Ink development

As demonstrated from textile electrodes listed in the state of the art, the PEDOT should play a crucial role in the development of a conductive ink because presents excellent properties as a conductive polymer even if it is insoluble in water. To overcome this limitation, the much more used PEDOT:PSS was developed, whose chemical structure is shown in Figure 3.1. It is a polyelectrolyte complex formed by PEDOT and polystyrenesulfonic acid (PSS) to obtain a stable dispersion. A complex polyelectrolyte (PEC) is normally formed by a mix of aqueous solutions of polyanions and polycationes and can be either a complex soluble in water or an insoluble precipitate. In addition, the PSS interacts with the individual repeating units of the PEDOT polymer chain making it electrically neutral, otherwise it would present positive charges.

The PSS is historically the first polyelectrolyte used to form a PEC with the PEDOT and from 1990 it is considered an industrial standard. The advantages related to the use of the PSS as counter-action for the PEDOT are several, among them:

- wide commercial availability,
- formation of a stable suspension in water,
- formation of enduring films,
- transparency.

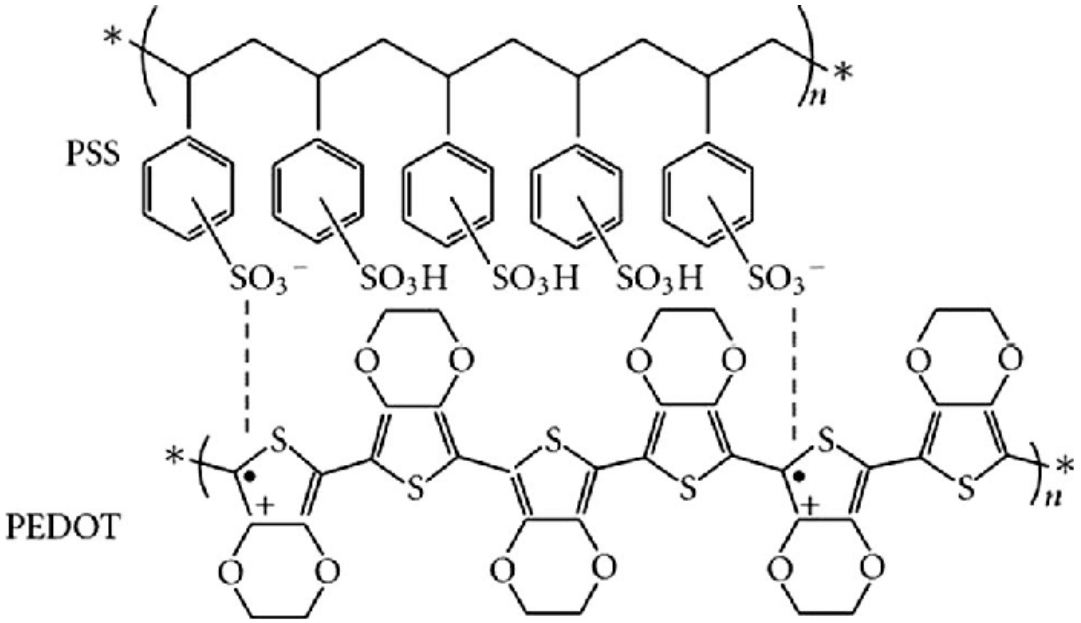

Figure 3.1 Chemical structure of the PEDOT: PSS.

The conductive properties of PEDOT:PSS can be improved with a process named secondary doping where organic compounds, including high boiling solvents like methylpyrrolidone, dimethyl sulfoxide, sorbitol, ionic liquids and surfactants are added to the polymer (Thomas et al. (2014)). This doping can increase the conductivity by many orders of magnitude by changing the properties of the solution in which it is suspended, as shown in Figure 3.2 (Kim et al. (2002)).

In this thesis, the PEDOT:PSS was doped adding ethylene glycol to the solution, mainly composed from water, changing surface tension of the environment in which the polymer is suspended. This leads the polymer to assume a different configuration in which the conduction is increased since the monomers are oriented along the axis σ, as shown in Figure 3.2 (Ouyang et al. (2004)). This improvement in the physical properties of the solution makes it also suitable as a transparent electrode, for example in touchscreens, organic light-emitting diodes, flexible organic solar cells and electronic paper to replace the traditionally used indium tin oxide (ITO). Owing to the high conductivity (up to 4600 S/cm), it can be used as a cathode material in capacitors replacing manganese dioxide or liquid electrolytes. It is also used in organic electrochemical transistors (Gualandi et al. (2016).

The conductivity of PEDOT:PSS can also be significantly improved by a post-treatment once deposited, with various compounds, such as ethylene glycol, dimethyl sulfoxide (DMSO), salts, zwitterions, co-solvents, acids, alcohols, phenol, geminal diols and am-

phiphilic fluoro-compounds. This conductivity is comparable to that of ITO, the popular transparent electrode material used for flexible organic devices.

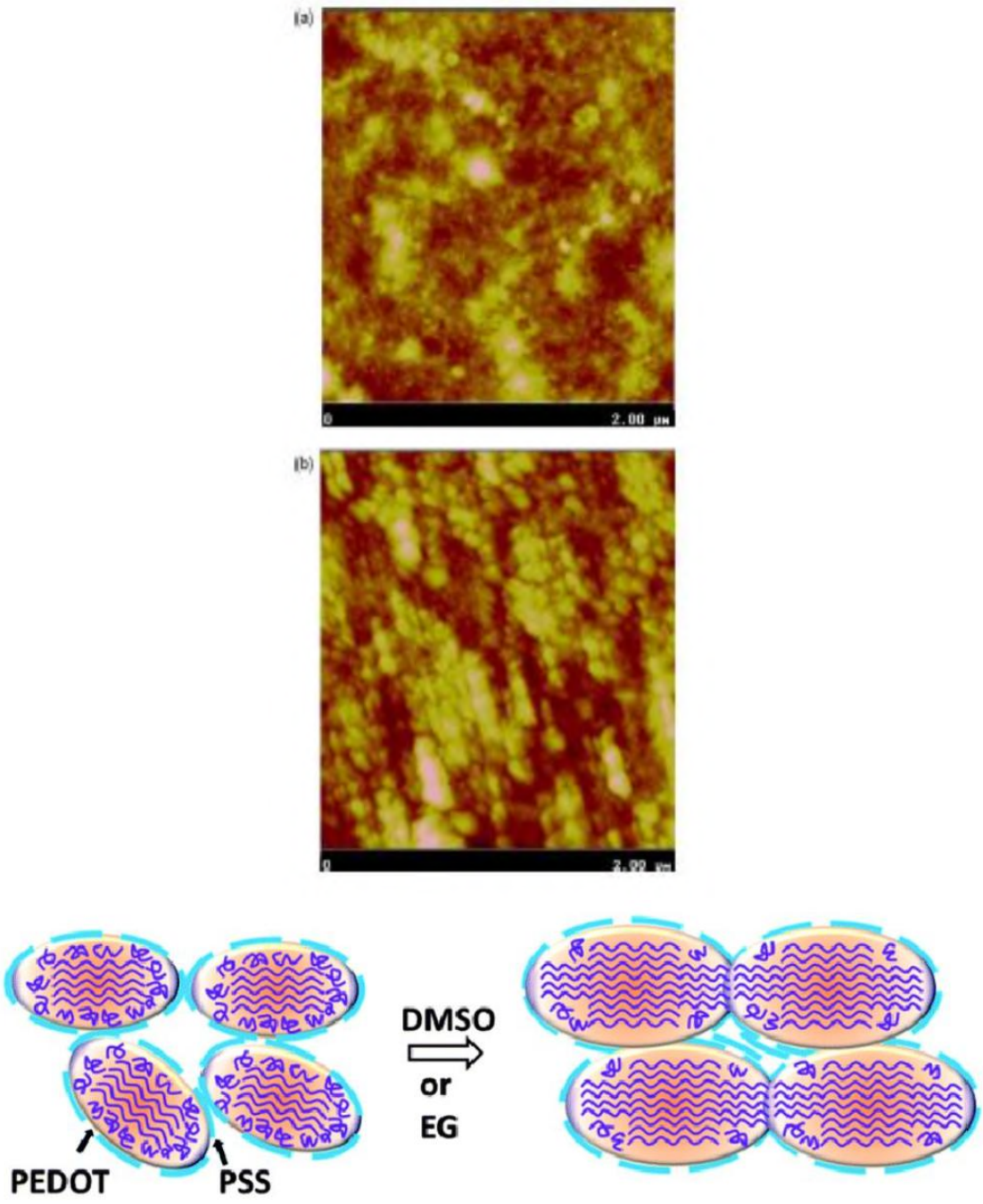

Figure 3.2 Top) AFM images of PEDOT:PSS obtained from a suspension with and without ethylene glycol, Bottom) Schematic model of structural modification in PEDOT:PSS with the addition of co-solvents.

Deposition of PEDOT:PSS-based inks

The PEDOT:PSS is commercially available in the form of liquid suspensions, usually watery, and most applications need it in the form of a solid compound. Several deposition techniques or polymerization are available, which are differentiated by:

- difficulty in preparing the solution and viscosity thereof,
- velocity in the deposition process,
- possibility to obtain a predefined pattern,
- waste of solution,
- thickness, homogeneity and adherence to the substrate of the obtained film.

The main deposition methods are related to solid substrates and they are divided between covering techniques, as spin coating, and printing techniques, the latter aimed at transferring on the substrate a layer with a specific shape whereas the former simply cover the whole available area. Among the coating techniques we can find: spin coating, spray coating and dip coating. Among the printing techniques: screen-printing, exographic printing, pad printing and ink-jet printing. The only printing technique that does not have a preformed layer to be transferred on the substrate and which therefore results as a sort of controlled coating is the ink-jet printing. For the purpose of this work, it is useful to analyze more in details some of these deposition methodologies such as dip coating, ink-jet printing and screen-printing. Each deposition process requires a specific treatment of the PEDOT:PSS, leading to a different ink formulation, in order to optimize the bond with the substrate or facilitate its distribution.

Water-based PEDOT:PSS inks are mainly used in slot die coating, flexography, rotogravure and ink-jet printing. At the same time, high viscous paste and slow drying is required in screen-printing processes; in such cases, PEDOT:PSS can also be supplied in high boiling solvents like propanediol. Finally, to overcome degradation to ultraviolet light and high temperature or humidity conditions, PEDOT:PSS UV-stabilizers are available.

3.1.1 Viscosity

The viscosity is maybe the most important parameter to adjust in the ink formulation in order to obtain a high printing quality because each printing procedure requires a specific viscosity. In addition to other chemo-physical parameters, the viscosity will be studied to optimize the polymer for the different printing procedures without affecting the conductive properties (Viswanath et al. (2007)). Viscosity is a characteristic property of all liquids: it measures the liquid resistance to flow or shear as well as the frictional properties of the fluid. It depends on the temperature and pressure: in this work, both are considered at room condition. Basically, two forms of viscosity can be identified:

- absolute or Dynamic viscosity,
- kinematic viscosity

Dynamic viscosity is the one measured in this context and required for specific deposition procedures as ink-jet printing or screen-printing. The most common unit for viscosity, also used in this work, is centipoise (cP), defined as 0.001 Pas. According to viscosity dependence on shear stress and on time, liquids can be divided into three categories:

- Newtonian: the viscosity is a constant parameter independent of the applied shear stress, i.e. the shear rate is a linear function of the shear stress,
- time-independent non-newtonian: the viscosity is a time-independent function of the shear stress, i.e. the shear rate is a non-linear function of the shear stress,
- time-dependent non-newtonian: the viscosity itself is time-dependent, therefore no shear rate function of the shear stress can be uniquely defined.

Ideal inks are newtonian fluids: actually, the ink dynamics depends on their composition. Polymer-based inks show a marked non-newtonian behavior, since long polymeric chains give rise to viscoelastic forces and can be clearly seen in the droplets ejected from the ink-jet printer. The best solution to modify the ink viscosity during its formulation is to employ different solvents, when possible. The main problem is with low viscosity inks, since most solvents have low intrinsic viscosity. To overcome it, a small quantity of a high-viscosity substance or a cross-linking agent can be added to the solution, which does not affect neither the surface tension nor the final electrical performance of the device. These liquid properties are tested by an instrument named viscosimeter, shown in Figure 3.3.

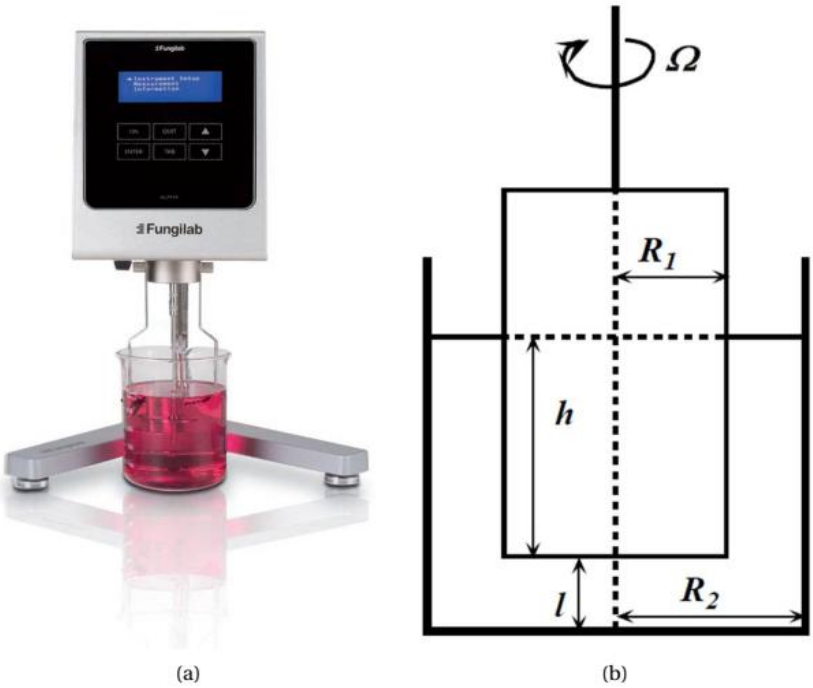

Figure 3.3 a) Fungilab® viscometer Alpha L. (b) Schematic of the working principle of a rotational coaxial-cylinder viscometer.

In particular, the viscometer employed during the work of this thesis was purchased by Fungilab®. The standard model can measure viscosity in the range 20-2000000 cP, but by the addition of an adaptor viscosities as low as 1 cP can be measured. According to the viscosity range, 18 rotational speeds can be set reaching a maximum resolution of 0.01 cP and a 0.2% of measurement repeatability. The working principle of this rotational viscometer, of coaxial-cylinder type, is schematized in Figure 3.3. The viscometer consists of an inner cylinder of radius R_1 and height h, and an outer cylinder of radius R_2. The latter, which contains the ink sample, is stationary, while the former, suspended by a fine wire, is rotated at a constant speed Ω (rad/s). The resultant torque T (dyne·cm) is measured by the angular deflection of the inner cylinder. If a newtonian fluid is considered, the dynamic viscosity is obtained from the following expression:

$$T = \frac{4\pi R_1^2 R_2^2 h \eta \Omega}{R_2^2 - R_1^2} = C \cdot \eta \cdot \Omega$$

where C contains all the constant specific of the instrument. Basically, given C, set Ω as input and measured T as output, the dynamic viscosity η can be evaluated as a proportional factor between T and Ω.

3.2 Dip coating

In this work, textile electrodes are fabricated by treating conventional fabrics with a highly conductive solution of PEDOT:PSS. We previously said how, in order to achieve reasonable conductivity values for the PEDOT:PSS, a second dopant should be added. The conductivity can be enhanced from one to three orders of magnitude by the addition of poly-alcohols (alcohols with more than two OH groups on each molecule, e.g. ethylene glycol, glycerol, sorbitol) or high-dielectric solvents (dimethyl sulfoxide, N-N dimethylformamide, tetrahydrofuran) (Chi et al. (2010); Marozas et al. (2011); Paradiso and Pacelli (2011)). The ethylene glycol was mixed with two times the PEDOT:PSS dispersion Clevios PH 500 (Heraeus Clevios – Germany) with a magnetic stirrer until a homogeneous solution was obtained. Woven cotton (250 µm thick) and polyester fabrics (400 µm thick) were used as received, and immersed for at least 48 h at room temperature in the polymer solution. Fabrics were then removed from the PEDOT solution and squeezed between metallic rolling cylinders to remove the solution in excess as shown in Figure 3.4. Samples were then annealed at 180 °C for 3 minutes, roughly the time needed for both water and second dopant to evaporate in order to avoid deterioration of the fabric mechanical properties. Dried fabrics were cut in 35 mm $\times$ 65 mm pieces and the surface resistance measured. In order to evaluate the properties of the conductive fabrics as surface bio-potentials electrodes, without any disturbance due to other materials getting in touch with the skin, the conductive fabric was sewed to a non-conductive 35 mm $\times$ 35 mm layered structure of foam (4 mm) and polyester, using simple cotton yarn. In order to obtain reproducible samples, all sewing was performed following an automatic procedure developed with an electronic embroidering machine (Brother Innovi's 955). After sewing, the active area of electrodes is reduced to 30 mm $\times$ 30 mm. The size of the electrodes, which is acceptable for ECG monitoring, has been chosen to ensure a good reproducibility of the custom fabrication process. The introduction of foam layers allows improving the contact between the electrode and the skin by ensuring a uniform pressure, which is especially beneficial in case of dry electrodes. In fact, some authors associate the baseline drift, which is a typical artifact in signals acquired by textile electrodes, to a variation in the contact pressure, which can be reduced by a soft layer of foam (Paul et al. (2014a)). The presence of the foam also allows keeping the electrode wet (physiologically or artificially) in order to reduce the contact impedance (Löfhede et al. (2012)).

In light of the extreme versatility of the fabrication technique was thought that an integration of the electrode in a garment could be obtained by selectively treating pre-defined portions of the garment with a similar procedure. The choice of woven cotton and polyester

fabrics was motivated by the idea of having common textile materials instead of rare and expensive ones. Notably, the proposed approach can be applied to any kind of textile material able to absorb and retain the conductive polymer. Furthermore, we chose flexible but unstretchable fabrics in order to reduce the effect of the stretch on the electrode-skin contact impedance (Kang et al. (2008)). In fact, flexibility and stretchability can confer to conductive textiles the ability to act as strain gauges, changing their impedance as a function of the stretch level (Carvalho et al. (2014)). Clearly, this feature is not desirable for an electrode, which should maintain its impedance constant despite the occurrence of mechanical deformations.

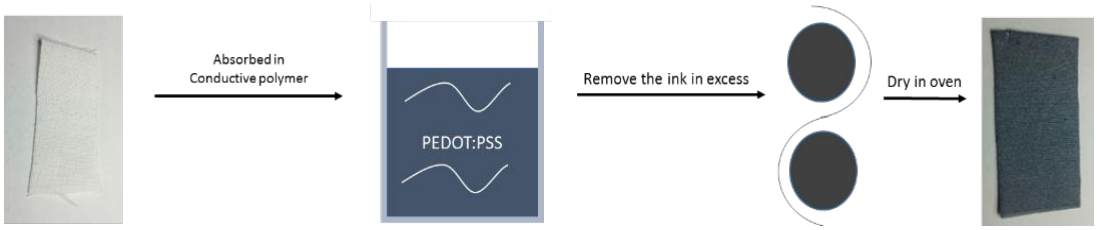

Figure 3.4 Schematic fabrication process used to develop dip coated textile electrodes

3.3 Ink-jet printing

The ink-jet printing operation consists in the formation of a tiny drop of ink which is deposited on the substrate. It allows producing electrodes with a specific geometry and a controlled amount of ink deposited on the substrate. To guarantee the success of this process, the viscosity of the ink must be low and the surface tension high, so that a sort of vapor droplets can be generated. The waste of substance is minimal due to the great precision of the technique, in fact this deposition method could reach a film thickness range between 1 and 500 μm.

As said, the ink viscosity plays a crucial role in the printing procedure, mainly because it is the parameter that could influence the amount of ink deposited on the fabric. The ink-jet printer used was a Dimatix Materials Printer DMP-2800 Series, Figure 3.5, that can jet a wide variety of fluids, including aqueous and solvent-based fluids, solutions and particle suspensions. The ideal fluid characteristics for this printer and its cartridges are viscosity of 10 centipoise (0.01 Pa sec) and surface tension of 30 dynes/cm. To maintain this condition, it is necessary to control the environment to avoid any particles aggregation in the ink. Many

times, in particular with inks composed of several components, it is difficult to control this parameter and the printer allows a fluid viscosity range equal to 2 - 30 cPs. The viscosity range is intended as an ideal viscosity to obtain a perfect printing process, but actually "printable" inks have a wider range of viscosity. From 10 cP to 18 cP, very good printing can be performed, with a very good control of the drop formation, vertical direction and reduced drop tails. Over 18-20 cP viscosity may be too high and the deformation of the piezoelectric crystal is not sufficient to eject a drop. On the other side, viscosities in the range 6-10 cP result in fair good printing with generally vertical drops but with a poor control on the drop volume: satellite drops can arise which do not allow the printing of very accurate patterns. The range 1-6 cP includes printable inks with poor or very poor control on the drop and the final result: these inks are generally used to create full non-patterned layers whose surface roughness is not a critical issue for the device performance. Under 1 cP the printing is almost impossible: the very low viscosity results in material waste during the cleaning cycles and in a very poor control of the droplets, which can be of various size, rarely vertical, and that are randomly deposited on the substrate. The cartridges are also compatible with most organic solvents and acrylate materials such as: a) Aliphatic alcohols (high boiling point better than low in all cases) b) Aromatic hydrocarbons such as anisole, trimethylbenzene c) Aliphatic hydrocarbons such as hexane, dodecane, d) Cellusolves e) Glycols f) Lactate esters g) Aliphatic and aromatic ketones including tetrahydrofuran (evaporates quickly) h) Polyethylene glycols, polypropylene glycols.

The ink-jet printing process used by Dimatix Materials Printer DMP-2800 involves the ejection of a fixed amount of ink, in form of droplets, from a chamber through a nozzle. The ejected drops fall onto a substrate under the gravity force and air resistance to form a pattern. The solidification of the liquid may occur through the evaporation of a solvent, chemical changes (for example the cross-linking of polymers) or crystallization. Often some post-processing treatments are required, as thermal annealing or sintering, i.e. the melting of metallic nanoparticles in metallic inks, achieved by heating to high temperatures. The ink-jet printing system employed in this research activity is a Drop-on-Demand (DoD) system, so called because it ejects an ink droplet from a reservoir through a nozzle only when a voltage pulse is applied to a transducer, i.e. only when the ejection is required. Dimatix Material Printer 2800 (DMP2800, FujiFilm) is a *piezoelectric* printer where the ejection of the droplet is caused by the mechanical deformation of a piezoelectric material under the application of an electric field. Before the printing process starts, the ink chamber is depressed by applying an appropriate bias to the piezoelectric crystal in order to prevent the ink from falling down from the nozzle (Start or Standby phase). A zero voltage is then applied to the piezo, which

is thus undeformed in its relaxed position, leading to the ink flow into the chamber from reservoir. In the next phase, the chamber is strongly compressed causing the drop ejection from the nozzle. Finally, the chamber is brought back to the initial decompressed condition to pull back the ink and to prepare the system for the next ejection. The main component of the DMP2800 are:

- *print carriage*: it is the physical support of the cartridge and it represents the core of the printer itself;
- *platen*: it is the substrate's holder. It can be heated until 60 °C and it is provided with a vacuum system. The platen temperature is an important printing parameter. Indeed, it affects the drying time of the ink-jetted droplets on the substrate, and it can be one of the major causes of the undesired nozzle clogging. The vacuum system has the function of holding the substrate on the platen during the printing process;
- *cleaning station - blotting pad*: it is the cartridge maintenance station, where the cleaning cycles are performed;
- *drop watcher station*: this is the system which allows direct viewing of the jetting nozzles, the face plate surrounding the nozzles, and the actual jetting of the fluid.

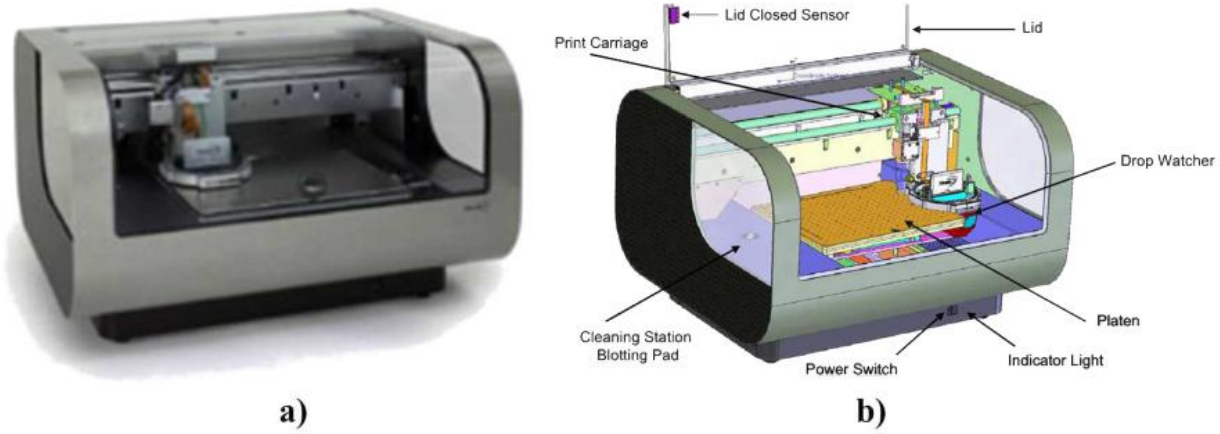

Figure 3.5 Picture a) and scheme b) of a Dimatix DMP2800.

The print carriage in Figure 3.6a is the core of the printing system. It is the support for the cartridge and it includes the fiducial camera, a very useful tool for alignment procedures and for evaluation of the printed pattern quality. During printing, the carriage moves horizontally

(X direction) above the substrate, while the vertical shift (Y direction) is achieved by means of the platen motion. In other words, the printing action proceeds through subsequent horizontal scans of the print carriage, and subsequent vertical shifts of the substrate. The cartridge, Figure 3.6b, is composed of two main parts: a *fluid module*, which contains a plastic bag acting as ink reservoir, and a *jetting module*, where 16 jetting nozzles, at a distance of 254 µm, are located in a single row and each orifice size is about 21.5 µm. Dimatix supplies two models of piezo-driven jetting cartridges which differ for the nominal drop volume they can eject: DMC-11601 and DMC-11610 models are able to jet 1 pL and 10 pL droplets respectively. Determining the spot size of the ink on the substrate is a fundamental operation to set an appropriate *drop spacing* in order to achieve the desired resolution of the printed pattern. The *drop spacing* is the distance between the center of two subsequent drops, both in X and in Y direction, which the printer deposits on the substrate to create the pattern. As shown in Figure 3.6c and Figure 3.6d, in the X direction the printer manages the ejection of a drop from the correct nozzle according to an encoder signal and to the image resolution corresponding to the drop spacing set. In the Y direction the distance between two subsequent spots is determined by the cartridge mounting angle (angle between the scan direction of the cartridge and the nozzle plate), but also by the intrinsic resolution of the printer, i.e. the distance between two subsequent nozzles in the nozzle plate (254 µm). The cartridge mounting angle is set manually through a rotating system, which allows the operator to rotate the cartridge at the desired angle by means of two graduated scales, Figure 3.6d. The drop spacing thus is adjustable between 5 µm and 254 µm.

Controlling the quality of jets ejected is crucial in order to achieve the best print quality. It can be done in two different and complementary ways: caring for the cartridge maintenance and monitoring the ink droplets ejection. The maintenance operations are supported both by software and hardware of the printer, and are designed in order to initialize and maintain the optimal jetting performances. In the cleaning station there is a replaceable adsorbing pad, which has the function of soaking up the ink from the nozzle plate. Four main functions can be combined to form Cleaning Cycles:

- **purging**: the fluid is pushed out of the nozzles by an application of air pressure to outside of fluid bag. Purging is required for the initial use of the cartridge to push air out of the fluid path, as air bubbles may cause nozzle clogging;
- **spitting**: a certain number of drops are jetted at a predetermined frequency in order to clean the nozzles and to keep fluid path surfaces wet;

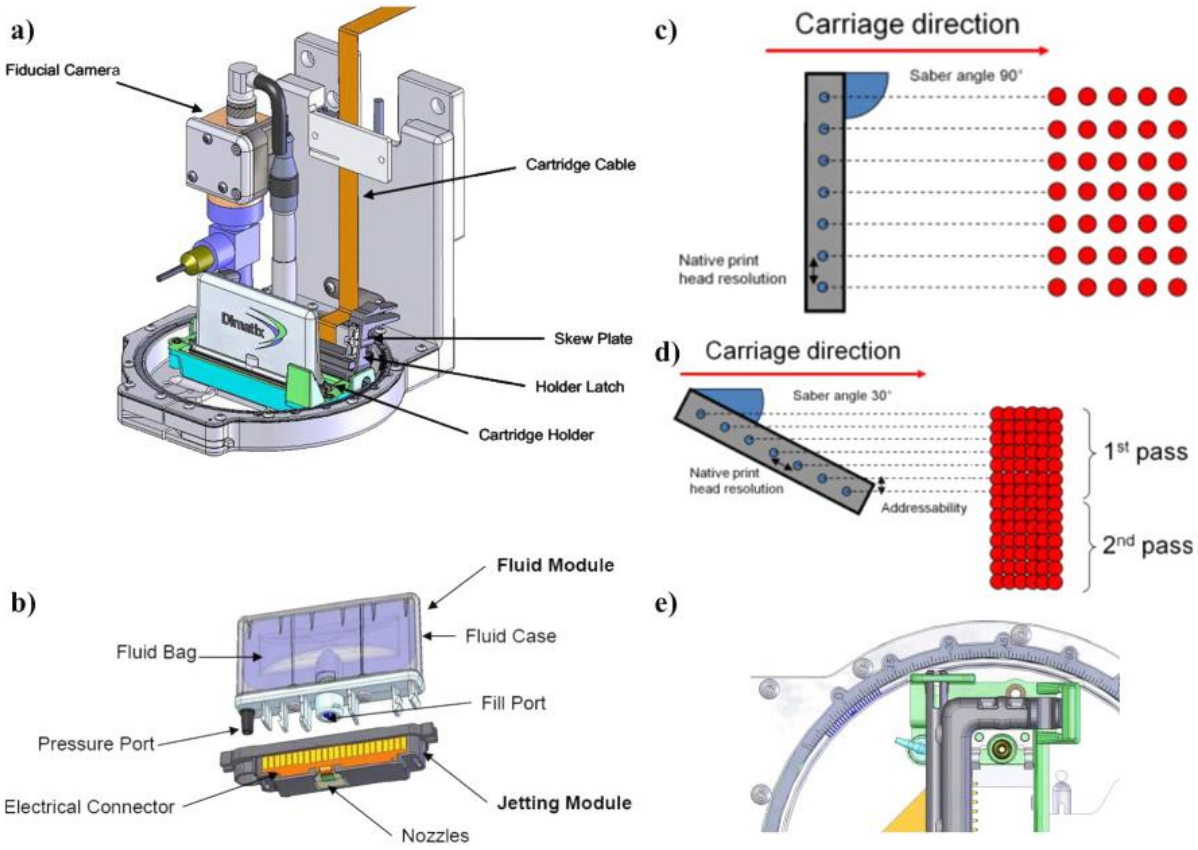

Figure 3.6 a) Print carriage; b) cartridge parts (fluid module and jetting module); c) and d) pattern resolution in X and Y directions as a function of the cartridge mounting angle e).

- **blotting**: the nozzle plate is kept in contact with the cleaning pad (no wiping) to remove the excess of fluids that may be present in proximity of the nozzles;

- **meniscus control**: in order to prevent ink from flowing out of the cartridge nozzles, a low vacuum is applied to the ink reservoir. The desired cleaning cycle can be performed before (almost mandatory to achieve satisfactory printing performances), during and after printing and also during resting time. Monitoring and adjusting the ink jets is possible by using the *drop watcher camera system*, including a replaceable *drop watcher pad* which collects the fluids ejected, and a digital camera with a magnification of 150x. During jetting observation several parameters can be set and/or modified;

- **firing voltage**: it corresponds to the bias applied to deform the piezoelectric crystal for the droplet ejection. It can be adjusted for each nozzle independently. Obviously, different inks require different firing voltages in order to reach the optimal jetting performances. Generally, a high firing voltage produces quite compact drops but with a long tail. Conversely, a low firing voltage permits reducing tails length, drop velocity and avoiding droplets scattering at the impact with the substrate (and, subsequently, obtaining a better print quality). On the other hand, a low firing voltage may bring to misdirected jets and increases the probability of clogging nozzles during printing;

- **jetting frequency**: it's the frequency of nozzles for ejecting droplets. It affects the print velocity, the print precision and it is strictly dependent on the particular pattern as described afterwards;

- **number of jetting nozzles**: as the jetting frequency, also the choice of the number of used nozzles is strictly dependent on the specific pattern and precision. If high precision and definition of the printed pattern are required, using a few jets is suitable. On the contrary, when rough layers of material have to be printed, the use of many nozzles leads to a faster print process together with a good uniformity of the material deposited. It should be noticed that printing with more than one nozzle implies to use adjacent nozzles: choosing the group of nozzles with the overall best jetting performances is really critical and sometimes it could be quite difficult. Checking the good jetting performance of the chosen nozzles just before printing is absolutely advisable.

To test this deposition process for the development of textile electrodes, the commercial ink PJET 700 provided by Heraus was used. It was selected because it presents the right

viscosity range required for this procedure, 5.0 - 20 cP. As textile substrate was selected a sheet of cotton and the ink was printed on a 1 mm $\times$ 5 mm area with the following settings:

- cartridge with 10 pl drop size,
- 10 µm or 15 µm drop space,
- Nozzles used: 2 side-by-side,
- Hot plate @60 °C,
- Print size: 2 mm $\times$ 5 mm,
- Number of layers: variable from 1 to 8.

3.4 Screen-printing

The screen-printing technique is the second printing procedure analyzed and the one we considered the best to functionalize the fabric with PEDOT:PSS in order to obtain textile electrodes. An organic solvent, called secondary dopant, was added to the commercial suspension of PEDOT:PSS, even in this case to increase its electrical conductivity. Finally other chemical compounds were added to the suspension to endow with specific features the conductive polymer layer. In this specific situation, this compounds is the (3-Glycyloxypropyl)trimethoxysilane (GOPS) that is a cross-linker often added to the PEDOT suspension to increase its stability in aqueous environment. This reticulating agent increases the resistance of the material to degradation in contact with water, increasing the number of bonds between the chains forming the conductive polymer.

For the ink was used a PEDOT:PSS formulation composed by one part of ethylene glycol and two parts of Clevios PH 1000, wherein, after the mixing, 1% of GOPS was added. The commercial PEDOT:PSS suspension is not suitable for directly carrying out screen printing, because the polymer particles can spread into the fabric by capillarity leading to the formation of active patterns with an ill-defined shape. After a series of tests was defined the appropriate amount of the solvent to evaporate from the PEDOT:PSS suspension before deposition, in order to obtain a viscous suspension that allows to print patterns with high lateral resolution. This final PEDOT:PSS ink presents an high viscosity and the mechanical features of a gel and was used for screen printing the patterns of conductive polymer onto the textile substrate by employing a stencil with a suitable shape and a fill blade. As said before, each printing

procedure requires inks with a specific viscosity and the original solution was composed from PEDOT:PSS with a viscosity range equal to 15 - 50 cP and ethylene glycol characterized from 16.9 cP whereas screen-printing inks have a viscosity higher than 50 KcP.

Figure 3.7 Screen-printing instrumentation composed of ink, frame and squeeze

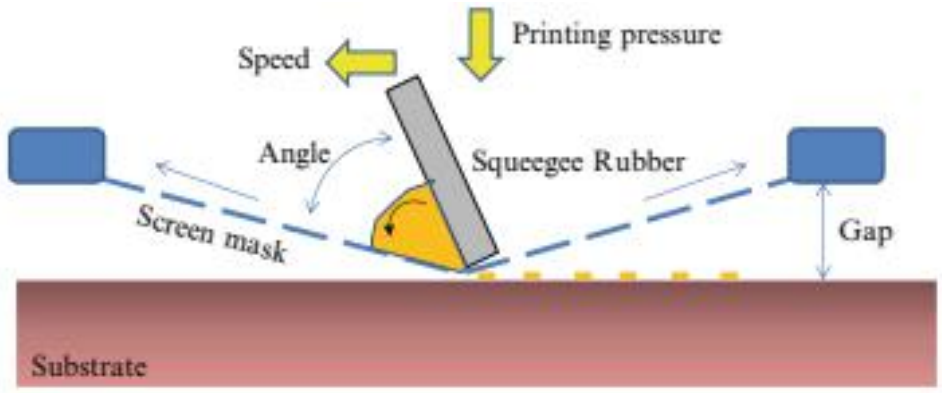

Figure 3.8 Schematized working principle of screen-printing deposition processand the parameters involved.

A schematic of the screen-printing process is shown in Figure 3.8. The screen is supported by the emulsion in the openings. The squeegee pushes down on the screen, causing the screen to come into contact with the substrate. When the squeegee is moved along the screen surface, it pushes the paste through the openings, which covers the desired areas of the substrate. In this process there are several variables that could affect the results and the main ones are listed in Figure 3.9 (Fletcher (2016); Pan et al. (1999); Suganuma (2014)).

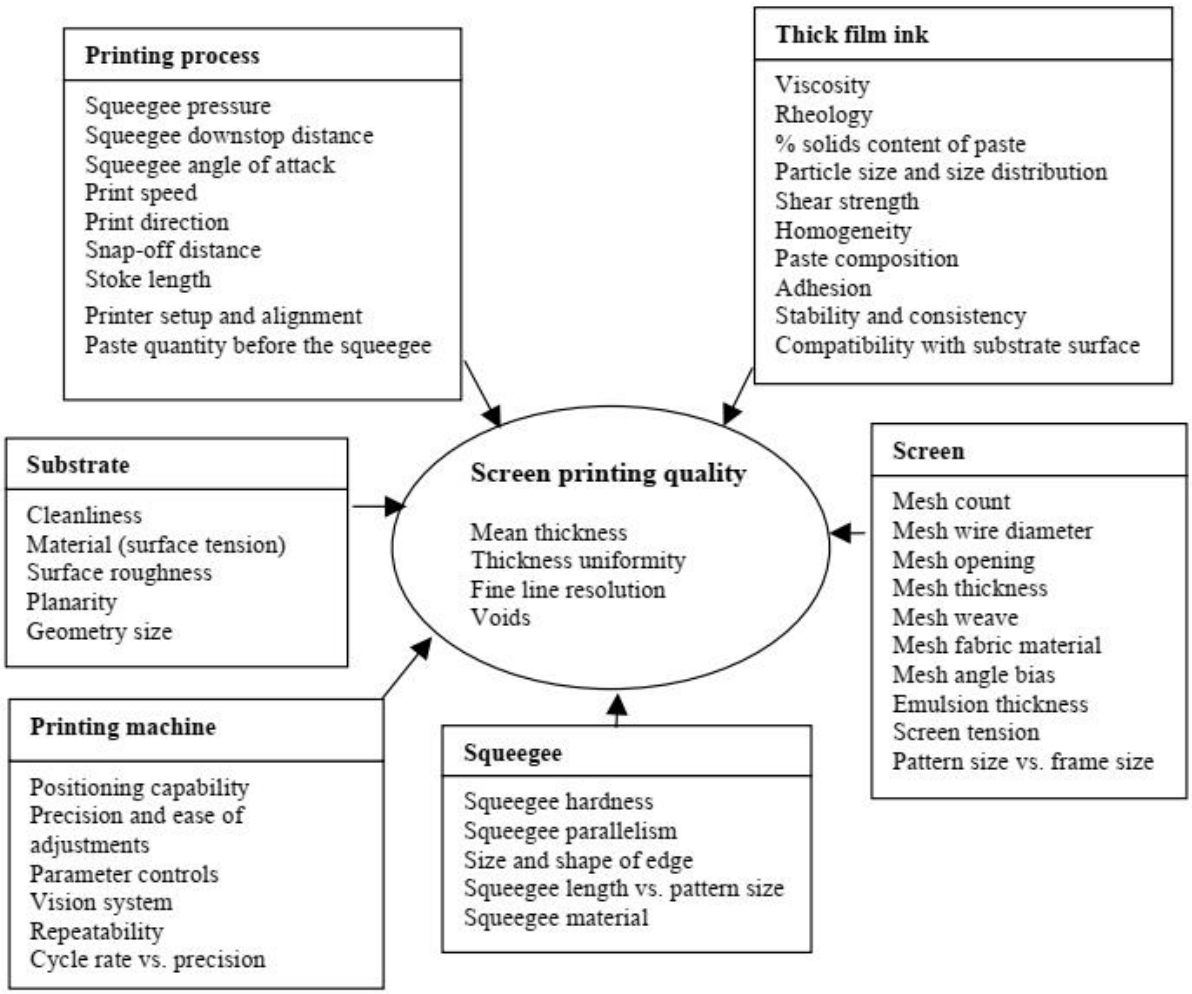

Figure 3.9 Factors that influence the screen-printing quality

The components of the screen-printing process include the printer, the substrate, the screen, the squeegee, the thick film ink, and the process parameters. Screen printing quality indexes include mean print thickness, thickness uniformity, fine line resolution, and the number of voids. The screen mesh count is a critical factor for controlling print thickness. Mesh count is the number of wires or openings (the linear distance between one wire to

the next adjacent wire) per linear inch. It is important also the mesh weave type, which includes plain weave, twilled weave, square weave, warp and weft wires, also influences print thickness. The screen mesh tension and the wire bias are two other important factors. Mesh tension is the tightness of the stretched mesh, measured in Newtons per centimeter. Proper mesh tension helps the ink release. If the tension is too high, it will be difficult to maintain proper snap-off distance. Furthermore, permanent damage can result if the yield point of the screen is exceeded. If the tension is too low, poor screen peel will result. Wire bias or mesh angle refers to the alignment angle between the mesh and the image. Biased screens with 30 degrees are recommended for fine line printing since they print more consistently. The screen mesh size is conventionally characterized by the number of wire strands per centimetre (spc), so larger spc values imply finer detail. To prevent screen blockage during printing, the maximum particle diameter should be around 15 μm. Particles above 20 μm can be removed by preliminary dry sieving. Mesh tensions are usually set around 30 N/cm, and printed film thicknesses are typically in the range 15 to 150 μm. In practice, there is a limit to layer thickness (and hence mask thickness) determined by the tendency of thick layers to crack during drying. At the other extreme, very thin layers tend to have high electrical resistance. After use, most screens can be safely cleaned with volatile esters (butyl acetate, ethyl acetate) or ketones (methyl isobutyl ketone, methyl ethyl ketone).

Mesh materials commonly used are stainless steel (type 304), monofilament nylon (polyamide), monofilament dacron (polyester), and metalized polyester. However, steel is preferred for making thick carbon electrodes because it possesses a greater open area, and thus allows more ink to be transferred for each pass of the doctor blade. Steel is also very resilient, readily resuming its original position after the passage of the doctor blade. Ink-free regions in the image are created by coating the mesh with a "mask" made of a rubbery, ink-repelling polymer, usually poly(vinyl acetate). This mask defines the shape of the image by providing a boundary for the ink. The reproducibility of the printed image depends on the mesh ability to form a gasket-like seal with the substrate when the doctor blade passes over it. The hole size and the wire diameter determine the thickness of the printed layer, while the wire spacing determines the resolution (and hence reproducibility) of the printed area. Many experiments in industry have been done and many models of the printing process have been developed since the mid-1960s (Horwood (1974)). Miller studied the relationships between the amount of paste deposited and the screening process such as the mesh size, paste rheology, line width, etc. (Miller (1968)). Austin described the effects on printing thickness of squeegee attack angle, squeegee blade characteristic, and substrate variations (Austin (1970)). Riemer presented a theory of the paste deposition process by screen printing. In his

theory, the ink roll in front of the squeegee is treated as a pump generating high hydrostatic pressure close to the squeegee edge to inject ink into the screen meshes (Riemer (1988)). Owczarek and Howland described a physical model of the screen-printing process (Owczarek and Howland (1990)).

3.4.1 Carbon black

Differently from the ink-jet printing, which requires a specific ink viscosity, the screen-printing procedure could be performed with several types of inks with various viscosities. For this reason, the ink composed of PEDOT:PSS and ethylene glycol was compared with a conductive commercial ink based on carbon black, the Electric Paint by Bare Conductive Ltd. Electric Paint is a nontoxic, water based, water soluble, electrically conductive paint that can be used in circuits as a painted resistor element, a capacitive electrode or can act as a conductor in designs that can tolerate high-resistance paths. This low-cost ink was chosen for its capability to adhere to a wide variety of substrates including paper, cardboard, wood, metal, plaster, some rubbers, plastics and many textiles. It can be easily applied using screen printing equipment. Its major benefits include low cost, solubility in water and good screen life. It is black in color and can be over-painted with any material compatible with a water-based paint.

The technical properties of this ink are listed below:

- Viscosity: Highly viscous and shear sensitive (thixotropic),
- Density: 1.16 g/ml,
- Sheet Resistance: 55 Ω/sq at 50 μm film thickness,
- Vehicle: Water-based,
- Drying Temperature: Electric Paint dry at room temperature for 5 – 15 minutes.

The drying time can be reduced by placing it under a warm lamp or other low intensity heat sources because high temperature environments could negatively affect both physical and electrical performance.

Electric Paint is a unique material that can be applied in many different ways, from a paintbrush to common printing processes like screen-printing. The best electrical performance can be reached with screen printing using a textile-type screen in order to achieve

a generous layer thickness. The developers suggest to use a 43T screen for its deposition and specify that is not compatible in any case with an ink-jet printer. The processing and handling information are summed up in Table 3.1.

Screen Printing Equipment	Manual
Screen Types	Polyester, stainless steel (43T – 90T gauge mesh)
Typical Cure Conditions	Room temperature (24°C) for 15 minutes
Typical Circuit Line Width	0.5 – 10mm (43T-mesh stainless steel screen)
Clean-up Solvent	Warm water and soap
Sheet Resistance	Approximately 32Ω/sq when using a brush or manual screen printing
Shelf Life	6 months after opening

Table 3.1 Processing and handling Carbon Black ink

When processed using manual screen-printing the expected sheet resistance is approximately 32Ω/sq. The below equation can be applied to roughly predict how surface resistance changes with the line shape:

$$Resistance = 19.77(length/width) + 12 \tag{3.1}$$

The results in term of printing deposition usually are studied with techniques able to investigate the quality of printing process by analyzing how the ink dried on the substrate. These techniques, as for instance the profilometry or the atomic force microscopy, require a smooth substrate as PEN, PET or PVC to analyze the surface after the deposition (Ping et al. (2012)). These techniques cannot be used with printed fabrics because the high irregularity of the garment surface (roughness) avoids any kind of comparison between different areas of the fabric and then it is impossible to evaluate the amount of ink deposited with these printing techniques.

As previously described for ink-jet printing, in addition to the geometrical resolution it is necessary to study the surface conductivity induced by the conductive ink. Also in this, case the amount of ink and conductive polymer deposited on the fabric surface could influence the surface conductivity. We could quantify this parameter by investigating the sheet resistance with a 4-probe measurement because with this printing technique we could treat a higher area.

3.5 Sheet resistance measurements

To characterize the textile electrodes, the sheet resistance was evaluated using an LCR meter (4284A by Agilent/HP Keysight) to perform a 4-probe resistance measure (Figure 3.10). This is an LCR meter with a frequency resolution from 20 Hz up to 1 MHz and accuracy of 0.01% which, through the four crocodile connectors, makes it possible to make measurements of resistance, capacitance, inductance, impedance, phase, conductivity, factor of dissipation, quality factor and reactance with the resolutions shown in Table 3.2.

Figure 3.10 Agilent/HP Keysight 4284A

Parameter	Range
| Z |, R, X	0.01 mΩ to 99.9999 MΩ
| Y |, G, B	0.01 nS to 99.9999 S
C	0.01 fF to 9.99999 F
L	0.01 nH to 99.9999 kH
D	0.000001 to 9.99999
Q	0.01 to 99999.9
Θ	-180.000° to 180.000°
Δ	-999.999% to 999.999%

Table 3.2 Agilent/HP Keysight 4284A parameters resolution

Each measure could be performed with two probes or four probes to analyze the response to an AC signal with a specific amplitude and frequency. This instrument was used in two different configurations to measure the skin contact impedance at different frequencies with two probes and the sheet resistance with four probes at a single frequency. In Figure 3.11, the setup used to record the sheet resistance separating the probes that inject the AC signal with the acquiring ones is presented.

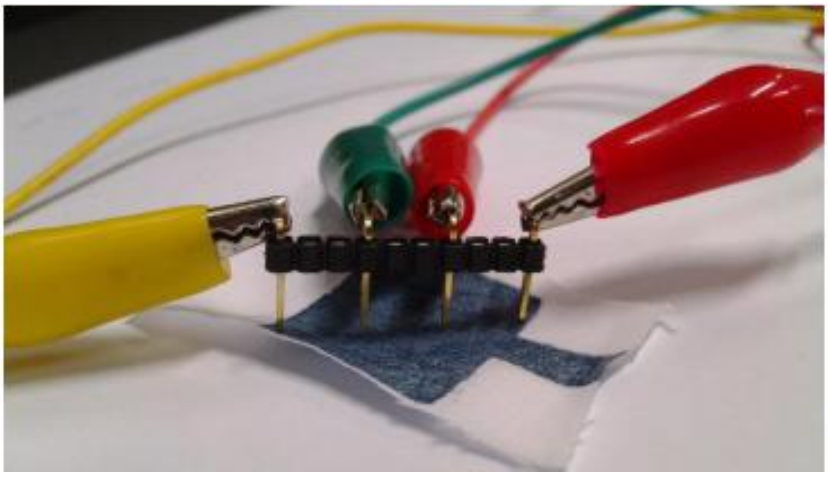

Figure 3.11 Interface between LCR meter and electrode surface for a 4-probe measurement

For the 4-probe measurement, the instrument cables were connected to a 4-pin interface with alligator clips, as shown in Figure 3.11 (Smits (1958)). With this setup, it was possible to measure the sheet resistance of fabrics treated with PEDOT:PSS, by injecting a sinusoidal signal with an amplitude of 0.5 V and a frequency of 20 Hz. The amplitude value was chosen to be lower than 0.8 V because at that voltage the electrochemical properties of PEDOT:PSS become not negligible and there is the possibility of an oxidation or a reduction of the polymer. With the 4-probes resistance measurements, the interface with four tips can largely remove the contribution of contact impedance between the probes and the conductive fabric. With a two-probe resistance measurement, in addition to the measure of the desired resistor there is the contribution of the internal resistance of the amperometer which, even if small, is not negligible. In Figure 3.12, on the leftm it is represented the scheme of the two-probe measurement, where R is the resistance that should be evaluated.

In Figure 3.12, on the right, it is represented the scheme of a measurement with four probes, whose contacts A and B apply a potential difference while the contacts A' and B' detect the voltage without being affected by the contact impedance. The contact impedance

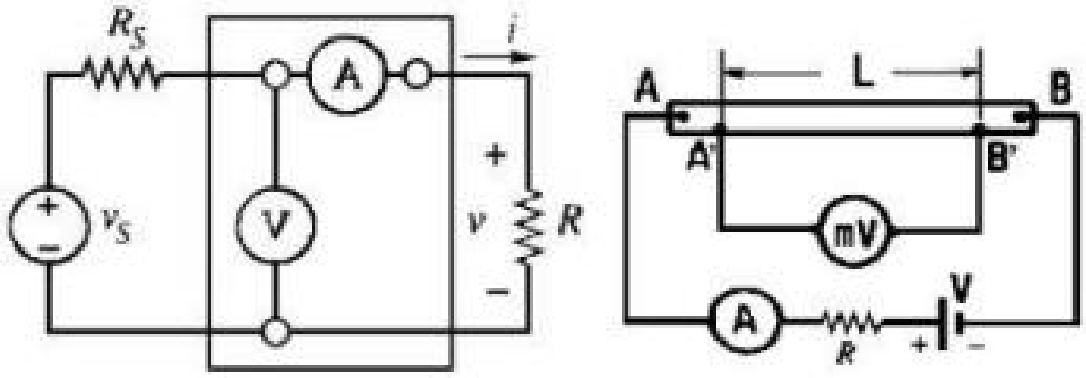

Figure 3.12 2-probe and 4-probe measurement electrical scheme

of A' and B' is smaller than the resistance of the voltmeter and therefore can be neglected, obtaining only the resistance related to the conductivity of the material to be measured.

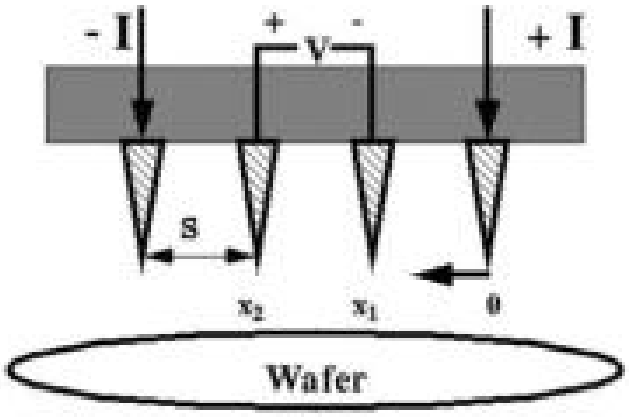

Figure 3.13 Schematic representation of a measurement interface

Taking into account the scheme in Figure 3.13, the resistivity can be computed in relation to the wafer thickness t. For thicknesses much larger than the pitch between the probes, there will be a current spreading circularly around them and then the system can compute the variation of the resistance as resistivity for the variation of the path in the circular area A. To compute the resistance due to a single probe in a path between x_1 and x_2 is necessary an integration between the two points, considering that in a system with the first external probe used as zero, to reach the third probe the integration interval goes from S to 2S

$$R = \int_{x1}^{x2} \frac{\rho dx}{2\pi x^2} = \frac{\rho}{2\pi}\left(\frac{-1}{x}\right)\Bigg|_{s}^{2s} = \frac{1}{2s}\frac{\rho}{2\pi}$$

Through the 4-probe measurement, it is possible to get a resistance value that is equivalent to the applied voltage in relation to the double of the current, therefore from the formula of the resistance it is possible to calculate the resistivity as the double of the experimental resistance multiplied by the product between the probes distance and π:

$$\rho = 2\pi s \left(\frac{V}{I}\right)$$

In case the thickness was much smaller than the distance between the probes, ($t << s$) then there would be a minimal surface current distribution limited by the thickness of the conductive material. In this case the area of the circular current flow pattern around the probes will change in relation to X and the thickness and it will be equivalent to twice π multiplied by the product between the probes distance and the thickness. Integrating the resistance, the result is the resistance value related to the resistivity, the natural logarithm of 2, the thickness of the substrate and π

$$R = \int_{x1}^{x2} \frac{\rho dx}{2\pi xt} = \frac{\rho}{2\pi t} (\ln x) \Big|_{s}^{2s} = \frac{\rho}{2\pi t} \ln 2$$

As in the previous case, resistivity can be obtained with the following formula:

$$\rho = \frac{\pi t}{\ln 2} \left(\frac{V}{I}\right) \approx 4.53t \left(\frac{V}{I}\right)$$

From this formula, it is evident that in the case of a thickness much smaller than the distance between the probes, the resistivity is completely independent from the second parameter, s.

Another aspect to take in account is the resistance of the ink to the stress that the fabric could receive during the everyday use. The principal two actions that could reduce the conductivity of the deposited film are the washing procedures and the physical stress induces by the stretch or the folding of the fabric.

The first one has been tested evaluating the sheet resistance after a series of washing cycles. The protocol used to reproduce the washing process is the following. Washing was simulated following the ISO 105-C10:2006 standard, which was designed to establish the effect of washing cycles on the ink fastness on textile substrates. To recreate mild washing conditions, as per standard requirements, the printed textiles are placed in an aqueous solution containing 5% of a low-duty laundry detergent for clothes and gently stirred at 40°C for 20 min. At the end of the process, the soap is washed away with clean water and, after

removing the excess water by pressing the wet fabrics with paper towels, the fabrics are dried in an oven at 70 °C for 15 min (Standards (2010)).

Stretching was simulated by recreating the conditions that could be experienced by the electrodes when they are embedded in a stretchable smart garment. To achieve this aim, the electrodes, which were screen-printed on the stretchable substrate, were stretched to 100% of their length three times.

3.6 Screen-printed textile electrodes

The proposed textile ECG electrodes consist of a sheet of cotton fabric with conductive properties. As mentioned earlier, this fabric has been treated by screen-printing with an ink based on PEDOT:PSS. The chosen HERAUS CLEVIOUS PH1000 PEDOT:PSS solution is composed of 1.0 wt% - 1.3 wt% of polymer in a water suspension, with a nominal viscosity ranging from 15 - 50 cPs. According to several studies, the conductivity of a polymer increases dramatically upon the addition of organic solvents such as dimethyl sulfoxide (DMSO) and ethylene glycol (Kellomäki et al. (2012)). The ink used for screen printing is composed of two components of PEDOT:PSS, one component being ethylene glycol and the other being 3-glycidoxypropyltrimethoxysilane (Elschner et al. (2010)). To improve the geometrical resolution of the screen printing process, the viscosity of the ink was increased by reducing the water:polymer ratio (Kim et al. (2017); Li et al. (2012); Taleat et al. (2014)). This was accomplished by drying the solution in an oven at 90°C until its density became similar to that of acrylic inks. To deposit the ink on a specific area, it was transferred onto the textile substrate through a polyester screen with 43T mesh delimited by a wax stencil using a rubber squeegee. Immediately after the deposition, the electrodes were dried in the oven at 70°C. This process needs to be executed in a timely manner since the ethylene glycol would start spreading through the fabric, thereby affecting the printing precision. This is the primary obstacle for drying the printed electrodes at room temperature. Several geometries have been tested taking in account the best way to connect the electrodes to the instrumentation and to obtain a stable and high-quality signal. The design was modified several times, by customizing the stencil mask to recreate the desired geometry. The changes applied to the electrodes where aimed at improving the connection between the electrodes and the instrumentation, as demonstrated in Figure 3.14. In such figure it is shown the electrodes design evolution passing through the addition of a channel to connect the instrument to acquire the signal. For the same reason, a snap button was also applied to connect the cable

directly to the electrode. In the first case, the connection was performed via alligator clips whereas in the second one the snap cable was connected with the electrode by using an Ag/AgCl snap button clipped to the fabric.

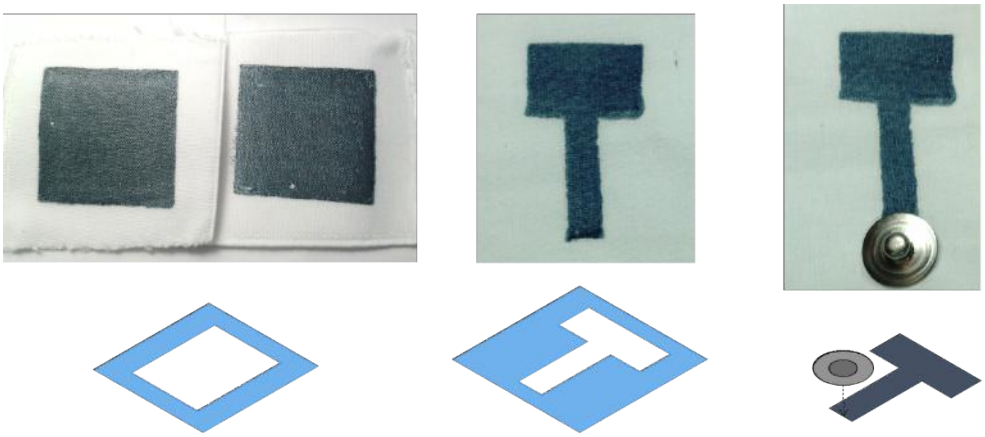

Figure 3.14 Geometrical evolution of textile screen-printed electrodes

Several preliminary tests were performed with the last configuration, by applying the electrodes on the skin with a medical tape. After this preliminary validation, the deposition technique was further improved by using a specific mesh with the required geometry. We were then able to produce two prototypes of the screen-printed textile electrodes, the first one for the ECG signals acquisition and the second one to detect the sEMG as the one shown in Figure 3.15.

To measure the ECG signal, the prototype described above was developed on a woven cotton as textile substrate for the screen-printing deposition because of its low cost, revealing how the proposed technique is less aggressive than the previous ones on the fabric (Pani et al. (2016b)). The active area of the electrode was a 20 mm $\times$ 20 mm square, so that they could be comparable in size with commercial disposable surface electrodes as the CDES000024 by Spes Medica Srl. This area has a square shape, with an additional conductive path (1.5 x 0.5 cm) employed to apply a connector and pick up the signal, Figure 3.16. In order to improve the skin-electrode contact, a thin foam layer was sewed on the back of this area. Such a soft layer of foam has positive impact on the mechanical contact of the fabric on the skin (Paul et al. (2014a)) and helps to preserve wet the electrodes (Löfhede et al. (2012)). A thin strip of polymer was used to bring the signal out from the active area to a point where it could be acquired by the measurement instrumentation. To obtain a stable electric contact, a metallic snap button was crimped on the fabric at the end of the strip. Neither the button nor the strip

Figure 3.15 The screen-printed PEDOT:PSS ECG electrode

was conceived to be in contact with the skin, to avoid altering the electrical characteristics of the electrode interface with the skin so, when the electrode was fixed to the skin by adhesive tape, this part was flipped back.

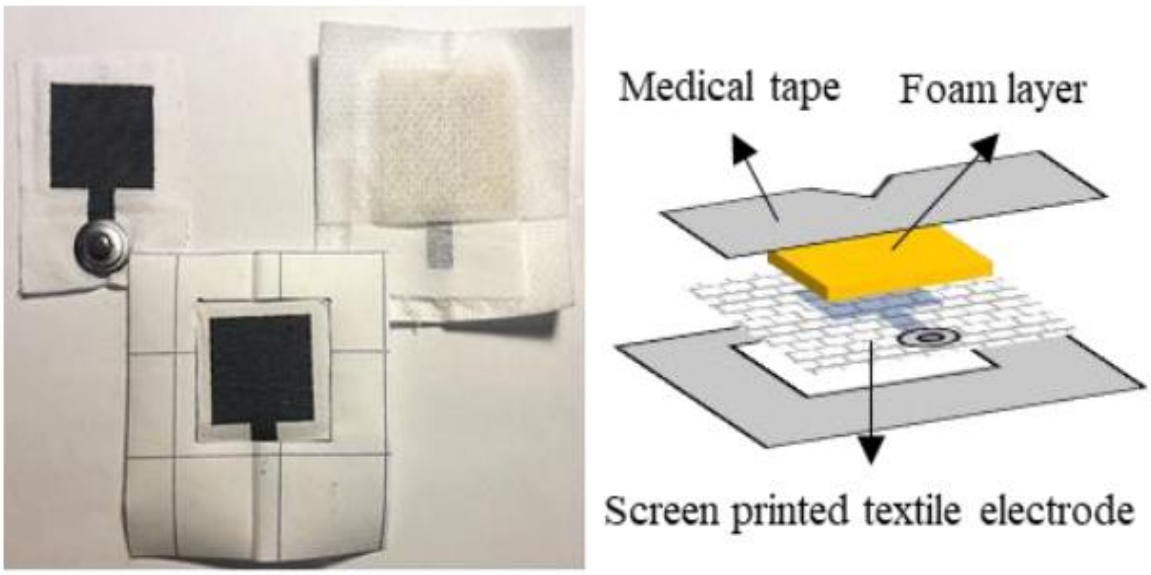

Figure 3.16 Screen-printed textile electrode fabrication. On the left, different views of the prototypical electrodes; on the right, their expanded parts view.

3.7 Prototypical screen-printed textile EMG electrodes

To detect the sEMG signals, different textile electrodes were developed with a standard screen-printing procedure on fabrics, with a conductive ink composed of HERAUS CLEVIOUS PH1000 PEDOT:PSS, Ethylene Glycol and GOPS, as described in previous works related to ECG signals acquisition (Achilli et al. (2018)). After the deposition on the textile substrate, the ink was dried by placing the electrodes in oven for 15 minutes at 70°C. For the deposition, a 43T mesh with a mask containing two different geometries was used. The first one (ø24) is the union of a round shape with 24 mm of diameter and a rectangular path (5 mm x 15 mm), whereas the second one (ø10) is composed of the same channel and a 10 mm diameter round shape, Figure 3.17. The channel was added to the electrodes as a mean to acquire the signal through a crocodile connection clipped directly onto the fabric. The two different shapes were established to fairly compare the performance with standard Ag/AgCl gelled electrodes. The electrodes used for this comparison were the CDES000024 by Spes Medica Srl with a 24 mm diameter and their 10 mm gelled snap button. To obtain better performances as sEMG electrodes, a few features were added to textile electrodes. A 2-mm-thick layer of foam placed on the fabric on the opposite side of the active area was added to maintain both a homogeneous and continuous pressure, and a wet skin condition during the acquisition (when a liquid electrolyte is added, as performed in the experimental sessions). In fact, the foam absorbs the liquid, preserving a homogeneous hydration level throughout the measurement. The foam was coupled to the fabric by using the same medical tape that was used to apply the electrodes on the skin. This tape was shaped and placed on the fabric, with the precaution of isolating the channel and the snap button from the skin. A spot was also provided to apply a few drops of saline solution between the electrode and the skin surface. In addition, textile electrodes were tested also with a solid hydrogel to evaluate the similarities with standard EMG gelled electrodes.

3.8 Prototypical screen-printed smart shirt

There are two possible approaches for developing a sensorized garment able to detect physiological signals. The first one entails the deposition of the conductive ink directly on the fabric composing the t-shirt, the second one the embedding of finished free-standing textile electrodes in the garment. To obtain signals with a good quality, we require in both

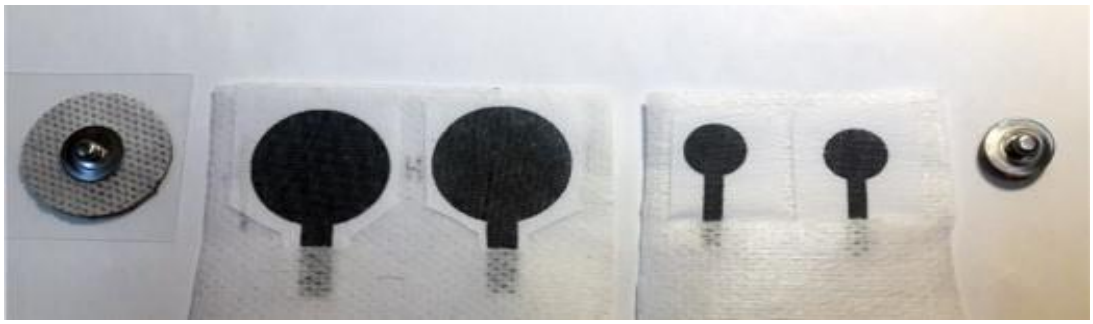

Figure 3.17 EMG screen-printed textile electrodes compare to disposable gelled electrodes (from left to right: 24 mm gelled Ag/AgCl electrodes, Ø24 and Ø 10 textile electrode pairs, and 10 mm reduced gelled Ag/AgCl electrodes)

cases a t-shirt with a high adherence to the skin to guarantee a continuous contact of the electrodes with the skin and, at the same time, a low contact impedance. To avoid the problems associated to direct printing on elastics surfaces and avoid the non-negligible degradation of the textile electrodes after the wearing procedure, where the expansion could crack the conductive electrode surface, it was decided to screen-print the textile electrodes onto a non-stretchable cotton fabric and to provide the integration by applying them on the t-shirt (Figure 3.18). The textile electrodes were placed inside the shirt with an adhesive patch in the positions defined by the required acquisition protocol, as detailed hereafter. The connection between the fabric and the measuring instrumentation was simplified clipping the electrode with an Ag/AgCl snap button placed in the external part of the t-shirt to avoid the signal acquisition from the metallic button in contact with the skin.

In the prototypical smart t-shirt, two textile electrodes were embedded in order to derive a chest-band level version of the frontal lead I for the ECG acquisition. Four electrodes were positioned to detect the sEMG signal during specific voluntary exercises. These electrodes were placed following a precise set up sketched in Figure 3.19, according to (Criswell Eleanor (2011)), symmetrically with respect to the sagittal plane in order to recorder the activities of the muscles of interest. In particular they were placed on the external oblique abdominal muscles, referring to the anatomical atlas, being important muscles for the stabilization of the vertebral column, enough on the surface to be easily detectable (Criswell Eleanor (2011)).

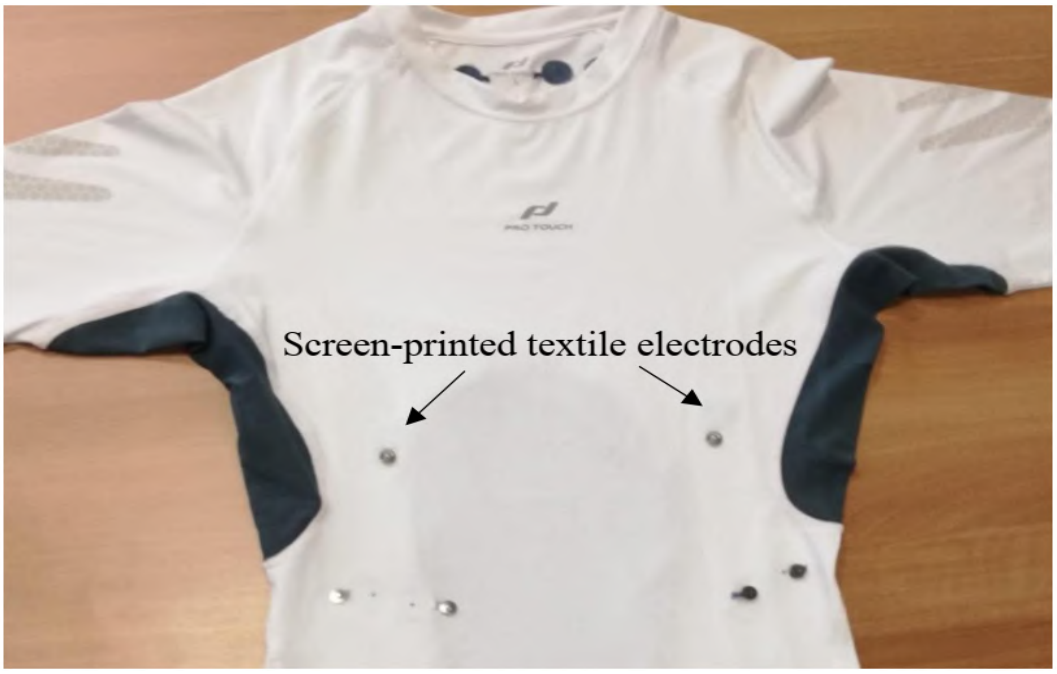

Figure 3.18 Smart shirt with embedded screen-printed textile electrodes for the detection of ECG and EMG signals

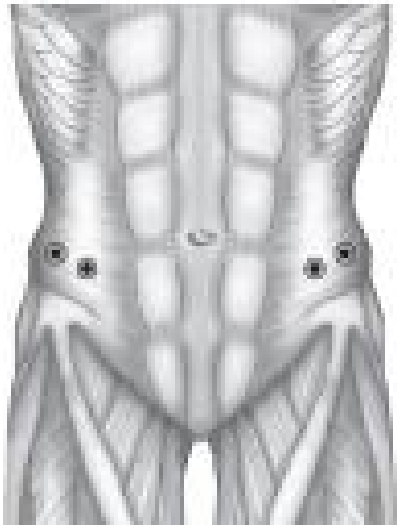

Figure 3.19 Electrodes position during EMG acquisition with smart shirt

Chapter 4

Textile electrodes characterization

4.1 ECG electrodes

The prototype of the screen-printed textile electrode for the acquisition of the ECG signal was tested in two main conditions, with benchtop measurement and with human subjects. With the first analysis is possible to recreate a controlled environment with a high reproducibility to fairly compare textile electrodes with the standard benchmarks. Conversely, the acquisition of the ECG on human subjects is strictly dependent on the physiological variability between subjects but actually represent the most important validation testbed to compare the performance of the electrodes as ECG sensors.

To completely assess the electrodes performance, we studied how the presence of an electrolyte could have an impact on the effectiveness of the electrodes. For this reason, we studied first the performance of dry textile electrodes and then we added a saline solution or a layer of solid hydrogel. The addition of an electrolyte could introduce few advantages as the improvement of the adherence of the fabric to the skin but, most important, it could play a crucial role in reducing the skin-contact impedance. Nevertheless, it represents the less important approach to this aim, since textile electrodes are conceived for unobtrusive monitoring of electrophysiological signals and the presence of adhesive layers goes in the opposite direction in terms of comfort.

4.1.1 Benchtop Measurements

Standard AAMSI for Xtratek

Although there is a lack of standards for textile electrodes, it is possible to assess their performance by observing the limits reported in the ANSI/AAMI EC12:2000/(R)2010 for disposable gelled ECG electrodes (ANSI/AAMi (2000)). In this standard a series of limit values is reported, summed up in Table 4.1, in terms of DC offset, AC impedance, noise, stimulated defibrillation recovery and bias.

Requirement description	**Test conditions**	**Units**	**Value (Min/Max)**
Impedance at 10 Hz for individual electrode pair.	Pairs connected gel-to-gel, impressed current not exceeding 100 μA	kΩ	2 (max)
Offset voltage	Pair connected gel-to-gel, after 1 min. stabilization	mV	100 (max)
Combined offset instability and internal noise	Pair connected gel-to-gel, after 1 min. stabilization period, in the passband of 0.15 to 100 Hz, for 5 min	μV	150 (max)
Defibrillation overload recovery Rate of change of polarization potential After test, 10 Hz electrode impedance	Pair connected gel-to-gel, 5 seconds after each of four discharges of 200 volts During 30 sec. interval following polarization potential measurement	mV mV/sec kΩ	100 (max) 1 (max) 3 (max)
DC voltage offset	Pair connected gel-to-gel, continuous 200 nA DC current applied over clinical use period (period > 8 hours)	mV	100 (max)

Table 4.1 Summary of the performance requirements of the standard ANSI/AAMI EC12:2000/(R)2010 for disposable ECG electrodes.

NOTE—All tests shall be performed at 23° C ± 5° C, and 40% ± 10% relative humidity.

AC impedance

The impedance of a pair of electrodes connected gel-to-gel can be determined by applying a 10 Hz sinusoidal current with known amplitude and observing the amplitude of the resulting

voltage across the electrodes. The magnitude of the impedance is the ratio of the amplitude of the voltage to that of the current. An adequate current generator can be assembled utilizing a sinusoidal signal (voltage) generator with a 1 (MΩ) (or greater) resistor in series with the electrode pair. The level of the impressed current should not exceed 100 μA p-p.

DC offset voltage

The DC offset voltage shall be measured by connecting two electrodes gel-to-gel to form a circuit with a DC voltmeter having a minimum input impedance of 10 MΩ and a resolution of 1 mV or better. The measuring instrument shall apply less than 10 nA of bias current to the electrodes under test. The measurement shall be made after a 1-minute stabilization period but before 1.5 min have elapsed.

Combined offset instability and internal noise

After a 1-minute stabilization period, the output voltage of the test circuit shown in Figure 4.1 shall not exceed 150 μV p-p over 5 min. Output voltage shall be measured with an instrument having a frequency response range of 0.01 to 1,000 Hz and a minimum input impedance of 10 MΩ. Alternatively, an oscilloscope with 1 MΩ input impedance may replace the 1 MΩ resistor shown in Figure 4.1. Component tolerance shall be ±10% and capacitors shall be non-polar.

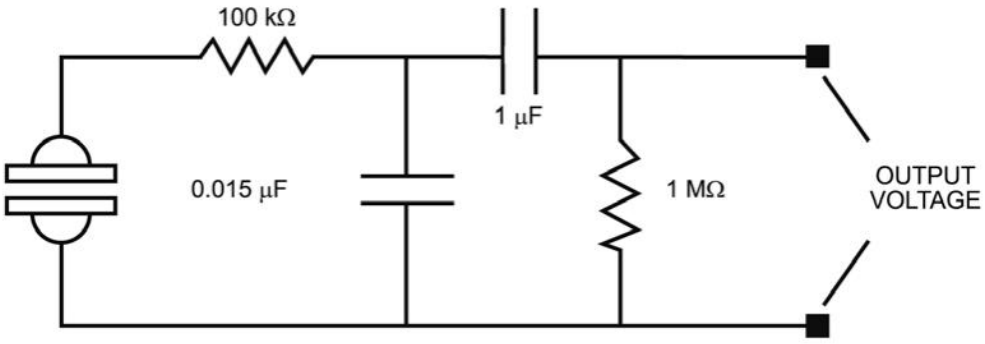

Figure 4.1 Test circuit for offset instability/internal noise determination

Defibrillation overload recovery

This test simulates the electrode response to an electrical defibrillation and describes its voltage reduction that permit to an ECG trace to return at its original state and shall be conducted as follows:

- a) A pair of electrodes shall be connected gel-to-gel and joined to the test circuit schematized in Figure 4.2 with switch SW1 closed and SW2 and SW3 open.

- b) At least 10 seconds must be allowed for the capacitor to fully charge to 200 V; switch SW1 is then opened.
- c) The capacitor is immediately discharged through the electrode pair by holding switch SW2 closed for a time long enough to discharge the capacitor to less than 2 V (this time shall be no longer than 2 seconds).
- d) Switch SW2 is opened and SW3 is closed immediately, thereby connecting the electrode pair to the offset measurement system.
- e) The electrode offset is recorded to the nearest 1 mV 5 seconds after the closure of switch SW3 and every 10 seconds thereafter for the next 30 seconds. The overload and measurement are repeated three times.
- f) The test sequence above is repeated for *n* electrode pairs. For all electrode pairs tested, the 5-second offset voltage after each of the four discharges of the capacitor shall not exceed 100 mV, and any difference in adjacent 10-seconds values (after the initial 5 seconds period) shall not exceed ±11 mV (±1 mV/sec).

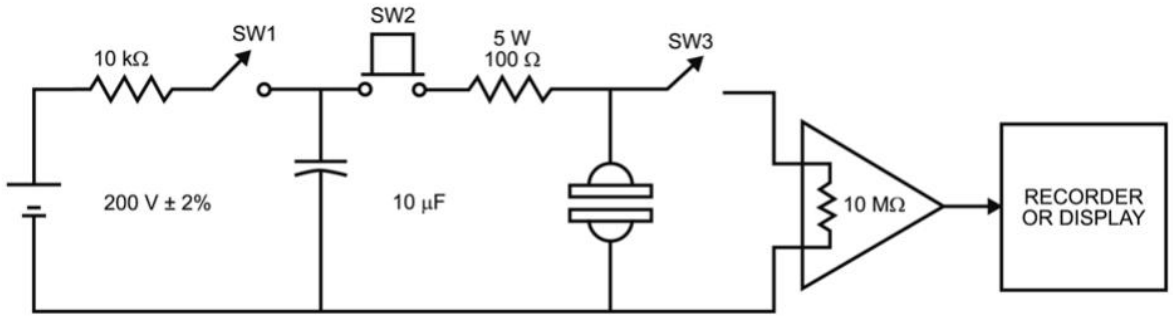

Figure 4.2 Defibrillation overload test circuit (all capacitor and resistor values have a tolerance of ±10%)

Bias current tolerance

A 200 nA DC current shall be applied to a pair of electrodes connected gel-to-gel, utilizing a current source consisting of at least a 2 V voltage source connected in series with an appropriate current-setting resistor. The potential across the pair of electrodes should be monitored with a DC voltmeter having a minimum input impedance of 10 MΩ, a resolution of 5 mV or better, and an input bias current of less than 10 nA. The differential voltage across the electrodes should be measured at least once per hour over the period of observation. The

initial offset voltage should be measured within 1 to 5 minutes after joining the electrodes and before the bias current is applied. The offset voltage change caused by the applied bias current is then measured relative to the initial offset voltage.

4.1.2 Xtratek ET-65A ECG electrode tester

To perform these measurements on ECG electrodes, with the specific requirements described above, the Xtratek ET-65A ECG electrode tester, produced by Xtratek, Lenexa, Kansas, USA, was adopted, by courtesy of Spes Medica Srl (Figure 4.3) (Hoof (2013).

Figure 4.3 Xtratek ET-65A ECG electrode tester

The Xtratek ET-65A electrode tester is a self-contained, portable instrument designed for electrical performance testing of gelled disposable ECG electrodes. The ET-65A performs all five of the tests described in the standard for gelled electrodes analyzed above. These tests require a pair of electrodes attached so that their gel layers are connected together. This instrument is widely used in the process of patenting as demonstrated from the following patents: EP0542294A1, EP3237056A1, US20100308282A1 (Copp-howland (2010); Martins (2017); Uy (1995)). According to the standard ANSI/AAMI EC12:2000 for disposable ECG electrodes (ANSI/AAMi (2000)), the XTRATEK ET-65A electrode tester must perform the five tests described above in the following measurement conditions:

AC Impedance

The AC impedance can be determined from the average value recorded through the electrode pair at either 5, 10, or 20 Hz with a level of impressed current not exceeding 100 μA peak-to-peak. For our test was imposed a 10 Hz frequency and recorded the average value over 3 measurements with an imposed limitation at 2 kΩ.

DC Offset Voltage

The DC offset determines the polarization potential (voltage) generated by an electrode pair connected gel-to-gel and was performed repeatedly every 20 seconds for 5 times and considered the average value.

Combined Offset Instability and Internal Noise

The instrument determines the peak voltage generated by the electrode pair in the pass band of 0.15 Hz to 100 Hz during a 5 minutes test period. The internal noise value was recorded every 30 seconds for 5 minutes and in the benchtop characterization it was considered as noise the highest value reached over this time.

Defibrillation Overload Recovery

Determines the value of polarization potential across the electrode pair and rate of change of the recovery slope after each simulated defibrillation. The recovery was tested 4 times and for any repetition the DC offset and the recovery slope were recorded.

Bias Current Tolerance

The instrument determines the DC offset voltage change across a pair of electrodes subjected to a continuous 200 nA DC current and reports the DC Offset value bias every 8 hours to study the bias and the related polarization.

The instrument accuracy is reported hereafter:

- DC millivolts: ± 0.8 mV (± .5% of full scale),
- AC impedance: ± 0.8 ohms (± .5% of full scale),
- Timing operations: ± 1%.

The standard refers to adhesive gelled electrodes that are tested in couples by putting their active surfaces in contact. Since such electrodes present either solid or liquid hydrogel, and an adhesive support, the measurements are characterized by the perfect contact between the two electrodes under test. To achieve comparable results with non-gelled and non-adhesive electrodes, such as those proposed in this study, the physical coupling between the two electrodes was ensured by pressing them one against the other with a reciprocal force of 9 N. This force was removed while testing the textile electrodes with the adhesive solid hydrogel. The sample size chosen for these tests consisted of five pairs of electrodes.

4.1.3 Benchtop impedance measurement by LCR meter

By using the Xtratek ET-65A, the impedance can be measured only at the specific frequency of 10 Hz, since this value is imposed by the standard (ANSI/AAMi (2000)). Because of this limitation, to investigate how the PEDOT:PSS electrodes work at different frequencies, the same LCR meter 4284A by Agilent/HP Keysight used for the evaluation of the sheet resistance was adopted. The measurements were performed coupling the active surfaces of two electrodes at a time. As said before, this device allows acquiring the impedance in a frequency range from 20 Hz to 1 MHz. The characteristics of the ECG signal must be considered while defining the upper limit of the frequency range for this analysis. The QRS complex is the sharpest waveform in the signal; although low-amplitude signal components as high as 500 Hz have been detected and studied (Mason et al. (2007)), the level of the noise could overcome the signal of interest at such frequencies. At the same time, the QRS complex of infants can contain significant components up to 250 Hz (Rijnbeek et al. (2001)). This is why the analysis was carried out applying an AC sinusoidal current, with a 0.1 mA amplitude, at different frequencies from 20 Hz to 300 Hz (10 frequency points: 20, 25, 30, 40, 60, 80, 100, 150, 250 and 300). Remarkably, this benchtop impedance measurement does not depend on the skin condition; hence, the variability can only be ascribed to the electrode characteristics.

Impedance measurement

Before any physiological signal acquired in this work was recorded, the coupling between the electrodes and the skin measuring the skin contact impedance was analyzed. This measurement was performed using the electrodes in the same configuration adopted for

the ECG (or EMG) recording, connected with the LCR meter adopted for the impedance benchtop measurements. This parameter was tested at the same frequencies of the previous analysis, but applying an AC sinusoidal signal with a 500 mV amplitude, keeping the injected sinusoidal current below 1 μA. It is worth recalling that this type of measurement on the human skin, differently from the benchtop impedance, is heavily affected by the skin conditions; hence, the results should be carefully considered and cannot be generalized. To estimate the skin-electrode impedance related to a single electrode, we divided by two the modulus of the measured impedance, which is actually the series of three impedances, i.e. the skin contact impedance of the first electrode, the negligible impedance contribution of the body, and the skin contact impedance of the second electrode (Pani et al. (2016b)), Figure 4.4. Obviously, such an approach only leads to a rough average estimate of the skin contact impedance, which would be justified by the assumption that the skin condition under the two electrodes is similar. Even though this hypothesis is questionable when the skin contact impedance is high, such as for dry electrodes, it is good enough when some electrolytes are added, because of the better coupling with the skin. In any case, due to the variability of the skin condition between subjects, and from time to time for the same subject (Beckmann et al. (2010), such an estimate provides acceptable information for the purposes of this work. In the same configuration two Ag/AgCl electrodes have been used to measure the skin contact impedance on the same points, obtaining a reference complex impedance and this leads to a good estimation of the skin-textile electrode contact impedance (Pani et al. (2016b)).

4.2 ECG acquisition for non-clinical assessment

Beyond the bench tests with the Xtratek ET-65A ECG electrode tester and the impedance measurements, screen printed textile electrodes were also tested in real ECG recording conditions. This study was performed according to the principles outlined in the Declaration of Helsinki of 1975, as revised in 2000. Four healthy voluntary subjects belonging to the research group (aged 33 ± 6 years, BMI 24 ± 2 kg/m2) were enrolled, and their informed consent for the acquisition protocol was obtained. During the measurements, the subjects were comfortably seated in a room with a constant temperature of about 23°C. A 1-min delay between electrode positioning and impedance measurement was adopted to allow the stabilization of the skin– electrode interface. For evaluating the relationship between the skin contact impedance and the signal quality, the different electrolytes introduced before were added to textile electrodes.

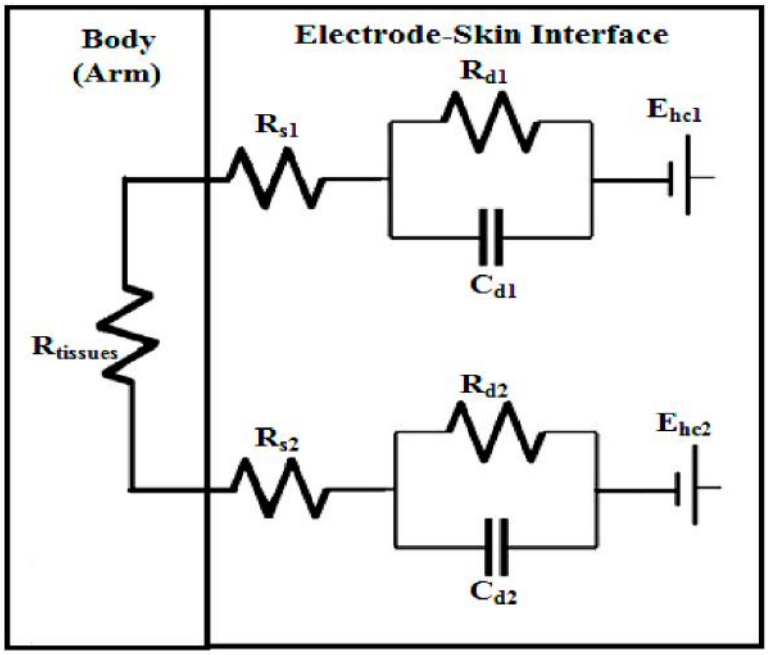

Figure 4.4 The simplified schematic diagram for the electrodes system used in the study.

Lead I of the ECG was recorded according to the Mason-Likar modification (Mason and Likar (1966)) of the standard 12-leads system (Malmivuo and Plonsey (2012)). Such an approach, typically adopted for ECG stress tests, allows reducing the electromyographic interference compared to the standard positioning. The signal ground electrode was also placed according to the Mason-Likar scheme, thus in a neutral position with respect to the recording site. Since this electrode is not directly involved in the bipolar lead measurement, a disposable gelled Ag/AgCl off-the-shelf electrode (CDES000024 by Spes Medica Srl) was used. To compare the performance of the screen-printed textile electrodes and that of traditional, disposable, gelled Ag/AgCl electrodes, the same placement was adopted for both. For this purpose, the measurement with the proposed textile electrodes was first performed, either under dry conditions or with different electrolytes. Then, the electrodes were replaced with the disposable Ag/AgCl electrodes for a comparative recording. As an alternative to such an asynchronous recording, two couples of electrodes (textile and Ag/AgCl) could also be applied for a synchronous recording (Marozas et al. (2011). However, a different signal amplitude can be experienced on the two parallel leads only because of the slight difference in the heart vector projection (Pani et al. (2016a). As the ECG signal will be analyzed in this study, including its amplitude features, the asynchronous approach was preferred.

The ECG signal was recorded using a 32-channel Porti7 system by TMSI shown in Figure 4.5. The Porti7 is a 32-channel ambulatory and stationary system for physiological research. it comes with unipolar electrophysiological inputs (ExG), bipolar electrophysiological inputs (BIP) and auxiliary inputs (AUX) for measuring EEG, ECG, EMG, but also movement, position, respiration, etc. The Porti7 includes TMSi's proprietary TAS2 (True Active Signal Shielding) technology for clean signals and data completely free of power-line interference and cable movement artifacts. It does not include hardware filters (other than anti-aliasing) so the raw data is always available and quick recovery ensured. The ExG inputs are configured as a reference amplifier: all channels are amplified against the average of all connected inputs. The BIP inputs are used to measure two physiological signals differentially to each other. Using these ExG and BIP channels, signals like EEG, EMG, ECG, EOG, EGG etc. can be measured.

A single bipolar channel was used to perform the ECG lead I measurement, and a passive ground lead was connected to the reference electrode placed on the subject. The device features a high-resolution analogue-to-digital converter (22 bits) without any analogue high-pass filtering stage. This method compensates for the large converter range for the baseline drift of the signal. The resolution on the bipolar channels is 71.5 nV, and the noise level is $<1\ \mu$V at the lowest sampling rate. The sampling frequency for the ECG signals was set to 2048 Hz. The input impedance of the recording systems is in the order of 1 TΩ, which is high enough to consider the instrument to be sufficiently insensitive to the skin–electrode impedance level. The polygraph can be connected with the PC via bidirectional optical fiber with the possibility of alternative connection via Bluetooth and this allows a real time saving of acquisitions in .poly5 file format through the TMSi PolyBench software, which also allows the setup of the measurement configuration by deciding the sampling frequency. With this software is possible to create a profile for any recorded subject to have an easy view of the signals and, during the acquisition it is also possible to apply filters at a graphical level for viewing in real time filtered signals without changing in any way the saved signals. In this work the signal was recorded and visualized in real time on TMSi PolyBench, and the raw digital data were exported into Matlab for all the subsequent signal analyses.

4.2.1 Morphological ECG features

A clinical evaluation of the ECG signal could be performed with simple measurements of the intra-beat timings and amplitudes (Clifford et al. (2006)). A common way to achieve

Figure 4.5 32-channel TMSI Porti7 with ExG (left) and BIP (right) cables

this goal is the averaging over several beats to either reduce noise or average out short-term beat-to-beat interval-related changes. The complex heart rate-related changes in the ECG morphology (such as QT hysteresis) can indicate the presence of problems. However, an expert clinician can extract enough diagnostic information to make a useful assessment of cardiac abnormality from just a few simple measurements.

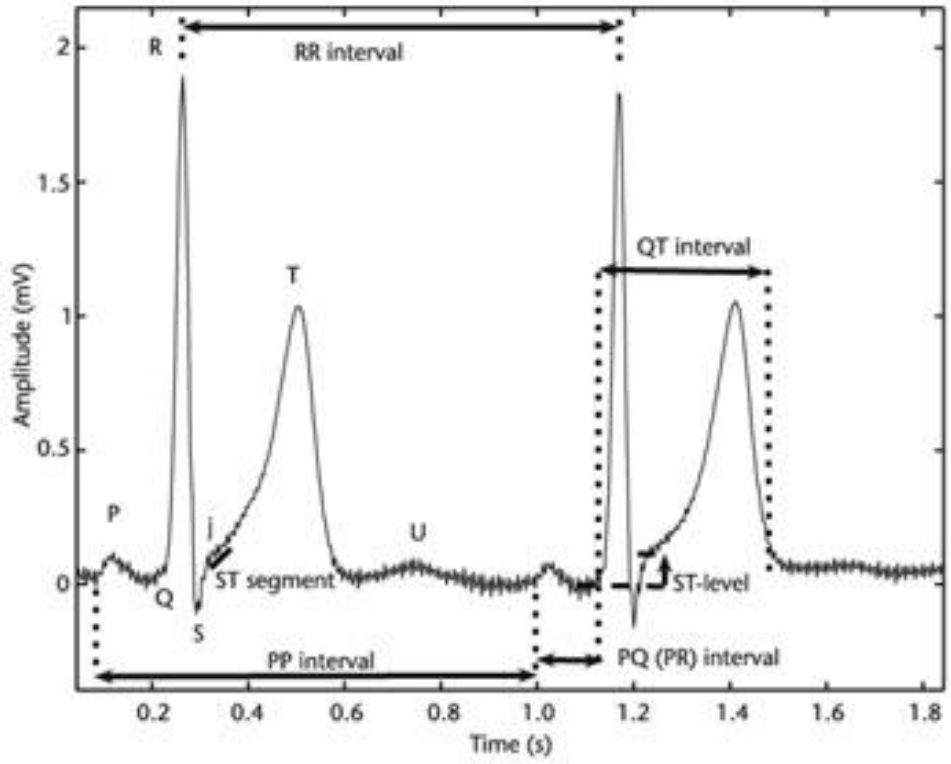

Figure 4.6 Standard fiducial points in the ECG (P, Q, R, S, T, and U) together with clinical features

Figure 4.6 shows the most common clinical features, and Table 4.2 illustrates typical normal values for these standard clinical ECG features in healthy adult males in sinus rhythm, together with their upper and lower limits of normality. Note that these figures are given for a particular heart rate. It should also be noted that the heart rate is calculated as the number of P-QRS-T complexes per minute, but is often calculated over shorter segments of 15 and sometimes 30 seconds. In terms of modeling, we can think of this heart rate as our operating point around which the local inter-beat interval rises and falls. Of course, we can calculate the heart rate over any scale, up to a single beat. In the latter case, the heart rate is termed the instantaneous (or beat-to-beat) heart rate, $HRi = 60 / RR_n$,of the n_{th} beat. Each consecutive beat-to-beat, or RR, interval will be of a different length (unless the patient is paced), and a correlated change in ECG morphology is seen on a beat-to-beat basis.

Feature	***Normal Value***	***Normal Limit***
P width	110 ms	20 ms
PQ/PR interval	160 ms	40 ms
QRS width	100 ms	20 ms
QTc interval	400 ms	40 ms
P amplitude	0.15 mV	0.05 mV
QRS height	1.5 mV	0.5 mV
ST level	0 mV	0.1 mV
T amplitude	0.3 mV	0.2 mV

Table 4.2 Typical Lead II ECG Features and Their Normal Values in Sinus Rhythm at a Heart Rate of 60 bpm for a Healthy Male Adult

These values could be changed by several parameters as heart rate, respiration patterns, drugs, gender, diseases, and ANS activity. QTc is defined as αQT where α is equal to $\sqrt{RR^{-1}}$. About 95% of normal healthy adult have a QTc between 360 ms and 440 ms. Female durations tend to be approximately 1% to 5% shorter except for the QT/QTc, which tends to be approximately 3% to 6% longer than for males. These intervals tend to elongate with age, at a rate of approximately 10% per decade for healthy adults. Often, the RR interval will oscillate periodically, shortening with inspiration (and lengthening with expiration). This phenomenon, known as respiratory sinus arrhythmia (RSA) is partly due to the Bainbridge reflex, the expansion and contraction of the lungs and the cardiac filling volume caused by variations of intrathoracic pressure. During inspiration, the pressure within the thorax decreases and venous return increases, which stretches the right atrium resulting in a reflex that increases the local heart rate (i.e., shortens the RR intervals). During expiration, the reverse of this process results in a slowing of the local heart rate. In general, the normal beat-to-beat changes in morphology are ignored, except for derivations of respiration, although the phase between the respiratory RR interval oscillations and respiratory-related changes in ECG morphology is not static.

Delineator

All these feature were extrapolated from the signals acquired with textile and gelled Ag/AgCl electrodes with the aid of the delineation algorithm designed by Martinez et al. (Martinez et al. (2004)).

They developed and evaluated a robust single-lead ECG delineation algorithm based on the wavelet transform, where first the QRS complexes are detected; then, each complex is delineated by detecting and identifying the R peak, onset and end. Then, P and T wave peaks are identified and delineated, identifying onset and end. The QRS detector algorithm was validated on several manually annotated datasets and marked a sensitivity of Se=99.66% and a positive predictivity of P+ =99.56% over the first lead of the validation databases (more than 980,000 beats). With this delineator good results were obtained also with textile electrodes as demonstrated in Figure 4.7 where the algorithm was executed on an ECG signal acquired with a wet screen-printed electrode.

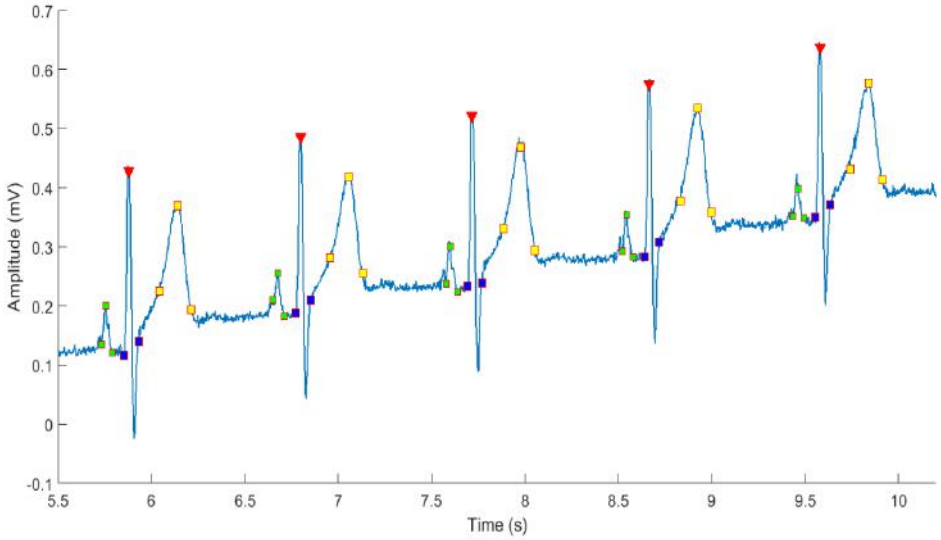

Figure 4.7 QRS detection of an ECG signal acquired with wet screen-printed textile electrodes.

The ECG signal is comprised of multiple sources and the recording is made through electrodes on the skin, which capture more than just the electrical activity of the heart. The primary electrical components captured are the myocardium, muscle, skin-electrode interface, and external interference as shown in Figure 4.8.

The common frequencies of the important components on the ECG are:

- Heart rate: 0.67 – 5 Hz (i.e. 40 – 300 bpm)
- P-wave: 0.67 – 5 Hz
- QRS: 10 – 50 Hz
- T-wave: 1 – 7 Hz

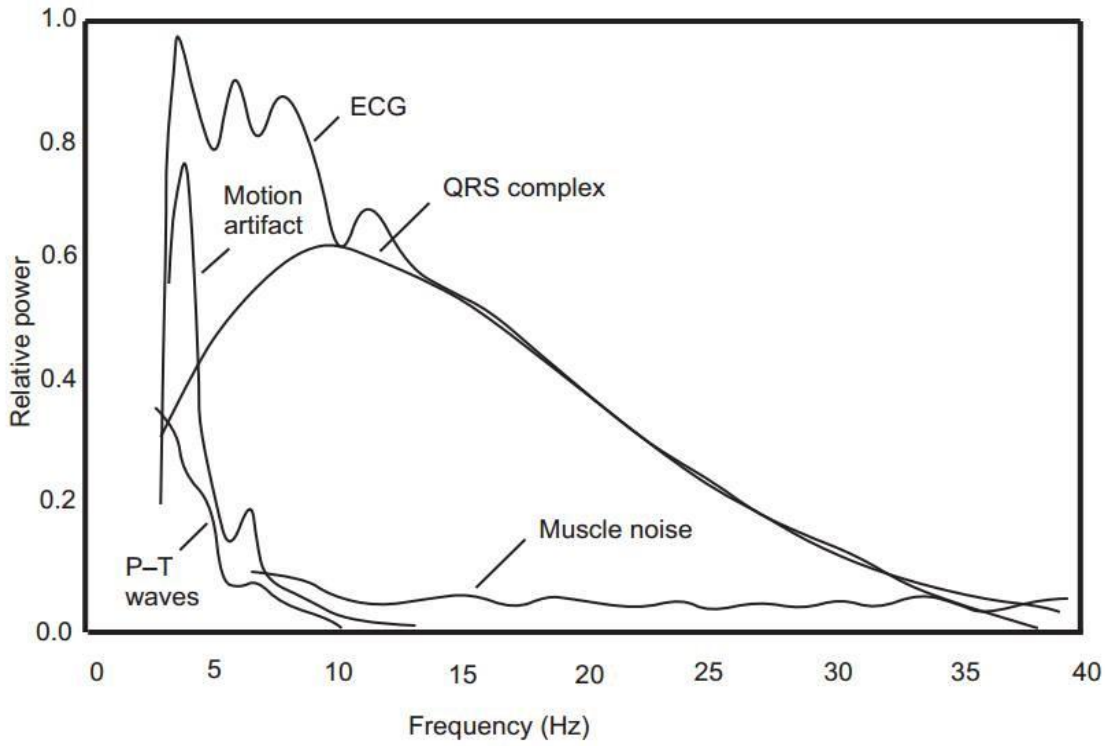

Figure 4.8 Relative power spectra of QRS complex, P and T waves, muscle noise and motion artifacts based on an average of 150 beats.

- High frequency potentials: 100 – 500 Hz

The common frequencies of the artifact and noise on the ECG are:

- Muscle: 5 – 50 Hz
- Respiratory: 0.12 – 0.5 Hz (e.g. 8 – 30 bpm)
- External electrical: 50 or 60 Hz (A/C mains or line frequency)
- Other electrical: typically >10 Hz (muscle stimulators, strong magnetic fields, pacemakers with impedance monitoring).

In this work the skin-electrode impedance represents a crucial aspect because this interface is the largest source of interference in the acquisition producing a DC component of 200-300 mV. Compared to the electrical activity of the heart, which is in the range of 0.1 to 2 mV, it is clear the contribution of this parameter for the quality of the signal. The interference seen from this component is magnified by motion, either patient movement, or respiratory variation.

Spectral and Cross-Spectral Analysis of the ECG

The short-term spectral content for a lead II configuration and the source ECG segment are shown in Figure 4.9, (Clifford et al. (2006)). The peaks in the power spectral density (PSD) at 1, 4, 7, and 10 Hz, corresponding approximately to the heart rate (60 bpm), T wave, P wave, and the QRS complex, respectively. The spectral content for each lead is highly similar regardless of the lead configuration, although the actual energy at each frequency may differ.

Figure 4.10 illustrates the PSDs for a typical full (12-lead) 10-second recording.

Experimented PSD Methods

In the state of the art, to analyze the ECG signal, there are several power spectral density estimation methods and the most common ones are the FFT and Welch. Fast Fourier Transform (FFT) is an algorithm to compute the Discrete Fourier Transform (DFT) and its inverse. The DFT is obtained by decomposing a sequence of values into components of different frequencies. This operation is useful in many fields but computing it directly from the definition is often too slow to be practical, especially because a n-point FFT is a way to

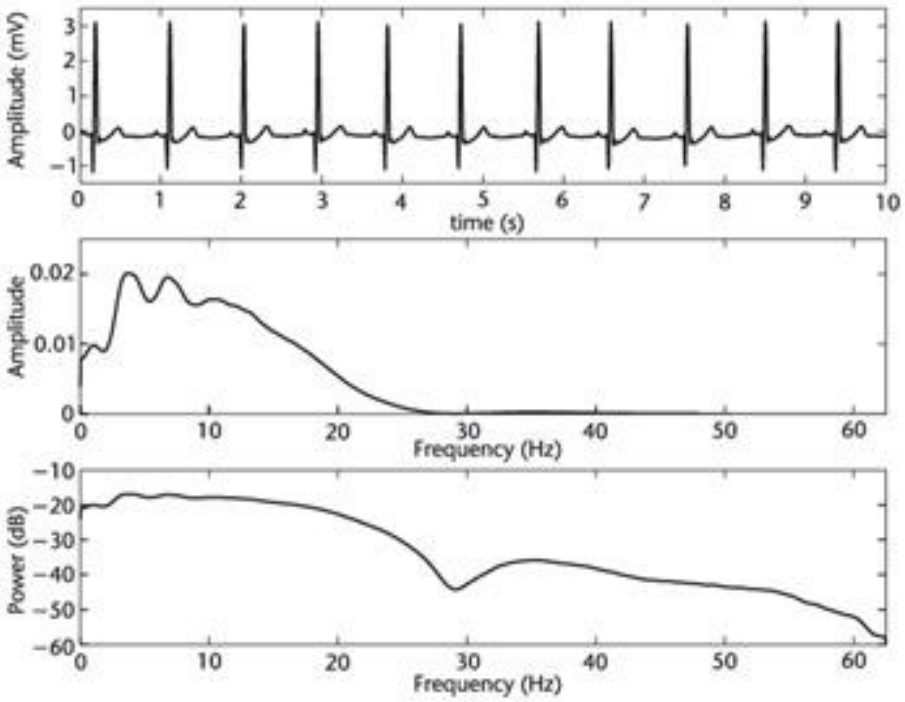

Figure 4.9 Ten seconds of 125-Hz typical ECG in sinus rhythm recorded with a lead II placement (upper plot) and associated linear and log-linear periodograms (middle and lower plots, respectively). A 256-point Welch periodogram was used with a hamming window and a 64-point overlap for the PSD calculation.

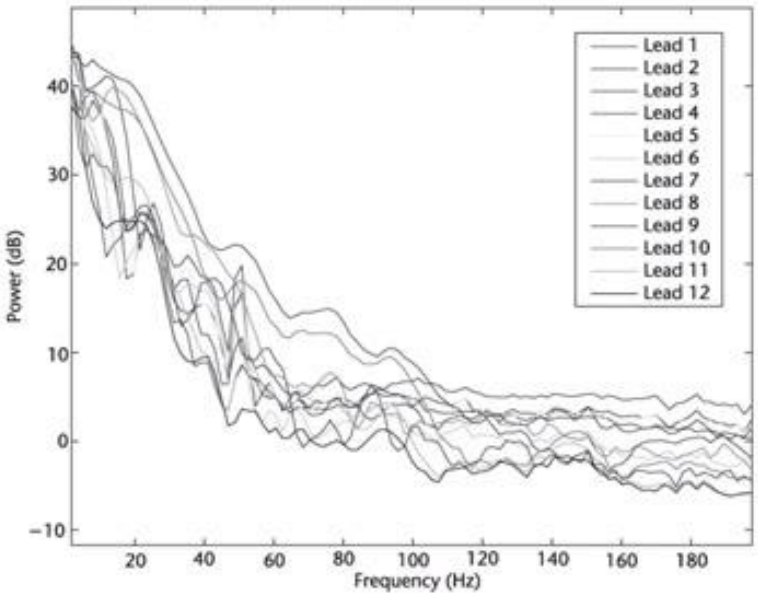

Figure 4.10 PSD (dB/Hz) of all 12 standard leads of 10 seconds of an ECG in sinus rhythm. A 512-point Welch periodogram was used with a hamming window and with a 256-point overlap.

compute the same result more quickly. An FFT computes the DFT and produces exactly the same result; the only difference is that an FFT is much faster than DFT and requires a power-of-two number of samples in time (or a zero padded sequence). Welch's method is another widely used PSD estimation method. The method is based on the concept of using periodogram spectrum estimates, which are the result of converting a signal from the time domain to the frequency domain. Welch's method is an improvement on the standard periodogram spectrum estimating method and on Bartlett's method, in that it reduces noise in the estimated power spectra in exchange for reducing the frequency resolution. Due to the noise caused by imperfect and finite data, the noise reduction from Welch's method is often desired. In our study, rectangular window with 4 seconds and 25% overlap were used for this method (Yucelbas et al. (2013)).

This power spectral density estimation method was selected to quantify the performance of ECG electrodes and compare it with the one obtained with the gold standard. As shown in Figure 4.11, this approach was used also with textile electrodes, for example in (Scilingo et al. (2005)), and the result of this comparison was considered also in our work to study the screen-printed textile electrodes performance.

4.3 Clinical ECG validation

The limitation of this analysis is the implementation of scripts designed for the extrapolation of parameters without any validation in terms of clinical analysis.

For this purpose, with the help of cardiologists, we performed another study on wet screen-printed textile electrodes able to validate them as clinical devices comparing their results with ones obtained with the gold standard. This test was performed acquiring the ECG on healthy subjects with a clinical instrumentation.

In order to evaluate the quality of the textile electrodes from a clinical perspective, the signals acquired with the textile electrode were visually inspected by the cardiologists to see the signatures typical of the different subjects' conditions. Marquette 12SL ECG Analysis Program was used to automatically compute the median beats and the principal measurements from the recorded 12-lead rest ECG traces. Even though the delineation algorithms are unknown, this solution produces a clinically accurate set of measurements. ECG recording and parameters measurements were performed with the 15-lead GE CardioSoft V6.71, featuring the GE Marquette 12SL ECG Analysis Program. GE Marquette 12SL ECG analysis program including ACI-TIPI, gender-specific criteria, 12SL with Right Ventricular

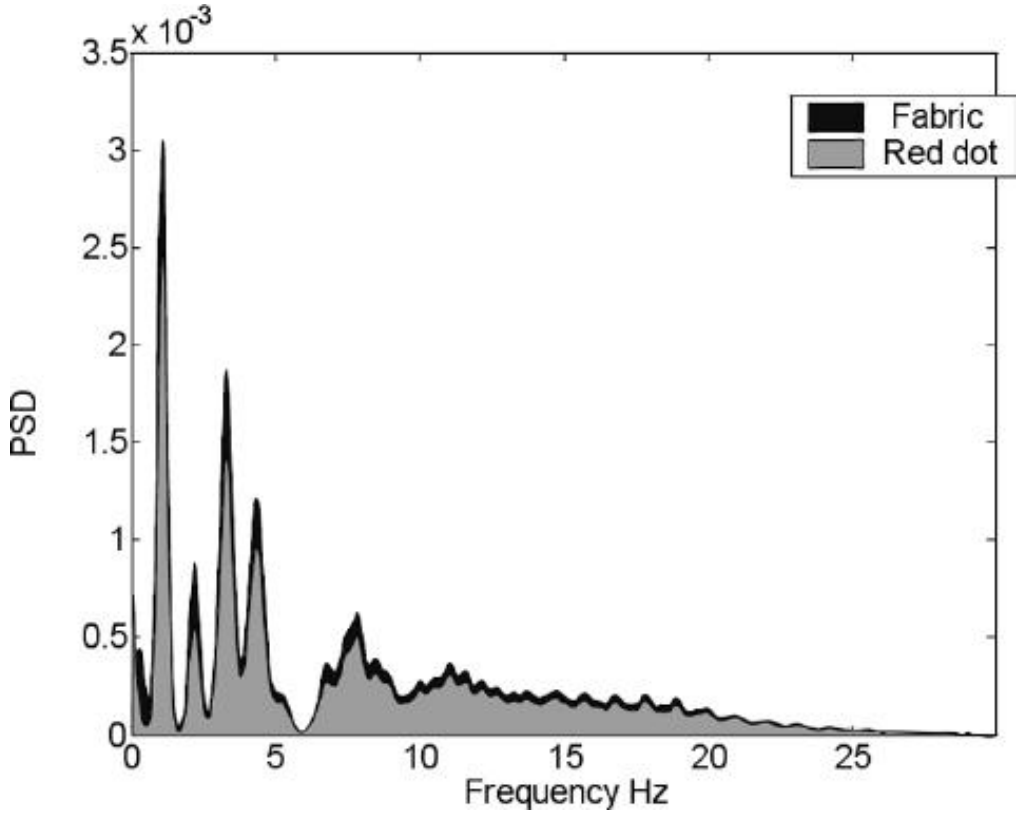

Figure 4.11 PSD curve of ECGs. Grey curve refers to ECG coming from Red Dot electrodes, while darker curve is related to ECG coming from fabric electrodes.

Involvement measurement and serial presentation of ECGs; 12SL is one of the most validated ECG analysis programs in the industry and was cited in over 150 independent publications. The data acquired with the Cardiac Acquisition Module (CAM-14) present the following features:

- Active Technology with "Type BF" floating isolated powered 14-channel acquisition module with built-in lead-fail detection,
- Input impedance >10 MΩ @10Hz,
- Sampling frequency: 500 Hz,
- Resolution: 4.88 µV/LSB @500 Hz,
- Peak-to-peak noise <15 µV (0.1 - 150 Hz),
- Internal impedance measurement, >600 kΩ lead-off detection.
- Baseline correction: Cubic Spline algorithm
- Common mode rejection: Measured: 100dB, calculated: >140 dB (123 dB with AC filter disabled)

Filter settings:

- High-pass filter @ 0.01 Hz,
- Low-pass @ 150 Hz,
- 50 Hz notch filter.

The study was performed following the principles outlined in the Helsinki Declaration of 1975, as revised in 2000; all the volunteers gave their informed consent to the measurements. Ten subjects (8 males, 2 females, aged 39 ± 8) were recruited by convenience sampling trying to include different conditions: healthy subjects (sedentary, trained, body builder, heavy smoker) and patients with aortic insufficiency, aortic stenosis and high hypercholesterolemia. ECG signals were recorded at rest, exploiting the standard clinical 12-lead configuration. No skin treatment was performed. In order to enable a comparison of the textile electrodes with commercial ECG electrodes, the cardiologist applied a set of ten off-the-shelf disposable gelled Ag/AgCl electrodes (FIAB F9079, foam with solid hydrogel) and performed a 10-second recording, annotating the value of the impedance showed by CardioSoft interface

on three precordial leads. Then, each commercial electrode was substituted by a textile one applied in the same point and fixed on the patient's skin thanks to a strip of adhesive medical tape. Owing to the state of the art, the adoption of two drops of saline (sodium chloride 0.9%) was considered, to wet the textile electrodes improving the signal quality (Pani et al. (2016b). A second 10 s measurement and impedance annotation was then performed. All the signal analyses were performed off-line.

The CardioSoft XML export module was used to save the 10 s traces, the medians and the automatic measurements set performed on them. In order to perform some post-analyses, a Matlab set of functions leveraging the XML Matlab Toolbox by Geodise (www.geodise.org/toolboxes/generic/xml_toolbox.htm, University of Southampton) was created. In particular, such functions were used to compute some parameters not directly available, such as the QRS amplitude on leads V_1, V_3, V_6 (QRS_{Vi}), the maximum QRS amplitude across all the leads (QRS_M), and the lead presenting such a high value (LM). The mean of the impedance modulus measured on leads V_1, V_3, V_6 by the device (ZV_i) was considered as indicative of the quality of the contact with the skin. The following clinical features were also considered:

- Ventricular frequency (HR),
- P wave and QRS complex duration,
- PQ and QTc intervals.

QT interval considered was the one corrected with the Bazett's formula. The measures obtained from the Ag/AgCl electrodes were compared to those from the textile ones by means of the two-tailed Student's t-test. Values of p 0.05 were set as the minimum level of statistical significance throughout the paper. Furthermore, as a measure of the broadband noise level, decimated wavelet denoising (WD) was performed on the lead LM to obtain the residual signal, and its root mean square (rms) was taken as index of the noise level. The parameters for the WD were the following: Bior 6.8 wavelet, 5 decomposition levels, soft thresholding, Heuristic SURE thresholding method assuming a non-white noise structure, soft thresholding.

4.4 EMG acquisition

To evaluate the performance of the textile electrodes as sEMG sensors, a comprehensive study was carried out, including voluntary muscular activations and electrostimulation protocols.

4.4.1 EMG electrodes characterization

The raw sEMG representation is the oldest form of signal presentation. When the sum of the single motor unit action potentials (SMUAP) reaches the skin, the sEMG emerges asn interference pattern whose peak-to-peak amplitude is associated to the strength of the contraction. Despite the fact that there is not a simple equation able to correlate the muscle force with the sEMG signal amplitude, the qualitative relationship between them has proved to be useful in many scenarios. These include biofeedback applications for the training of specific muscles, ergonomic assessments to establish the degree of muscles contraction or relax, biomechanics investigations to determine the role that individual muscles have in contribution to joint torque, as well as many other applications. In cases as the one in Figure 4.12, where this analysis is performed to validate textile electrodes with a performance similar to the gold standard, this investigation is not completely accurate because they are very similar in terms of amplitude values and time intervals (Scilingo et al. (2005)).

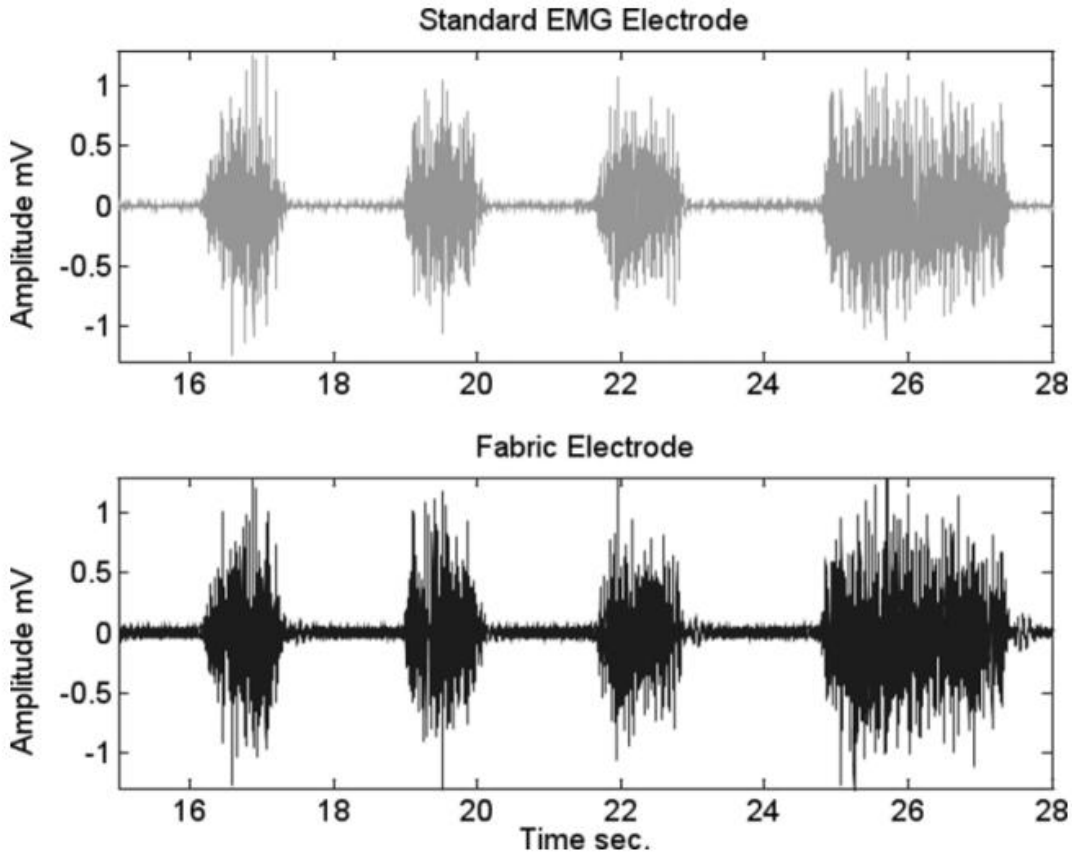

Figure 4.12 EMG of the left biceps brachi. Red Dot (upper) and Fabric electrode(lower).

Similarly to ECG signals, a more detailed investigation on the surface EMG could be performed in the frequency domain. In order to gain meaningful information from this type of calculation, the segment of data being studied must be stationary, meaning that the statistics of the signal do not change with time. The easiest way to ensure stationarity in an EMG signal is to constrain the muscle to perform a constant force, isometric contraction. Usually, parameters of the power spectral density used to provide meaningful information for the EMG frequency spectrum are the mean frequency, peak frequency, median frequency.

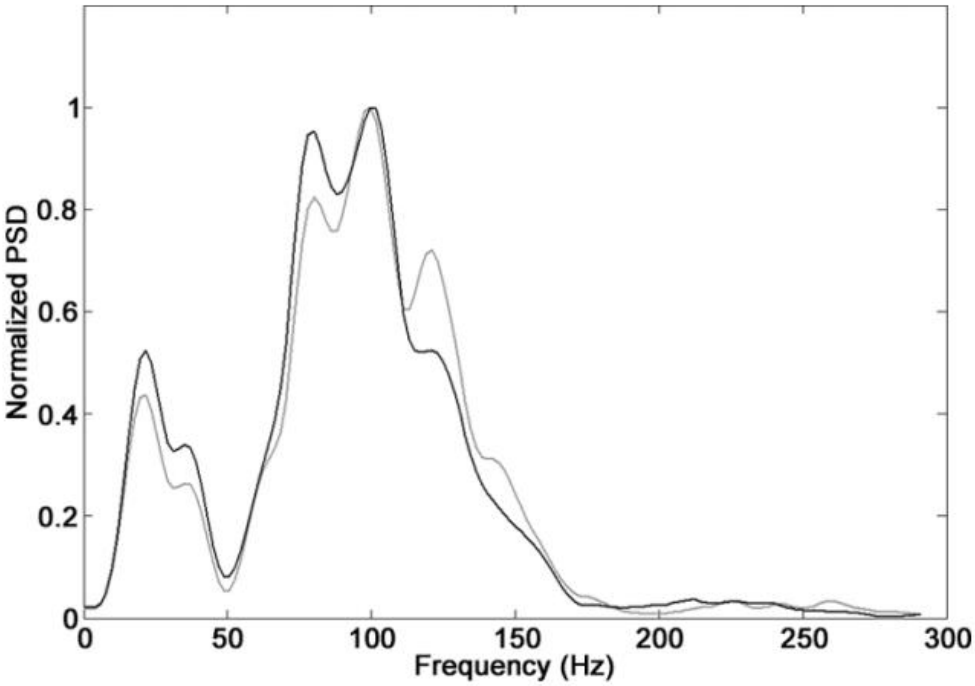

Figure 4.13 Normalized PSD of the EMG signal acquired by using Red Dot (lighter dashed curve) and standard (darker continuous curve) electrodes.

The spectral density of EMG power for a muscle shows the height of the curve to one determined frequency and indicates how much muscle energy is prevalent at that frequency, Figure 4.13. For instance, when a muscle is contracted, a filter from 20 to 300 Hz could represent almost all of the energy in the muscle spectrum. If a band-pass filter from 100 to 200 Hz is used, however, only part of the muscle energy would be observed. For illustrative purposes, we consider a work situation and a muscle fatigue, applying Power Spectral Density to signals at the beginning of the contraction and just before the point of release. During the initial part of the contraction, the median frequency of the spectrum may be slightly above 100 Hz. During muscle fatigue, there may be a shift towards the low to bring the median frequency to about 55 Hz. In fatigued muscles, the shape of the spectrum of frequency

changes in such a way that there is a decrease in the higher frequencies and an increase of the lower frequencies. This downward shift in the median frequency could be attributed to the synchronization of the motor unit recruitment models or to a slowing of muscle fiber conduction speeds.

The comparison of sEMG values between different subjects and for the same subject at different times is potentially problematic because anthropometric differences between individuals and the non-identical muscle contraction even on the same subject suggest that such comparisons should be approached with caution. Some factors that could influence these comparisons are: the thickness of subcutaneous adipose tissue, muscular length a rest, rate of contraction, muscle mass / transverse area, type of fiber, age, sex, changes in posture, interelectrode distance and skin impedance. The root-mean-square (RMS) calculation is considered to provide the most insight on the amplitude of the sEMG signal since it gives a measure of the power of the signal.

The RMS envelope of the EMG signal is calculated using a sliding window approach, with each window of data calculated according to the following equation:

$$RMS = \sqrt{\frac{1}{S}\sum_{1}^{S} f^2(s)}$$

where S equals the window length (points) and $f(s)$ equals the data within the window.

It is possible to compare the RMS values only for specific baseline rest conditions. However, during the movements, the comparison of the RMS amplitudes can be very misleading if sEMG data are not normalized first. There are several forms of normalization, each of which uses a kind of relative reference to sEMG amplitudes and calculate all other activities as a percentage of that reference. The most common method is represented by the isometric maximum voluntary contraction (MVIC). The patient is asked to run about three MVICs for the muscle group of interest. The central two seconds of a contraction lasting six seconds are recorded and then averaged over the three tests of the MVIC. Then, all the points of such excerpts are divided by the MVIC value, which represents a percentage between 0 and 100%. So, they are not absolute values in microVolt, but only a relative comparison against a maximal effort. In this way, the comparison between muscles and individuals may become possible reducing all muscle functions to this common feature.

This approach presents a series of advantages but at the same time is strictly limited by the physiological differences occurring during voluntary muscle contractions: even when an identical force is applied, the electrical response is different over time and all the more so from subject to subject. For this reason, we studied the sEMG signal under electrical

stimulation to increase the measurement repeatability and we studied the PSD only in rest condition to evaluate the presence of power-line interferences and their contribution with different kinds of electrodes and recording conditions.

Both electrical parameters and the characteristics of sEMG signals detected with the electrodes were analyzed.

Screen-printed electrodes were characterized in three different conditions: i) dry, ii) after the addition of a few drops of saline solution (0.9%) on the electrode surface, and iii) with a solid KCl hydrogel layer (Spes Medica Srl, Genoa, Italy) applied on the electrode surface. The results of the characterization were compared with those obtained from standard gelled Ag/AgCl electrodes (CDES000024 by Spes Medica Srl, Genoa, Italy). To ensure a like-with-like comparison, Ag/AgCl electrodes were used with their nominal diameter of 24 mm and with a reduced diameter of 10 mm obtained by cutting them with a hollow cutter punch. This choice maximizes the similarity between the proposed textile electrodes and the commercial ones. Indeed, the hydrogel added to our textile electrodes was the same used in the commercial Ag/AgCl electrodes considered for comparison.

The study population consisted of ten voluntary healthy subjects. The study was performed following the principles outlined in the Helsinki Declaration of 1975, as revised in 2000. All subjects signed an informed consent to the data acquisition and use, prior to the recording protocol.

The electrode characterization was performed on tibialis anterior while the subject was lying on an examination couch in semi-sitting position. Before electrode placement, the skin was shaved and gently treated by a skin preparation gel (NuPrep, by Weaver, Colorado, USA).

For each measurement, a couple of screen-printed textile electrodes was applied on the skin by means of a medical tape, with a distance between their centers equal to 30 mm for the 24 mm electrodes and 22 mm for the 10 mm ones. The electrodes separation avoids any direct conductive path through the fabric when the saline solution is added. A foam layer (5 mm thick) was placed over both electrodes and kept in place by means of a tubular net bandage in order to enhance the fabric adhesion onto the skin and to keep a stable and continuous pressure and skin humidity during the measurement. The same positioning was used during commercial electrode testing.

4.4.2 Electrical parameters analysis

The surface conductivity of the screen-printed textile electrodes was first analyzed. For this purpose, the sheet resistance of the functionalized textile substrates was measured by a 4-probes method.

After that, the skin contact impedance was measured. This is an important value to be used as reference when comparing other parameters such as the noise or the signal amplitude. The impedance was measured with a custom-made impedance meter (LISiN, Politecnico di Torino, Italy). This device converts a sinusoidal voltage input into a proportional current signal (200 nA peak-to-peak amplitude) and measures the voltage drop between the electrodes tested. The module of the impedance is computed through a Matlab routine as amplitude ratio between the measured voltage and injected current, for a frequency sweep in the range 10–1,000 Hz. For each measure, the impedance value at 50 Hz was extrapolated from the experimental dataset and used to compare the experimental conditions.

In order to quantify the noise contribution associated to the whole setup, a signal acquisition was performed with the subjects at rest, without any voluntary or induced muscular activation on the tibialis anterior.

To this aim, the DuePro amplifier (OT Bioelettronica, Torino, Italy), at 2048 Hz (bandwidth 10–500 Hz), and 16 bits of resolution, was adopted. During the measurement, the probe of DuePro was inserted into an armband fastened close to the ankle, in proximity to the electrodes, in order to minimize the wires length, movements and electrodes traction, Figure 4.14. The signals were displayed in real time by connecting the amplifier via Bluetooth to an host PC running a custom made acquisition software (LISiN, Politecnico di Torino, Torino, Italy) and then saved for the analysis and processing.

The detected signal was band-pass filtered in the 10-500 Hz frequency band and power-line interference was removed through spectral interpolation technique (Mewett et al. (2004). Noise estimations were then obtained by calculating the rms of the filtered signal over a 10 s window and validated by evaluating the same parameter in a quiescent period during the stimulation protocol. From the same 10 s long segments used for rms estimation, the power spectral density (PSD) of the noise was also estimated, by using the Welch's method with 4 s windows (1 s overlap). This analysis was performed for each subject in the typical range of the EMG signal, i.e. from 10 Hz to 500 Hz (Criswell Eleanor (2011).

Box-plots have been used for the representation of skin-contact impedance and rms of the noise distributions. In such figures, the median is highlighted, the box defines the 50% of the samples between the first and third quartile, and the wishers range from the minimum to

the maximum value, excluding the outliers (represented separately). The outliers are defined as data larger than q3 + 1.5(q3 – q1) or smaller than q1 – 1.5(q3 – q1), where q1 and q3 are the 25th and 75th percentiles, respectively, corresponding to approximately ± 2.7 σ and 99.3% coverage, if the data were normally distributed.

For skin-contact impedance and rms of the noise, at rest, a statistical analysis was performed by aggregating all the subjects testing the same electrode, and comparing the populations in pairs (Ag/AgCl electrodes against textile electrodes of the same size, in the different conditions). The values obtained with different electrodes and conditions were studied as distributions over the subjects and related with parametric and non-parametric tests. The first step was the execution of the Kolmogorov–Smirnov normality test for the distributions over the subjects in order to choose the correct statistical analysis between Student's t-test and the non-parametric Mann–Whitney U test. This distinction is necessary because the first one is a parametric test and could be used only with distributions normally distributed differently from the U test. Statistical significance was considered for $p < 0.05$. The Mann–Whitney U test is more widely applicable than independent samples Student's t-test, and for large samples from the normal distribution, the efficiency loss compared to the t-test is only 5%. The Mann–Whitney U test provides very similar results compared to ordinary parametric two-sample t-test on the rankings of the data (Conover and Iman (1981)).

4.4.3 EMG signal analysis

Because of the large variability of EMG patterns generated by voluntary muscular contractions, the approach followed in this work is similar to that described in (Botter et al. (2013), which is based on the study of the M-wave, representing the earliest sEMG response to the stimulation of the nerve associated to that muscle.

The same setup described before to record the noise was adopted. A DS7AH electrical stimulator (Digitimer LtD, UK) was added to stimulate the branch of the peroneal nerve innervating the tibialis anterior through two disposable stimulation gelled electrodes (bipolar nerve stimulation).

The stimulator was configured to transmit stimulation pulses with 300 µs duration, at 2 Hz. For each subject, the stimulation amplitude inducing a maximal M wave was identified at the beginning of the experiment, and kept constant throughout all the experimental conditions (i.e. different, tested electrodes). The average current value used for the stimulation was 24 ± 5 mA.

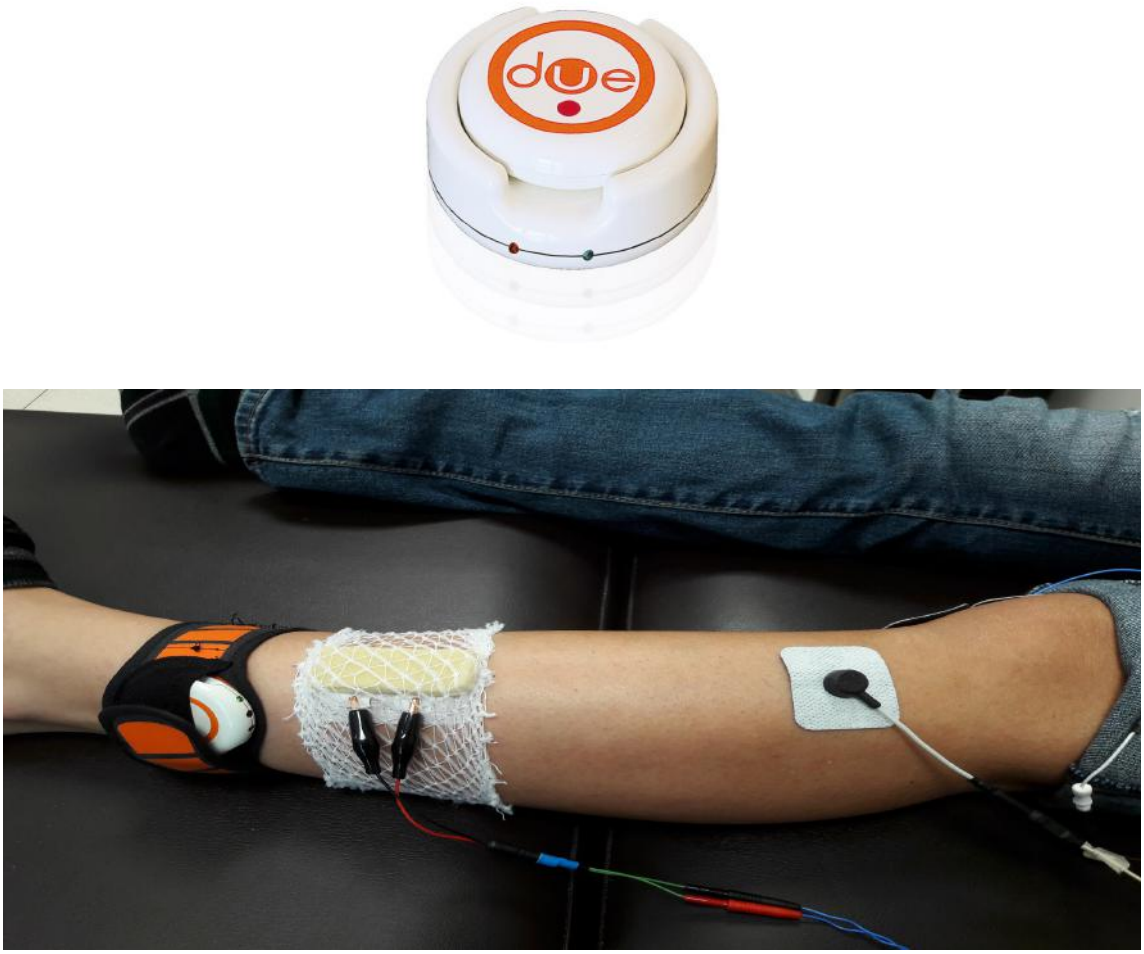

Figure 4.14 Top, DuePro amplifier (OT Bioelettronica, Torino, Italy), Bottom, Setup to compare textile electrodes with commercial electrodes during muscular stimulation

For each subject, electrode, and condition, the sEMG analysis was carried out on a prototypical M wave obtained by synchronized averaging of ten M waves occurring during that recording. The averaging procedure was adopted to reduce the effect of possible, subtle variability in the physiological responses to the electrical stimulation (Merletti et al. (1992)). With this process, it was possible to compare each signal acquired with textile electrodes with the one acquired by means of disposable gelled Ag/AgCl electrodes of the same size placed in the same position. The comparison was based on the similarity between the M-wave templates obtained with the textile and commercial electrodes. To this aim, a scatter plot of the individual samples of the two synchronized M wave templates was performed (one against the other), and three parameters where computed: slope, R^2 and normalized mean square error (NMSE). For these parameters, descriptive statistics have been provided in terms of mean and standard deviation, due to the physiological differences between the subjects in the different recordings.

4.5 EMG smart shirt

In all the tests, the different types of electrodes were positioned in the same point. The textile electrodes were fixed with double-sided adhesive tape to a stretch-fabric t-shirt with the goal of making them adhere to the skin as much as possible but at the same time leaving them able to follow the movements of the fabric during the exercise. After correctly positioning the textile electrodes, we proceeded with the connection to the electrodes to the biopotential recording system. Surface EMG signal was recorded by means of the 32-channel Porti7 system by TMSi, using four bipolar channels and placing the signal ground electrode on the third lumbar vertebra in order to avoid capturing undesired muscle activity. The protocol adopted included the following configurations:

- Short-circuit measurement (electrode against electrode)
- Subject at rest, sit
- Subject sitting with the torso bending laterally, at rest
- Isometric contraction of abdominal obliques
- Subject in motion: contraction of external obliques by torsion of the torso

The short-circuit and rest measurements were performed over one minute, while the exercises in isometry and in movement were repeated 10 times and each repetition had 5 seconds of contraction and 5 seconds of recovery. The exercises for the external abdominal oblique muscle were executed in a seated position to limit cable movement artifacts. For the activation of the external abdominal oblique muscles the subject was asked to perform a torso twist.

In order to analyze the effect of the motion artifacts affecting the proposed textile electrodes when they are not stably fixed on the skin, selective muscle activation exercises for external abdominal oblique muscles were executed by a single trained subject, following the instructions of a physiotherapist. Mild skin preparation was performed by gently abrading with NuPrep Skin Prep Gel by Weaver and Co.. The screen-printed and dip-coated textile electrodes could not acquire the signals in dry conditions due to their very high skin contact impedance, in the order of 10^6 Ω, as shown in the Results chapter. For this reason, the electrodes were wetted with a few drops of saline solution to reduce the skin contact impedance.

Chapter 5

Results

5.1 Preliminary printing tests

5.2 Dip coating

The dip coating procedure is the simplest between those studied in this work, but it presents many advantages in the fabrication process and in terms of physical properties. Figure 5.1 reveals the high homogeneity of the ink penetration between the fibers and the large amount of ink tends to decrease the sheet resistance of the fabric. For the lack of any spatial pattern resolution, this process was avoided in the fabrication of textile electrodes to prefer printing procedure were the ink could be deposited in an extremely controlled way.

5.3 Ink-jet printing

The ink-jet printing procedure shown in (Bihar et al. (2017)) was tested to develop printed textile electrodes based on PEDOT:PSS. As seen in the description of the ink-jet procedure, this printing process works only with cartridges that require an ink with a specific viscosity. For this reason the cartridges were filled with a commercial PEDOT:PSS formulation that already includes a series of organics solvents as secondary dopants. This ink is the HERAUS PJET 700 and presents a nominal viscosity of between 5.0 cP and 20 cP, depending on the external environment, completely compatible with the range imposed by the Dimatix cartridge.

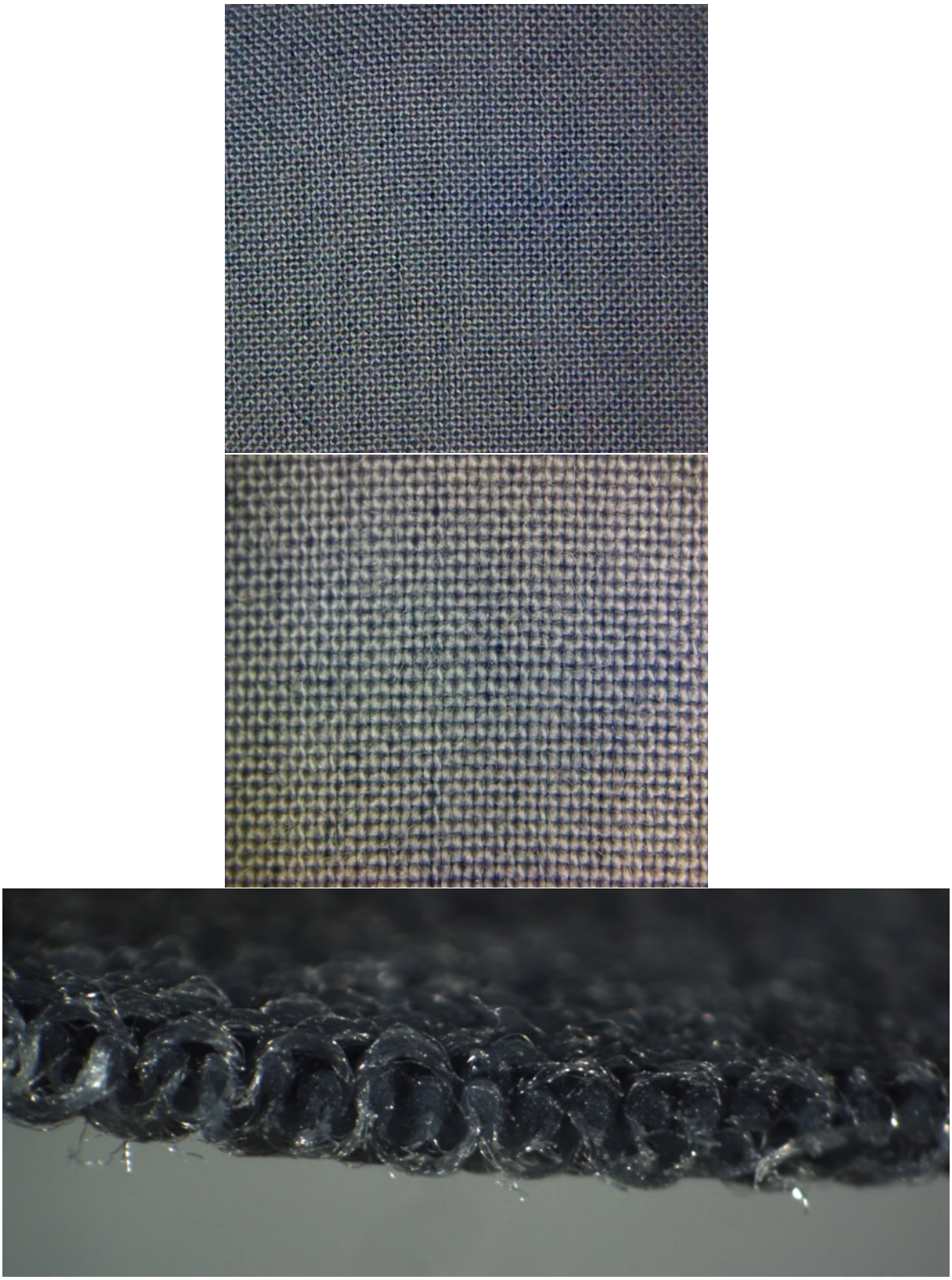

Figure 5.1 Detailed imagines of dip coated textile, top view and cross-section

Figure 5.2 presents the results in terms of resolution and conductivity measured on textile electrodes printed with the parameters listed before and a drop space equal to 10 µm.

Similarly, in Figure 5.3 are shown the results in terms of resolution and conductivity measured on textile electrodes printed with the same parameters and 15 µm of drop space.

5.4 Screen-printing process

5.4.1 Viscosity

The first step in the analysis of the screen-printing procedure was the research of the optimal ink for this printing process. Starting from the solution used for dip coating, several thickening tests were performed to increase the viscosity. Furthermore, the relation between the time in the oven (and another heating source) and the amount of water evaporated from the solution was studied, and the results presented in Figure 5.4.

Once established the inhomogeneous thickening obtained placing the polymer on an hotplate with a stirrer at 100°C was decided to heat it in oven at different temperatures. The optimal viscosity for the screen-printing process was chosen studying the results of the deposition with two different inks, one removed from the oven after 30 minutes and the other one after 55 minutes. The first one presents a viscosity equal to 17±2 cP and the second one, in Figure 5.5, a 100±10 KcP viscosity. The preliminary results of the deposition suggested the use of the second one and this was confirmed also from the direct comparison with a commercial ink designed for the screen printing, characterized by a viscosity equal to 70±10 KcP.

Both inks were used in the screen-printing procedure to establish if the one with the higher viscosity, shown in Figure 5.6, was the optimal one. From Figure 5.6 it is possible to appreciate the better resolution and the limited capillarity typical of this controlled process when a high-viscosity ink is used.

The viscosity is not the only parameter that should be checked in this deposition process; another aspect to obtain a good deposition is the mesh. By changing the number of lines in the mesh is possible to control the amount of ink deposited with the squeegee through the stencil. Once obtained the ink with the right viscosity, three different silk meshes, 18T, 24T

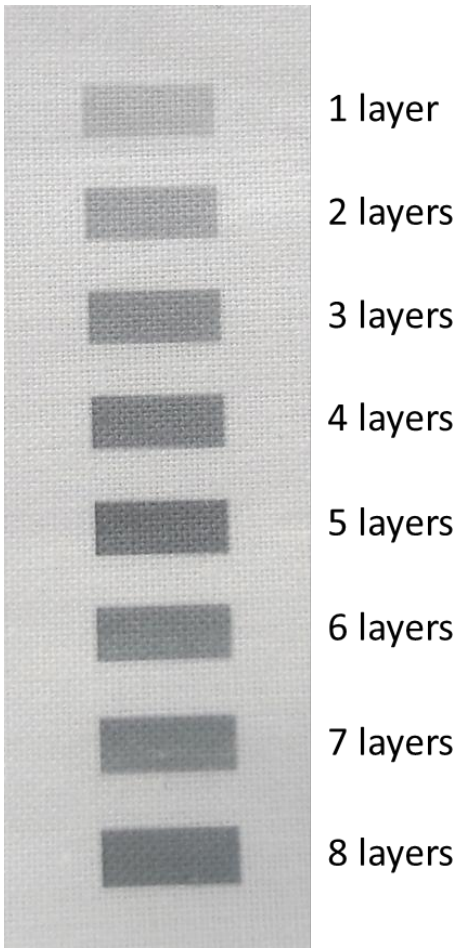

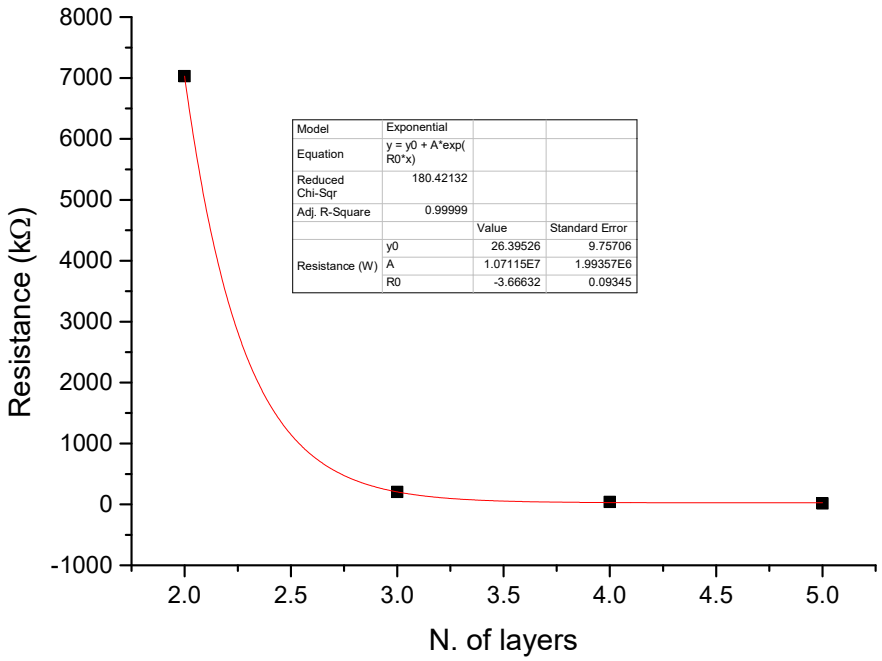

Figure 5.2 Electrodes printed with drop space 10 µm and their conductivity

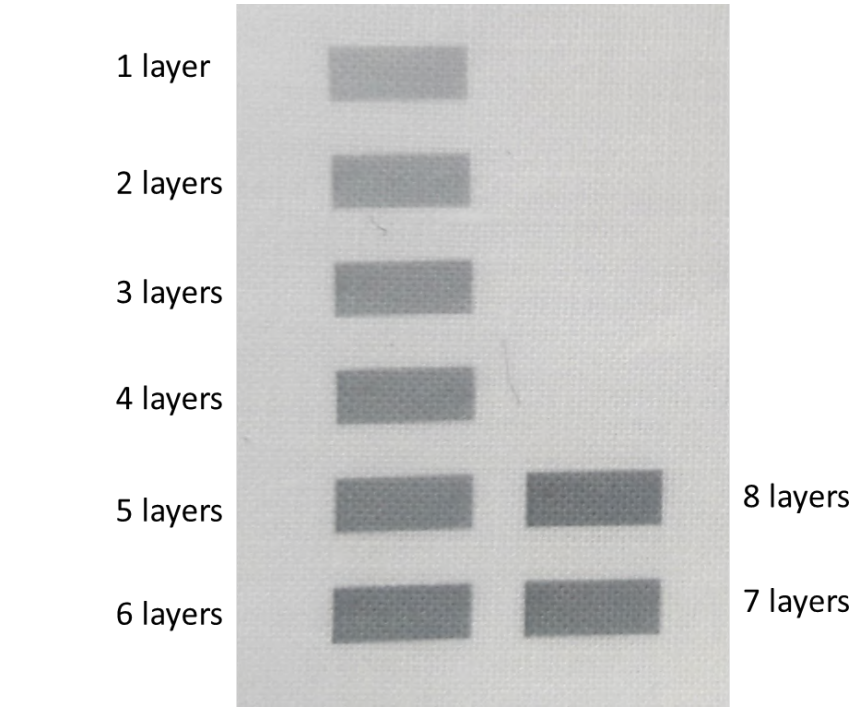

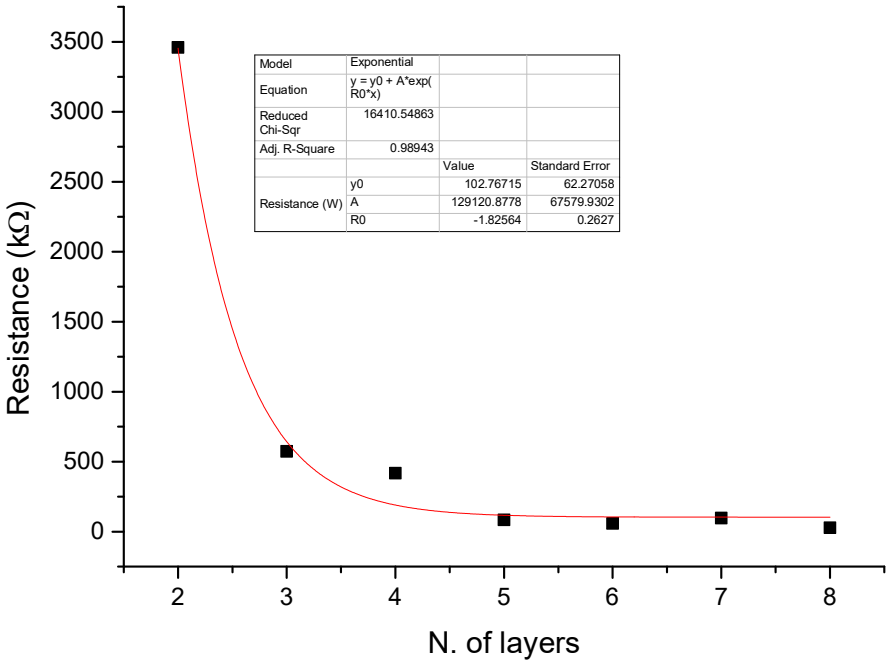

Figure 5.3 Electrodes printed with drop space 15 μm and their conductivity

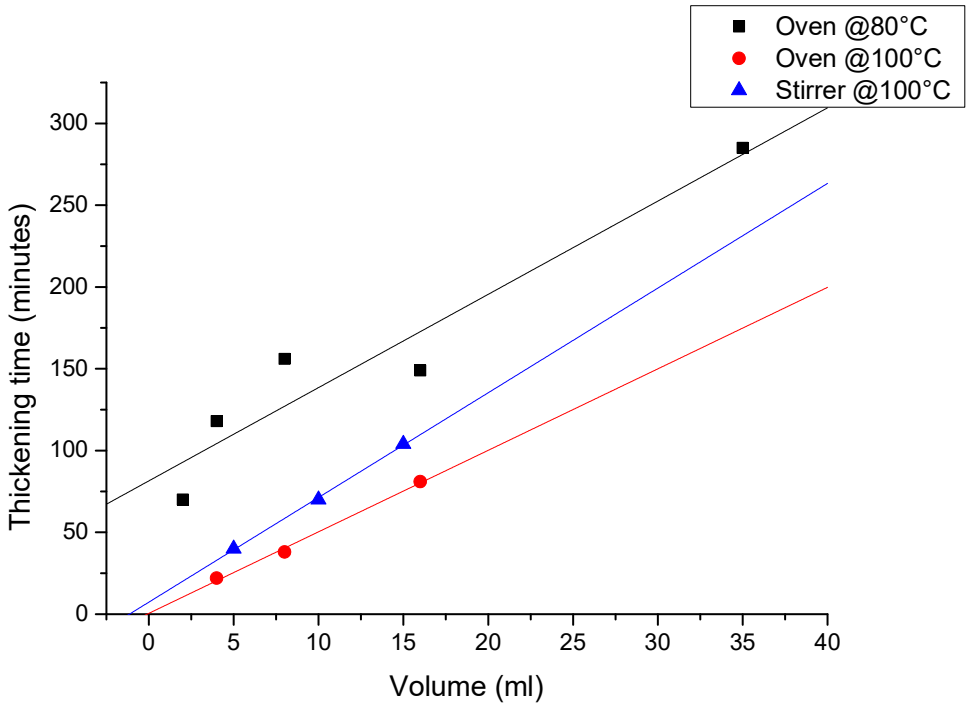

Figure 5.4 Relation between volume reduction and heating method

Figure 5.5 Conductive ink for screen-printing composed by PEDOT:PSS

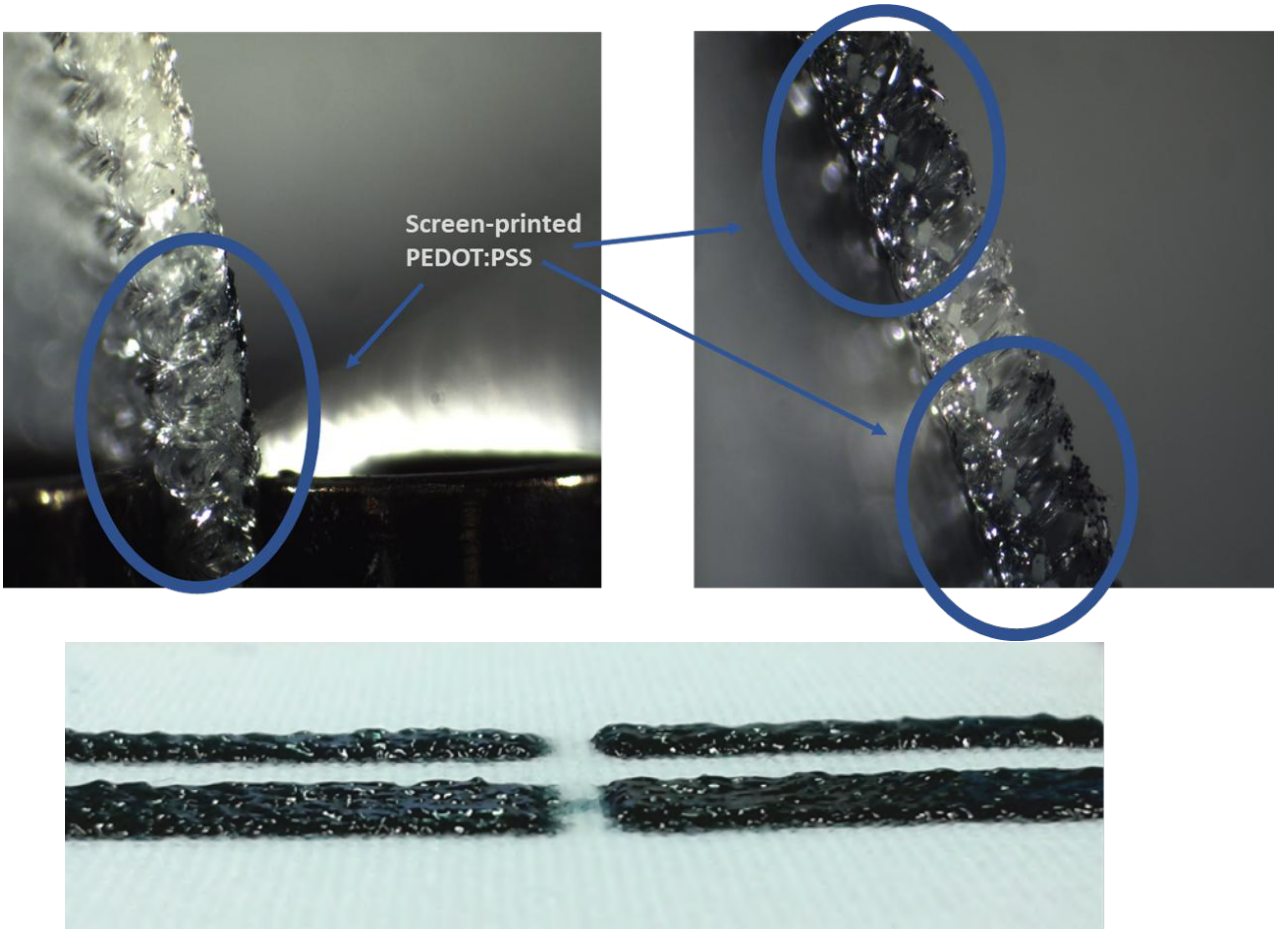

Figure 5.6 Top) Visual analysis of screen-printing tests with high (left) and low (right) viscosity, Bottom) Magnified image of the Ink with high viscosity deposited by screen-printing

and 43T, were tested on different substrates to evaluate the deposition. The mesh T number refers to the numbers of meshes per inch. The test was repeated on different substrates to evaluate how a different capillarity due to the different nature of the fibers could influence the results in terms of resolution and a preliminary result is reported in Figure 5.7.

Thanks to this comparison between different textile substrates, the optimal one was selected to continue the characterization the fabric: the one composed of 100% natural cotton fibers was chosen. On this substrate, further screen-printing tests were performed and the optical analysis demonstrated that the better results could be reached with a 43 T mesh, as shown in Figure 5.8.

5.4.2 Geometrical resolution

The nominal resolution indicated by the vendor of the 43T mesh frame (threads/cm) is equal to 0.3 mm and Figure 5.9 demonstrates that this performance was achieved even with our conductive ink.

The good results obtained with the polymeric ink on different fabrics introduced the possibility to develop smart clothes with screen printed electrode deposited on the finished garment.

5.4.3 Carbon black

This commercial ink is designed to be deposited by a screen-printing procedure to develop conductive paths on several substrates and the results obtained on a textile substrate as cotton showed a high quality in terms of conductivity and geometrical resolution, as shown in Figure 5.10.

Despite the good results obtained, it could not be used in the development of screen-printed textile electrodes because this ink presents a high hydrosolubility and a minimal moisture could remove the ink from the fabric. Textile electrodes should remain in contact with the skin for a long period and a minimal requirement is the resistance to humidity produced by the skin. For this reason, we have not investigated further this carbon black ink for textile electrodes.

The physical properties of the conductive ink based on carbon black facilitate to reach the goal to deposit by screen printing an electrode on a silicon surface. The elevated adhesion of

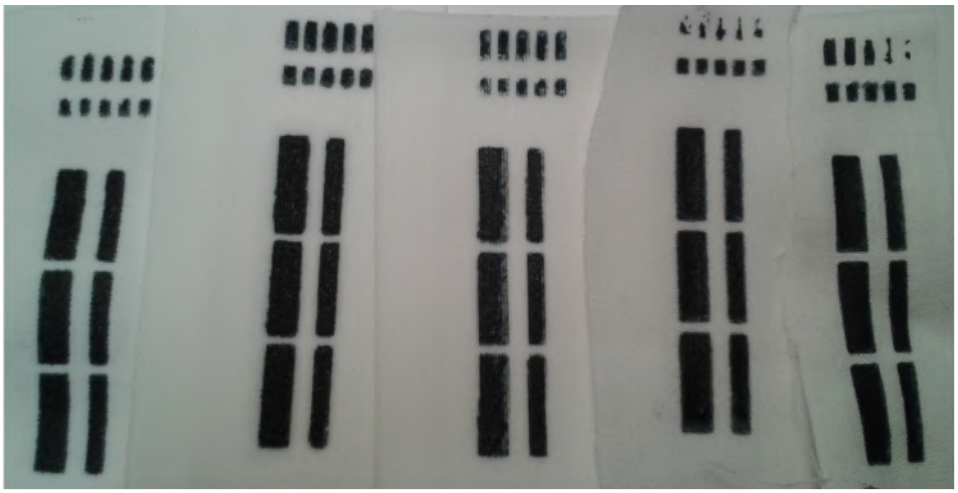

18T

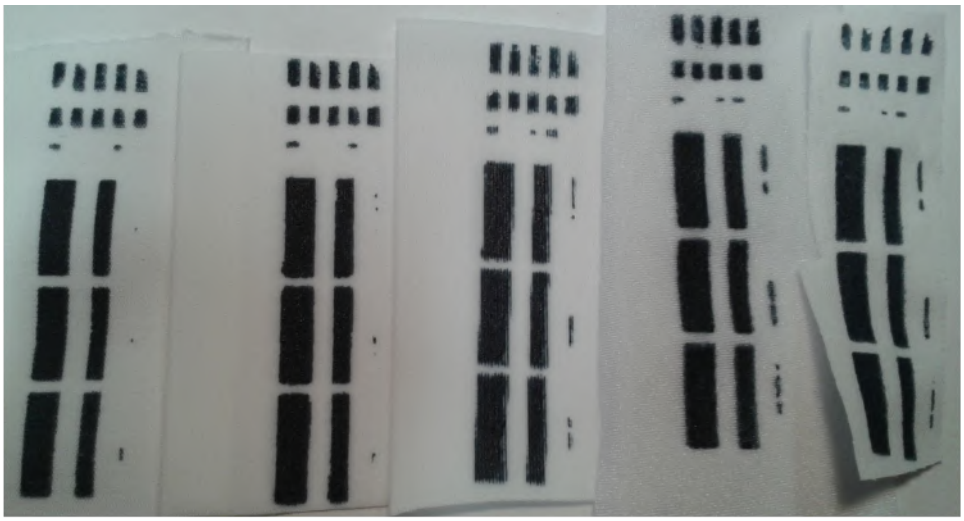

24T

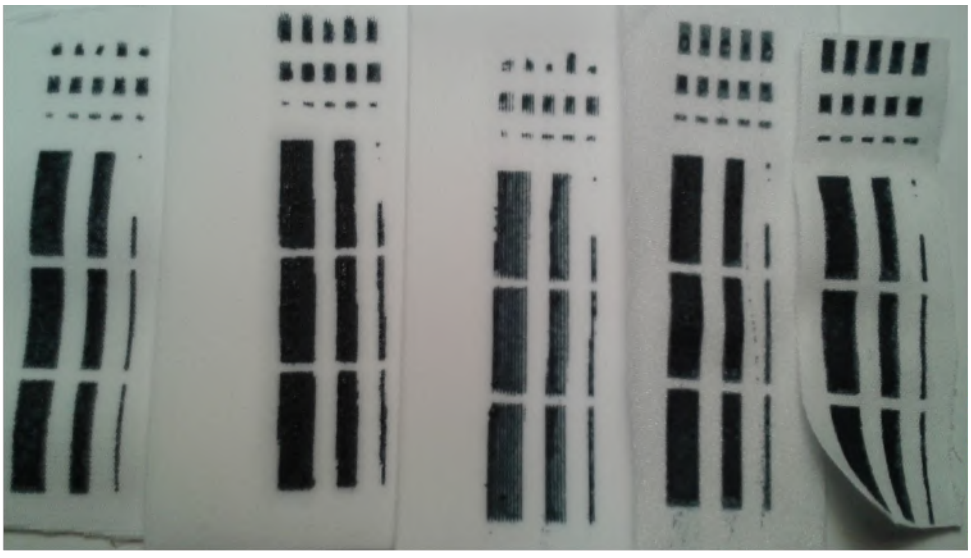

43T

Figure 5.7 Geometrical resolution obtained with different screen-printing frames (18T, 24T, 43T)

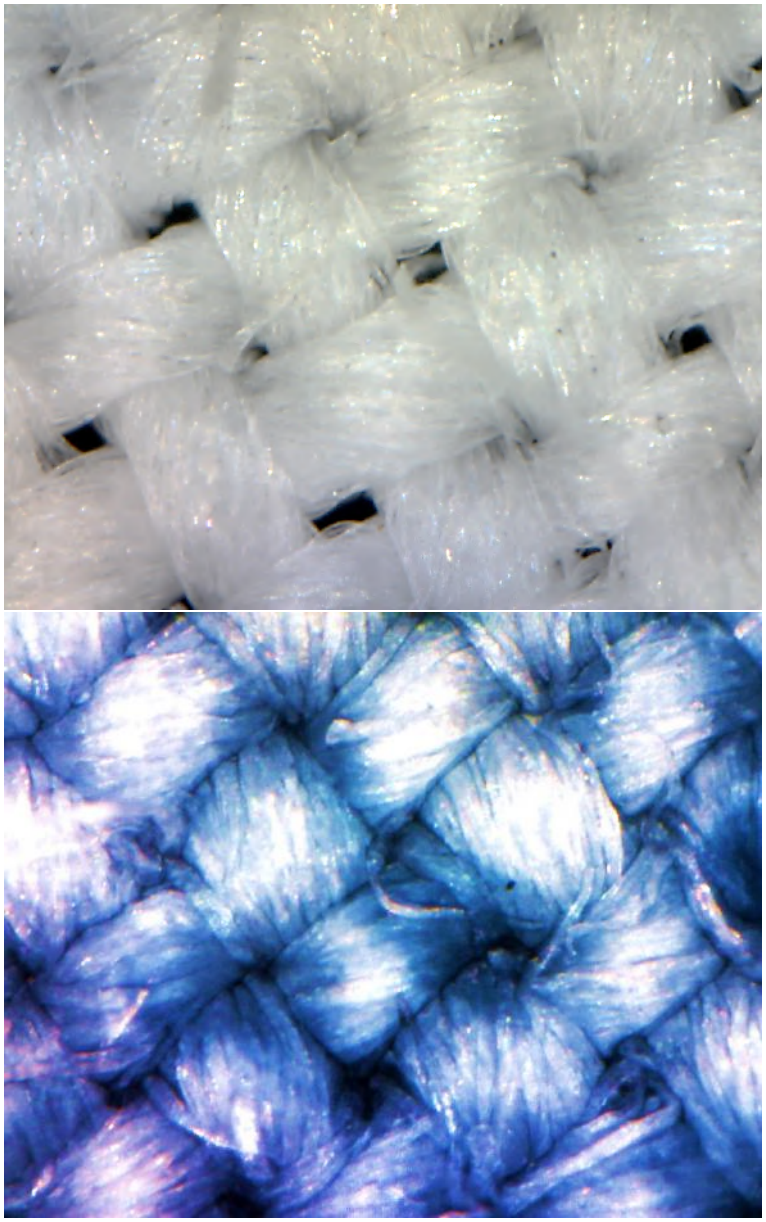

Figure 5.8 Cotton before and after screen-printing deposition observed with optical microscope

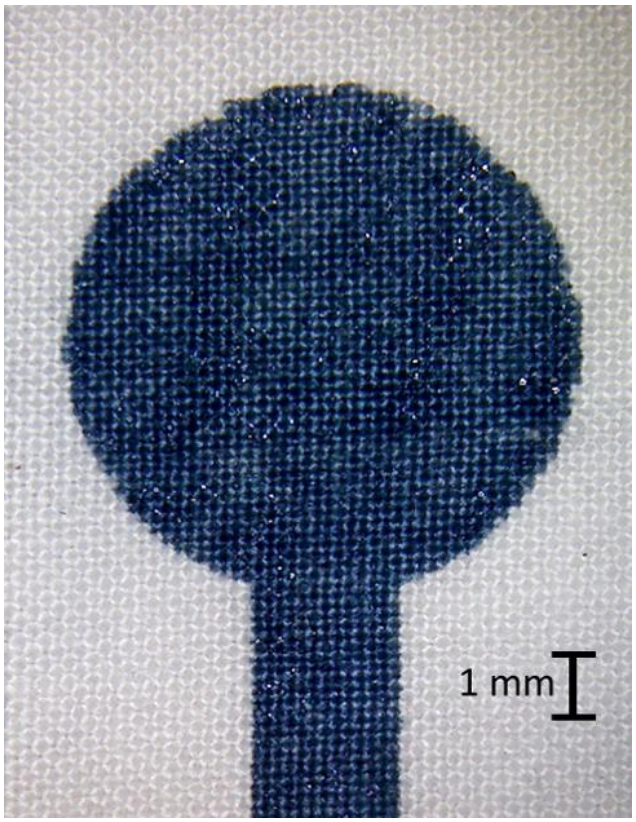

Figure 5.9 Detail of Ø10mm screen-printed textile electrodes

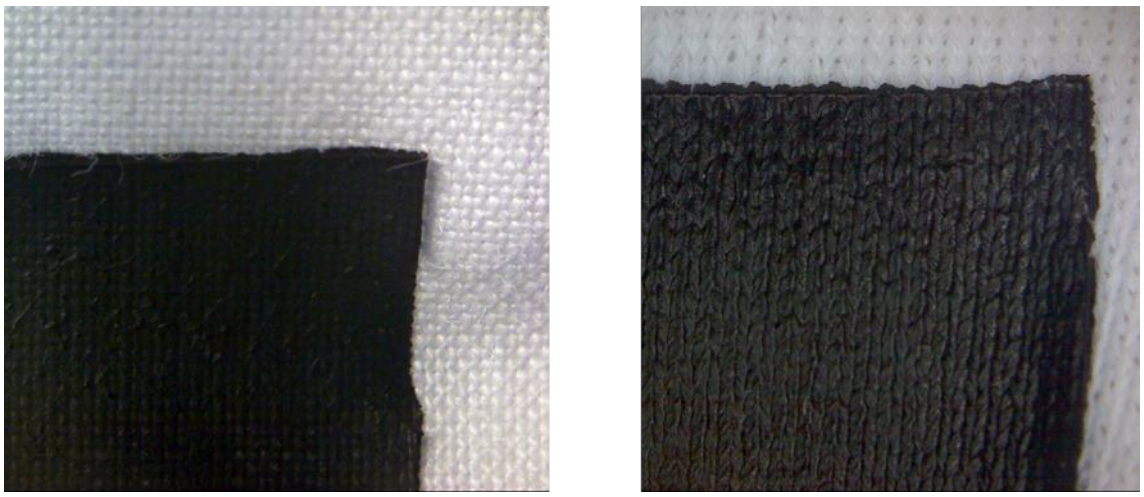

Figure 5.10 Screen-printed textile electrodes with carbon black ink on cotton (left) and elastic Lycra (right).

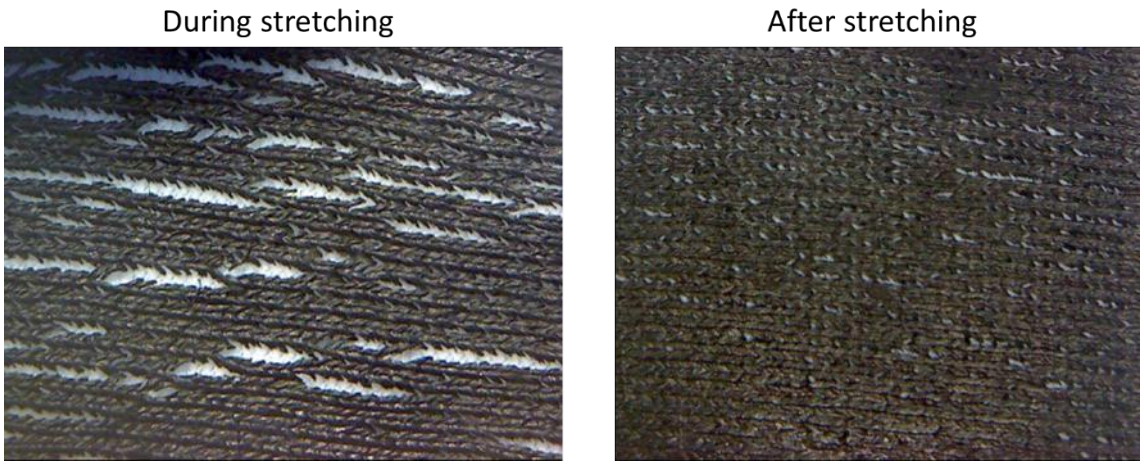

Figure 5.11 Visual comparison between cracks insurgence during the stretching procedure and film discontinuity after the stretch.

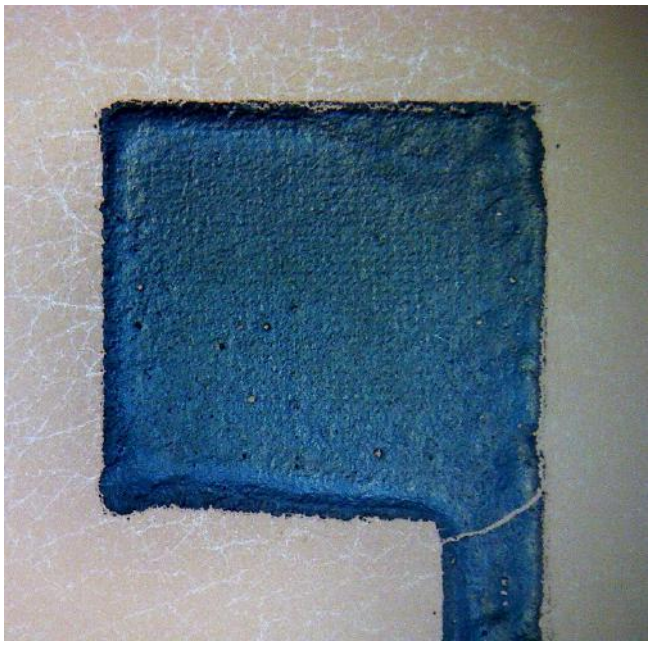

Figure 5.12 Screen-printed textile electrodes with carbon black ink on siliconic liner

this ink is a good result, but unfortunately it presents a rigidity that produces a discontinuity when applied a little stretch on the surface as shown in Figure 5.11.

5.4.4 Stretching resistance

The lack of flexibility recorded with the ink composed of carbon black was evident also with the PEDOT:PSS ink as shown in Figure 5.13.

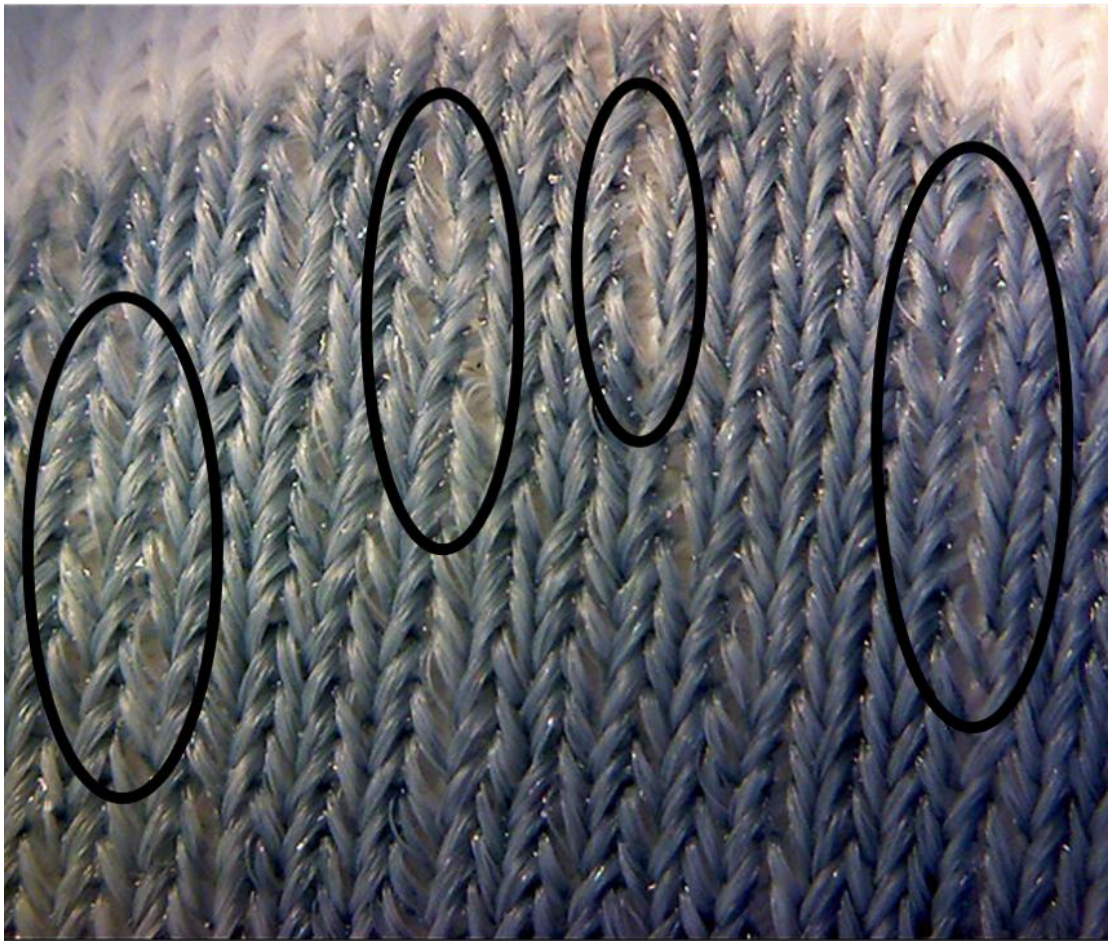

Figure 5.13 Stretched screen-printed electrode with highlighted cracks between fibers.

5.4.5 Sheet resistance

A detailed comparison between the sheet resistance obtained with the ink based on PEDOT:PSS deposited on different fabrics with different meshes is shown in Figure 5.14.

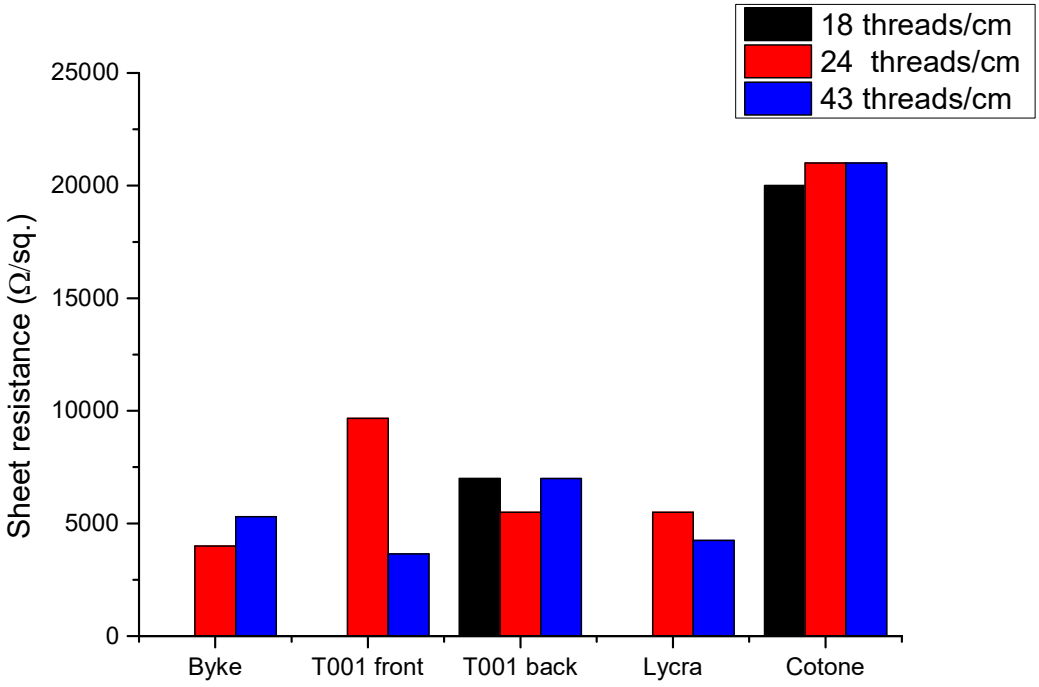

Figure 5.14 Sheet resistance measured for different substrates and meshes

5.4.6 Washing resistance

Daily use was simulated by repeated washing cycles and stretching tests with the protocol described in the previous chapters. To avoid the introduction of confounding factors in the analysis, the former test was performed only on non-stretchable samples (cotton), whereas the latter test was carried out only on the stretchable samples.

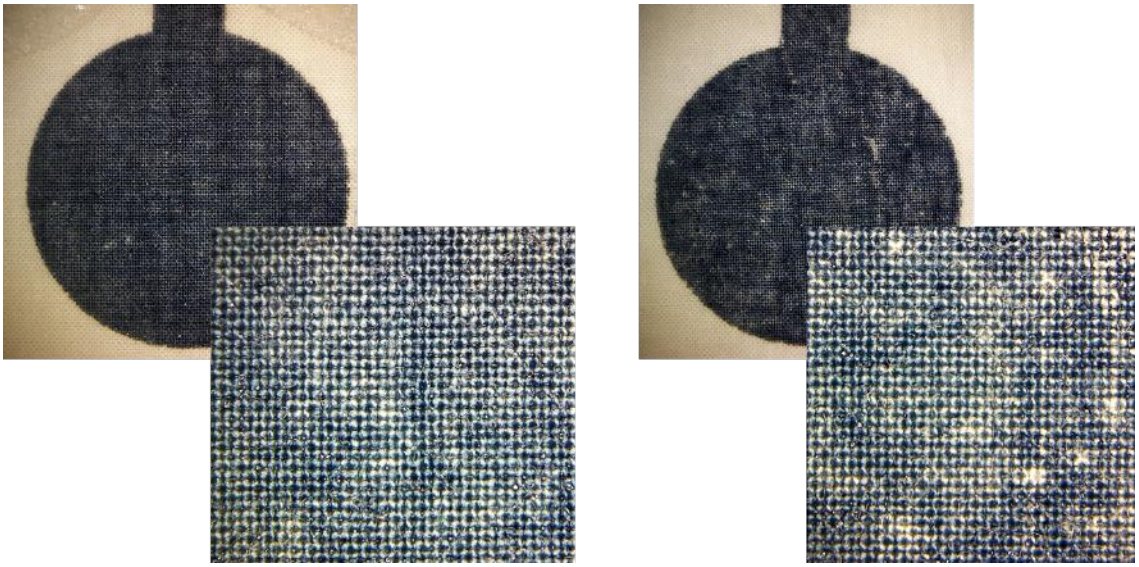

Figure 5.15 Visual comparison between textile electrodes before and after 20 washing cycles

Figure 5.15 shows how the ink layer is affected by these washing cycles and in Figure 5.16 is shown how this affects in turn the sheet resistance (average values over six samples, standard deviation and linear regression), measured with the LCR meter.

In (Achilli et al. (2018) is presented the variation of the noise and impedance parameters, measured with the Xtratek ET-65A according to the ANSI/AAMI EC12:2000/(R)2010 standard, by coupling pairs of textile washed electrodes in different conditions. For each washing cycle condition, a single couple of electrodes was tested.

Coupled screen-printed electrodes with different electrolytes exhibited a similar trend in terms of noise and impedance when increasing the number of washing cycles. After 10 cycles, a stabilization of the electrodes characteristics was observed, and no further degradation was perceivable. Compared with the ANSI/AAMI standard EC 12:2000, the impedance value measured with the Xtratek remained under the limits even after 20 washing cycles, whereas the noise, being closer to the limit before the treatment, exceeded it after 5 washing cycles only. This is relevant because the screen-printed electrodes could be exposed to washing procedures if placed on smart garments. Furthermore, they could also be used in a wet

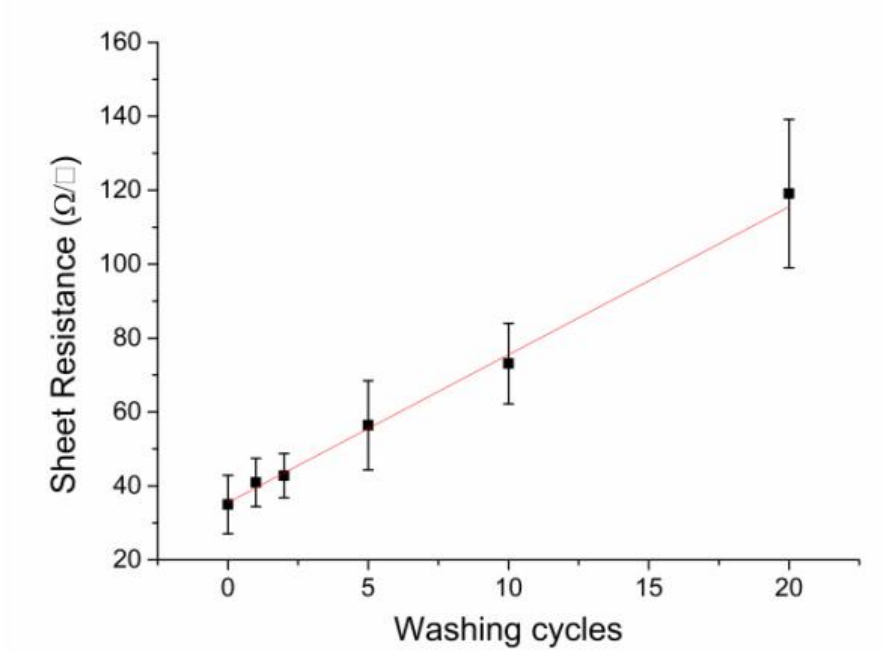

Figure 5.16 Sheet resistance for electrodes washed 20 times

condition during an athletic performance, or when covered by an electrolyte as saline solution during cardiac monitoring. Monitoring in these conditions is represented in Figure 5.18.

5.4.7 Stretching resistance

Stretching tests under dry conditions revealed an increment in the impedance and noise values, respectively increasing from 243 ± 1 Ω to 670 ± 30 Ω and from 48 ± 2 µV to 139 ± 2 µV after one stretching cycle of 100% in length. Despite the deterioration, the impedance was still within the ANSI/AAMI limits, whereas the noise slightly exceeded such limits. Even after repeating this stretching procedure several times, no significant variations were obtained with respect to just one cycle.

5.5 ECG-specific results

5.5.1 Benchtop measurements

In addition to sheet resistance, similarly to washed electrodes, brand new screen-printed textile electrodes were analyzed with benchtop measurements to evaluate the parameters

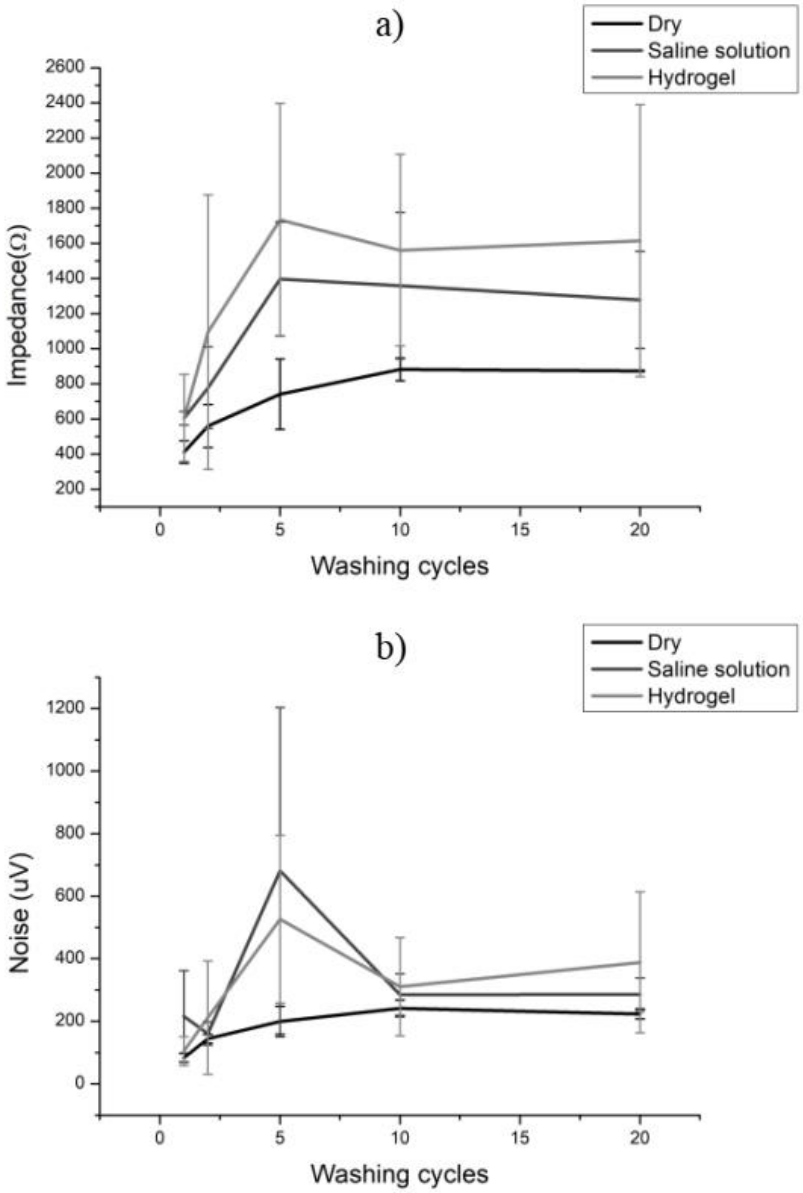

Figure 5.17 Impedance (a) and noise (b) measured on textile electrodes with Xtratek ET-65A in dry conditions and with saline solution and hydrogel between the active electrodes area.

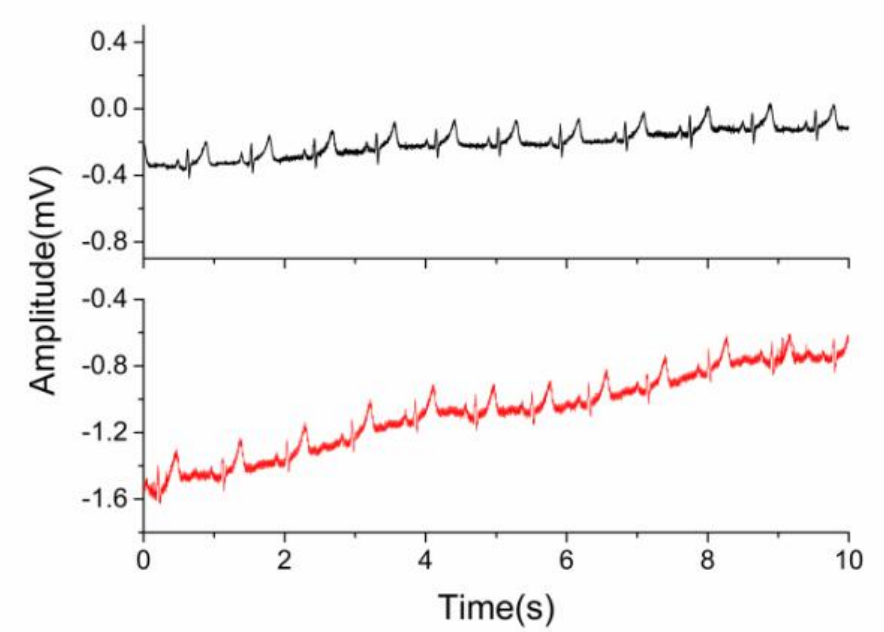

Figure 5.18 ECG signal recorded with textile electrodes washed 20 times under dry condition (top) and saline solution (bottom).

required by the ANSI/AAMI EC12:2000/(R)2010 standard for disposable ECG electrodes. Impedance (ACZ), noise, bias and SDR were analyzed under the controlled conditions described before under dry conditions and with the addition of electrolytes. The two former parameters are shown in Table 5.1 for the cotton samples. The value indicated represents the mean of the parameter over six measures for the impedance and ten measures for the noise, while the error represents the standard deviation.

	AC impedance	**Noise**
Dry	270 ± 6 Ω	60 ± 10 µV
Saline	450 ± 170 Ω	100 ± 60 µV
Hydrogel	600 ± 200 Ω	130 ± 30 µV

Table 5.1 ACZ and noise measured by Xtratek ET-65A coupling textile electrodes

In addition to such important parameters, the DC offset was also measured to assess the electrode performance. A stable value of 0 mV both in the dry condition and with saline was observed, whereas the addition of a solid hydrogel film resulted in a DC offset value of 2 ± 1 mV. In this condition, the DC Offset variation over a clinical use period of 8 hours and the polarization trend were also evaluated, and the results are presented in Figure 5.19.

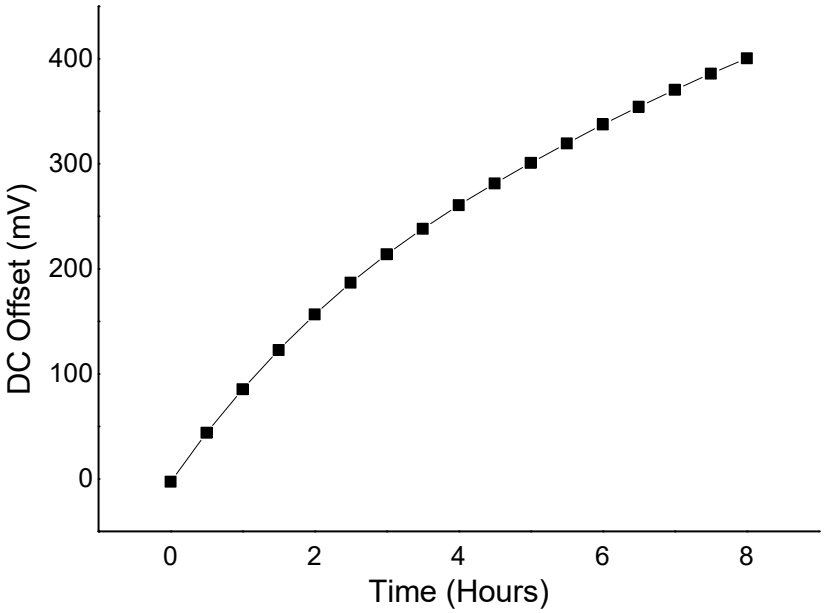

Figure 5.19 DC Offset Bias with textile electrodes and hydrogel over 8 hours

The measurements performed to simulate a defibrillation recovery using the screen-printed organic ink exceeded the limits imposed by the ANSI/AAMI standard and those of the Xtratek ET-65A (400 mV and 9.9 mV/s) for both offset and recovery slopes. For the stretchable substrate, tested only under dry conditions, the same results can be achieved in terms of DC offset and SDR, while the results in terms of impedance and noise were presented before.

5.5.2 Impedance between faced electrodes

The results of faced electrodes impedance are shown in Figure 5.20. As indicated by the impedance results obtained with the Xtratek ET-65A, the response to the addition of different electrolytes showed a similar trend over the different frequencies.

5.5.3 Skin contact impedance

The skin contact impedance obtained with screen-printed textile electrodes are shown in Figure 5.21a, in terms of their mean and standard deviation over the study population. To

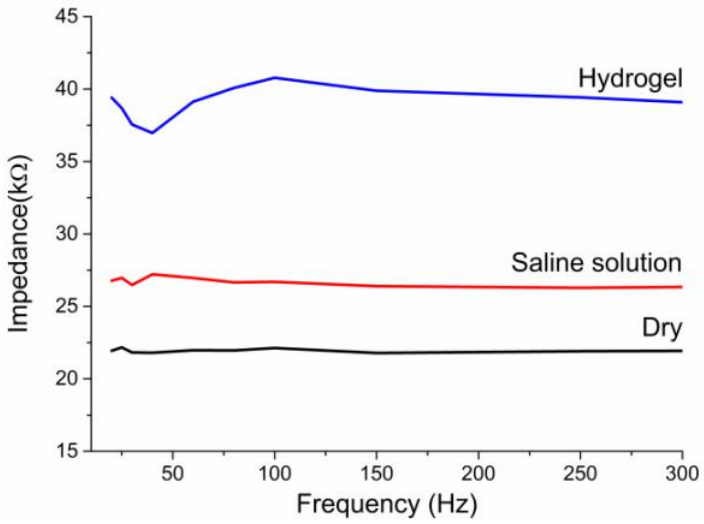

Figure 5.20 Impedance benchtop measurements using LCR meter

better identify the contribution of the electrolytes to this parameter, the same plot is shown in Figure 5.21b without the curve related to the dry condition. These curves exhibit a similar trend, as revealed by the Pearson's correlation coefficients presented in Table 5.2. Remarkably, such coefficients present an error lower than 10^{-13}.

	Saline	**Hydrogel**	**Ag/AgCl**
Saline	1	0.9996	0.9999
Hydrogel	0.9996	1	0.9995
Ag/AgCl	0.9999	0.9995	1

Table 5.2 Pearson's correlation coefficients obtained by comparing the textile electrodes.

The skin contact impedance measured for washed electrodes showed a different behavior compared to the bench tests. Since the subjects' skin was not treated for impedance reduction, in dry conditions the skin contact impedance at 20 Hz reached 16 MΩ on average, with brand-new screen-printed electrodes. Such a high value, incompatible with a good measurement, was due to the reduced contact pressure and the poor skin hydration. Several real recording conditions for a smart garment, such as athletes' performance monitoring or cardiac monitoring, take advantage of skin wetting. This situation was recreated by adding on the electrodes surface a few drops of saline solution or applying a solid hydrogel layer used in the disposable ECG electrodes. In this case, the skin contact impedance for screen-printed textile electrodes reached 100±30 kΩ when using saline solution and 80±20 kΩ when using

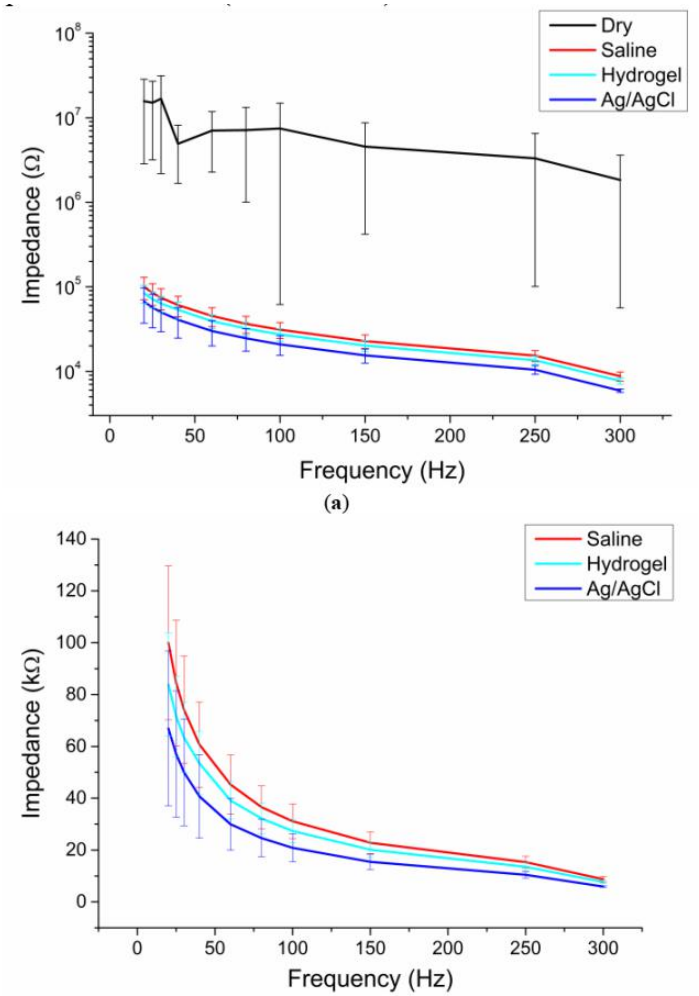

Figure 5.21 (a) Skin contact impedance measured before every ECG measurement, (b) impedance measured with the addition of electrolytes and compared with that of Ag/AgCl electrodes.

solid hydrogel. These results are comparable to the 70±30 kΩ impedance value measured with disposable gelled electrodes.

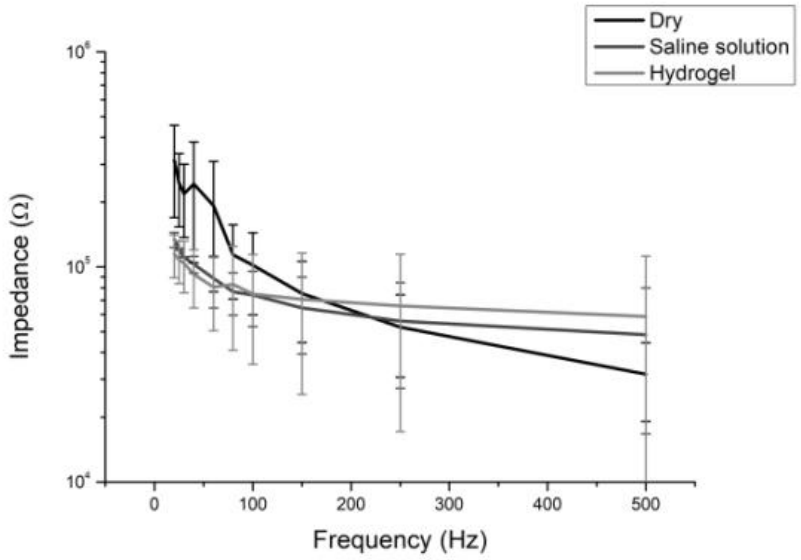

Figure 5.22 Variation of the skin contact impedance with the frequency for textile electrodes washed 20 times with or without electrolytes.

The performance of the screen-printed textile electrodes for ECG acquisition was assessed by comparing them with disposable gelled Ag/AgCl electrodes (CDES000024 by Spes Medica Srl). The results presented in this section are related to a single subject because of the physiological variability of the signals and, consequently, of the extracted features. Because of the excessively high value of the skin contact impedance under dry conditions, only the results with an electrolyte are reported hereafter. Three ECG excerpts obtained with brand new textile electrodes (saline and hydrogel) and Ag/AgCl electrodes are shown in Figure 5.23. The signals appear very similar, as also demonstrated by the PSD analysis, reported in Figure 5.24.

The QRS features (RR interval, QRS amplitude and QRS duration), extracted from the signals of the same subject over 60 s, are presented in Figure 5.25.

From these results, it is visible the high similarity between the gelled Ag/AgCl electrodes and the wet textile electrodes. This comparison was analyzed in detail in a clinical trial and the data extrapolated from this analysis demonstrated this similarity.

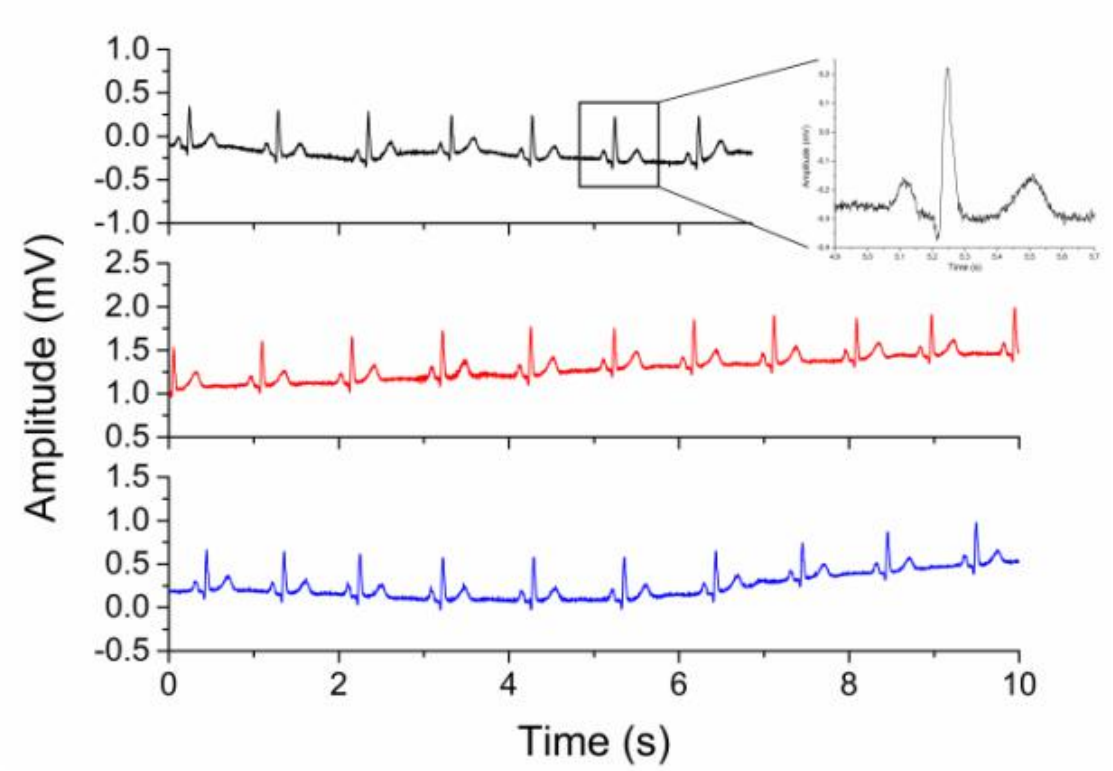

Figure 5.23 ECG signal recorded with different electrolytes with saline solution (top), hydrogel (center) and Ag/AgCl electrodes (bottom).

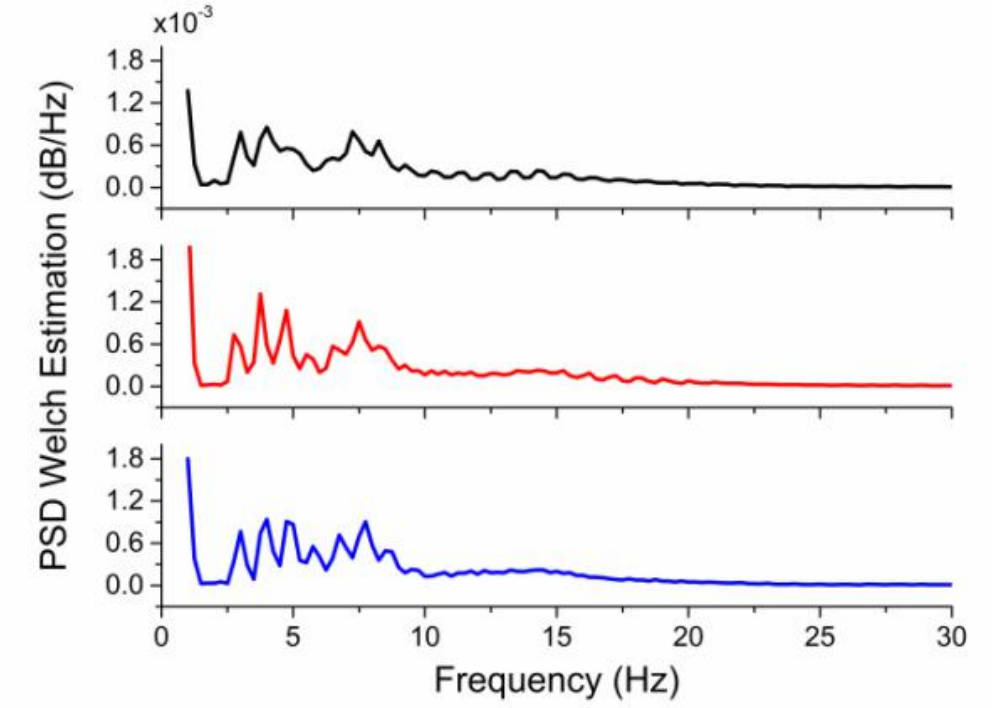

Figure 5.24 ECG power spectral density Welch's estimations with saline solution (top), hydrogel (centre) and Ag/AgCl electrodes (bottom)

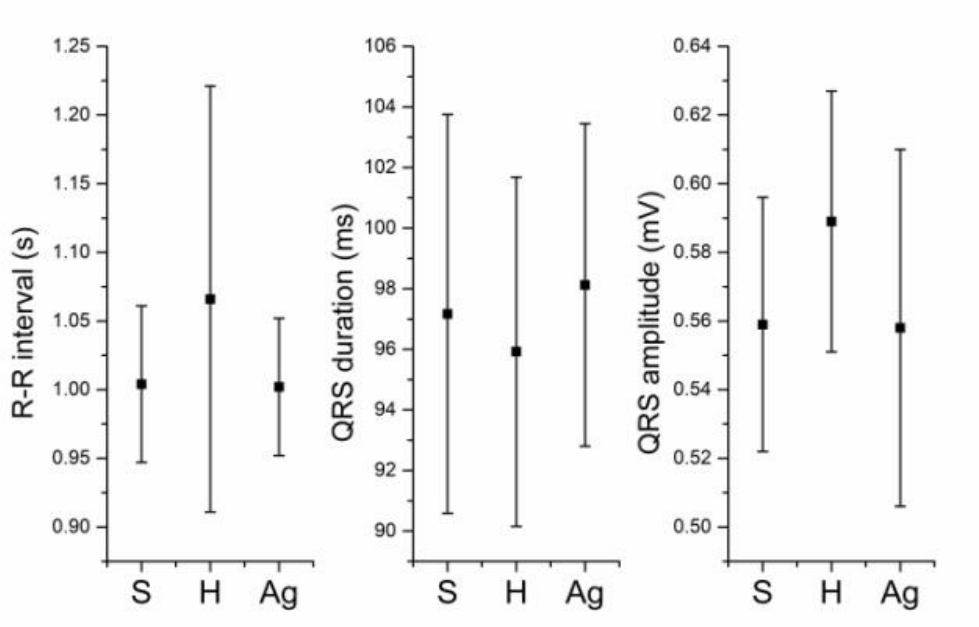

Figure 5.25 QRS features obtained with textile electrodes with added saline (S), hydrogel (H), compared with disposable Ag/AgCl electrodes (Ag).

5.5.4 Clinical features from textile ECG electrodes

A visual inspection of the ECG traces of the ten voluntary subjects reported a signal quality that can be considered adequate for diagnosis, without significant differences compared to disposable Ag/AgCl electrodes.

Dry textile electrodes failed in obtaining a skin contact impedance level below 600 kΩ, which is the limit in the GE ECG device to assert a lead-off alarm. In this case, CardioSoft stops saving the signal from that lead. It should be considered that the textile electrodes application (in this case accomplished through an adhesive medical tape) did not allow to press them on the skin, as would happen with an elastic band or t-shirt. Then, a high value of impedance is reasonable in this condition. By wetting the electrodes with saline, the impedance reaches remarkably low values, in the light of the abovementioned setup, even comparable to those achievable with the commercial electrodes and several times lower. To provide a clue on this parameter, we computed the grand mean (i.e. the mean, over the whole set of subjects, of ZVi) and the related standard deviation. The results are comparable when removing a single statistical outlier among the textile electrodes: 22 ± 23 kΩ for the Ag/AgCl electrodes and 29 ±31 kΩ for the textile ones (the outlier marked 378 ±219 kΩ due to the difficulty in applying the electrodes on the subject's skin) without statistically significant differences between the two types of electrode. From the analysis of

the measurements performed by the CardioSoft on the signals and medians, we obtained no statistically significant difference between the two populations of textile and Ag/AgCl electrodes for any one of the clinical features. The mean and standard deviation of such features are presented in Table 5.3.

Feature	**Ag/AgCl**	**Textile**
HR [bpm]	67 ± 13	66 ± 11
P duration [ms]	102 ± 13	101 ± 15
QRS duration [ms]	95 ± 6	93 ± 8
PQ interval [ms]	180 ± 80	190 ± 80
QTc interval [ms]	415 ± 20	415 ± 20

Table 5.3 Main temporal features comparison. Differences are not statistically significant.

About QRS_{Vi} and QRS_{M}, it is worth noting that alternate measurements with different electrodes in the same position can erroneously lead to ascribe to the electrodes the morphological differences descending from the physiopathological time variance of the ECG waveform (Kumari et al. (2017)). Taking into account the considerably larger ECG machine input impedance compared to the measured skin-electrode impedance, this parameter marginally influences QRS_{Vi} and QRS_{M}, Table 5.4.

Feature	**Ag/AgCl**	**Textile**
QRS_{V1} [mV]	1.4 ± 0.7	1.3 ± 0.4
QRS_{V2} [mV]	1.6 ± 0.5	1.6 ± 0.4
QRS_{V3} [mV]	1.6 ± 0.6	1.6 ± 0.7
QRS_{M} [mV]	2.1 ± 0.6	1.9 ± 0.5

Table 5.4 QRS_{Vi} and QRS_{M} features comparison. Differences are not statistically significant.

In terms of noise analysis, performed excluding the statistical outlier for the impedance, the rms for the Ag/AgCl electrodes was 2 ± 1 µV whereas, for the textile ones, 3 ± 2 µV. The difference was not statistically significant. Remarkably, these values are low if compared to the both QRS_{M} and peak-to-peak noise of the ECG machine, even though the presence of the notch filter surely influenced this result. Overall, textile electrodes were noisier, with a rms increase of 19% on average, except for a single subject (>300%). In that case, the subject's anxiety led to a noisy signal on which WD was too aggressive, in turn leading to larger

residual, despite the quite low skin-electrode contact impedance. The high quality of the results favorably compares to those achieved with the previous technology, with electrodes characterized by a wider active area (9 mm ^{2}) and applied after a mild skin treatment (Pani et al. (2016b).

5.5.5 Results with smart shirt

After this complete validation where the performance of screen-printed textile electrodes was tested in different working conditions, these electrodes were studied when integrated in a smart shirt. This possible use of screen-printed electrodes is interesting, because in this case the electrodes could be completely seamless and would not require any fixing element to maintain them in place.

At the same time, as demonstrated in Figure 5.26, they present a limitation in term of skin contact impedance, because the adhesion with the skin depends on the t-shirt adhesion, in turn. Even with an elastic shirt, like the one used in this case, it is difficult to guarantee a good contact for all the duration of the recording. After reaching a stable condition, it was possible to acquire the ECG signal with different configurations and the results are shown in Figure 5.26.

5.6 EMG electrodes

Taking in account the results obtained with wet textile electrodes in the detection of the ECG we used them also for the acquisition of the EMG. To perform this analysis, at first we used wet textile electrodes with the same instrumentation described before to record the ECG signal.

The first protocol we designed for the detection of the muscular activity concerned the placement of the electrodes on flexor carpi radialis and record a series of voluntary movements.

As shown in Figure 5.27, with wet textile electrodes it is possible to acquire signals with a high quality in terms of baseline drift and noise level.

This approach to the electromyographic signals is not completely reliable because their results are related to the physiology of the subject involved in the analysis. For this reason, if

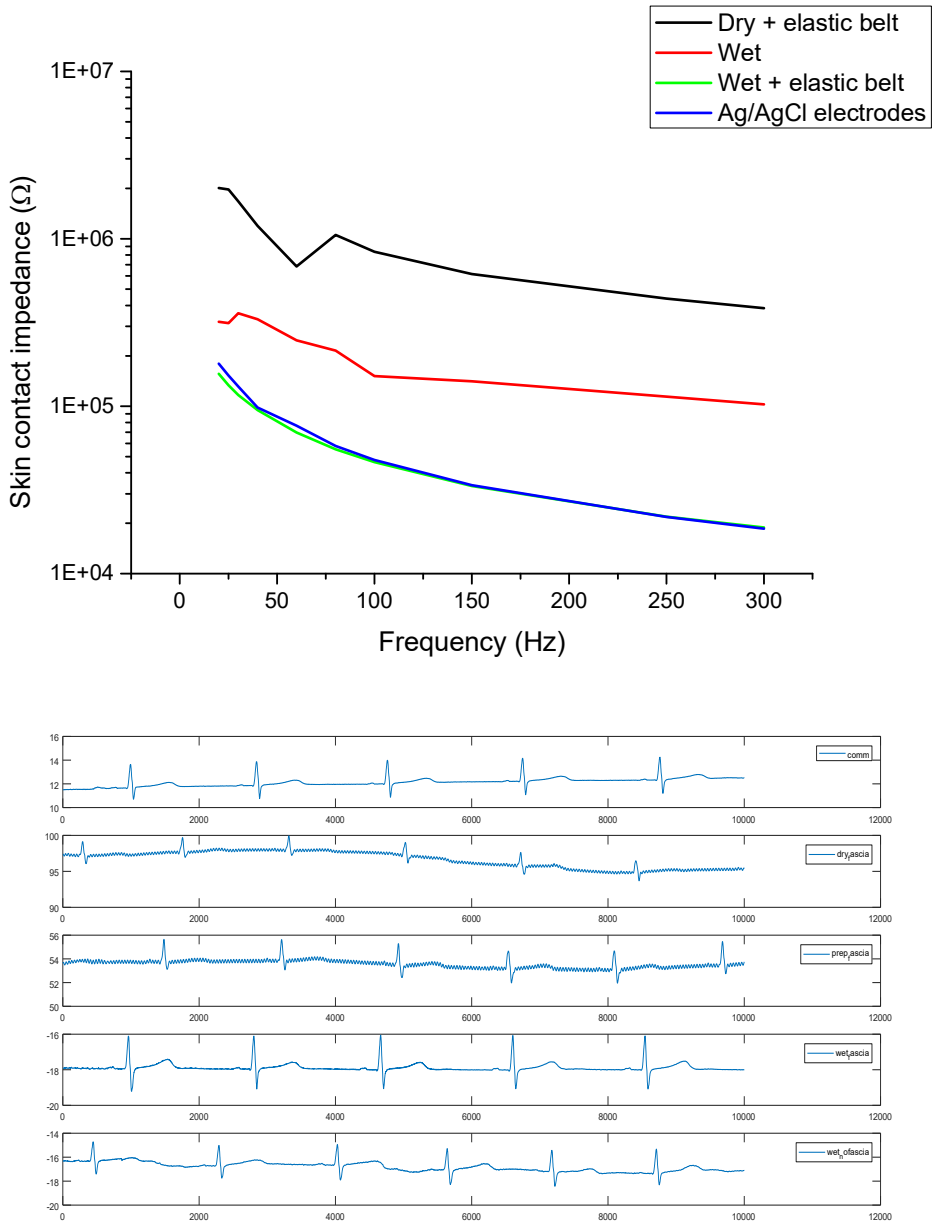

Figure 5.26 Skin-contact impedance and ECG signals recorded with smart shirt in different conditions.

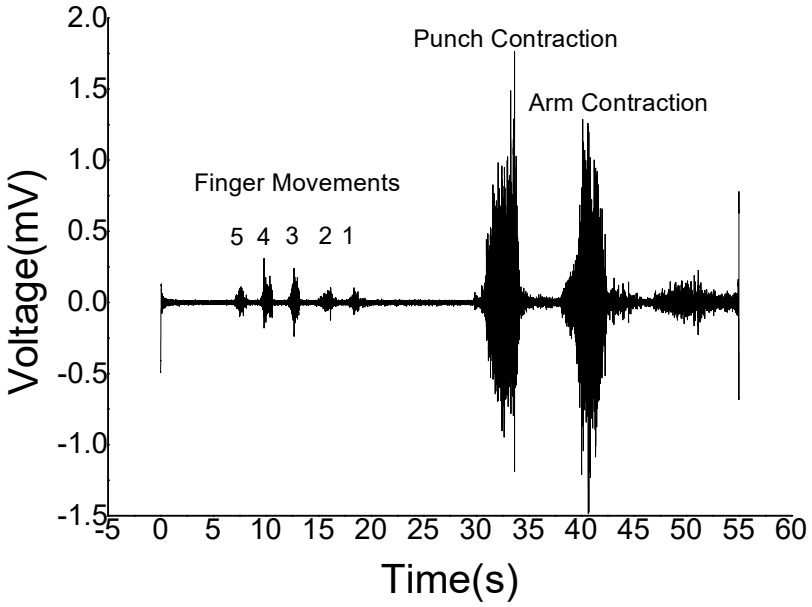

Figure 5.27 Voluntary surface EMG signal with markers related to specific actions

we ask to different volunteers to repeat exactly a specific movement or sequence of movements, the actual EMG will be different because of physiological variabilities (Chowdhury et al. (2013)).

To avoid the limitation introduced by a voluntary muscle activation, thus improving repeatability, we exploited a stimulated protocol. With the adoption of an electrical stimulator, and stimulating above the nerve innervating the muscle where the sEMG electrodes are placed, it is possible to study the electrical M-wave, like the ones shown in Figure 5.28, captured with electrodes in different conditions.

The sheet resistance measured for the textile EMG sensors was 390 ± 60 Ω/sq. and 410 ± 150 Ω/sq. respectively for the ∅24 and ∅10 electrodes.

The box-plot of the skin-contact impedance, measured in different conditions with both screen-printed and gelled electrodes, are shown in Figure 5.29. The results of the Kolmogorov–Smirnov test on these skin-contact impedance populations suggested the adoption of the U test. This test revealed a significant statistical difference between disposable gelled Ag/AgCl electrodes and dry textile electrodes of any size $p < 0.002$), and also for ∅10 electrodes with saline ($p = 0.0036$). Conversely, no statistically significant difference was found in the other cases (∅24 and ∅10 with hydrogel, $p > 0.7$ and ∅24 with saline, $p = 0.97$).

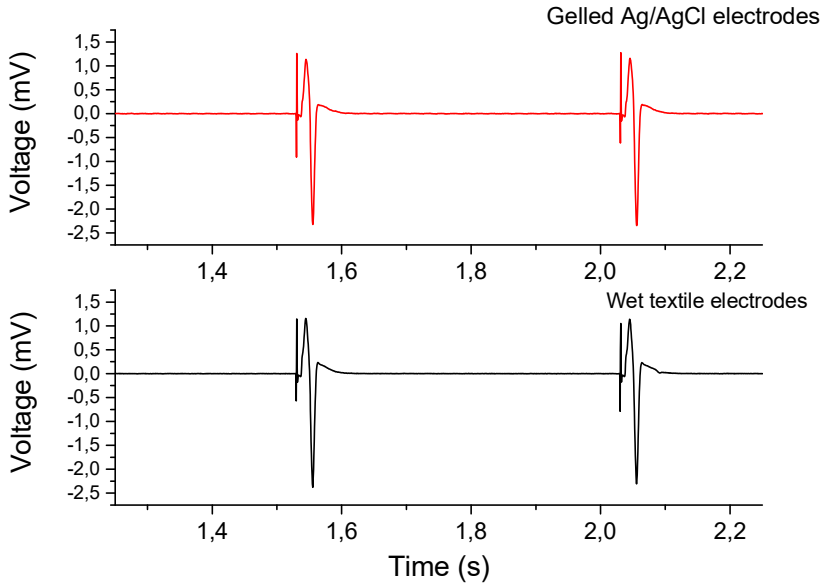

Figure 5.28 M waves recorded with gelled Ag/AgCl electrodes and wet textile electrodes

Figure 5.30 shows the *rms* of the signal at rest (noise) for all the electrode conditions. The Welch's PSDs of such signals, for a single subject in each recording shown in Figure 5.31. The same behavior observed at rest was also obtained during the stimulation protocol in the quiescent regions of the surface EMG signals.

The results of the Kolmogorov–Smirnov test on these noise populations suggested again the adoption of the U test, since distributions were not normal. This test revealed a significant statistical difference again between disposable gelled Ag/AgCl electrodes and dry textile electrodes of any size ($p < 0.0002$), but also for ∅24 electrodes with saline ($p = 0.0028$). Conversely, no statistically significant difference was found in the other cases (∅24 and ∅10 with hydrogel, $p > 0.10$ and $p > 0.85$ respectively, and ∅10 with saline, $p > 0.97$).

During electrical stimulation, the average M-wave per each electrode in each recording condition was computed. Figure 5.32 presents two examples of average M-waves obtained on the same subject with all the electrodes tested in this work, considering the different measurement conditions for the textile ones.

Figure 5.33 presents the linear regression model adopted to compute the parameters used to compare the disposable gelled Ag/AgCl electrodes with their textile counterpart, for a single subject and the larger electrode size (∅24). The average parameters obtained from the linear regression, along with their error expressed by the standard deviation over 10 subjects, are reported in Table 5.5.

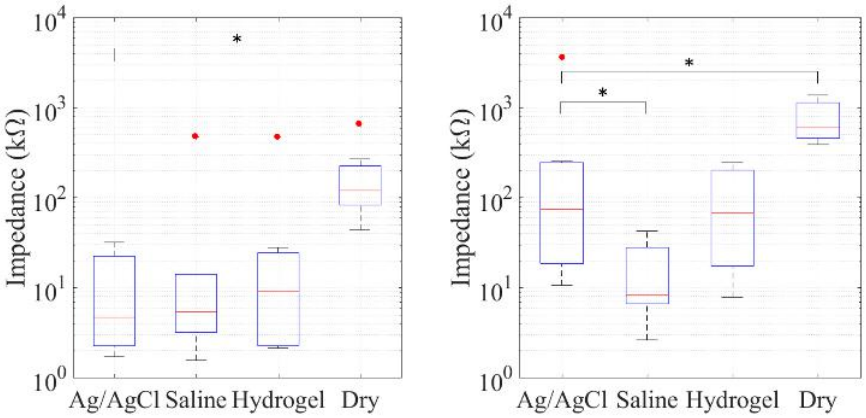

Figure 5.29 Box-plot of the skin-contact impedance for each electrode size and measurement condition (from left to right, for ∅24 and ∅10)

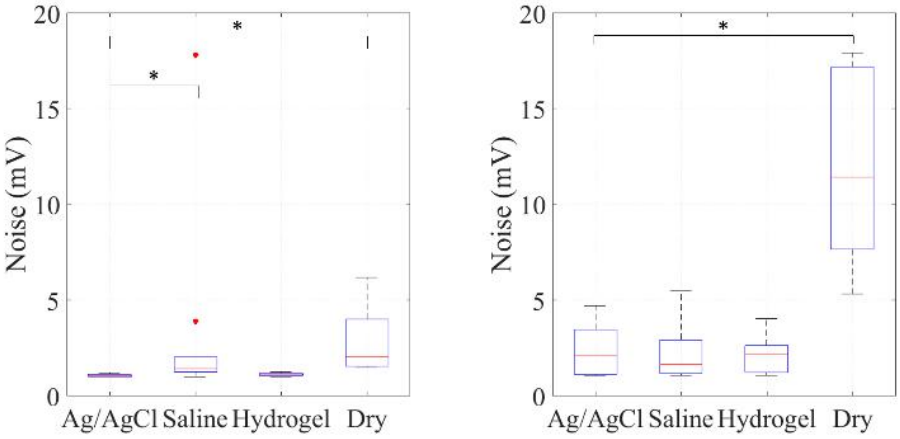

.

Figure 5.30 Box-plot of the rms of the noise for each electrode size and measurement condition (from left to right, for ∅24 and ∅10).

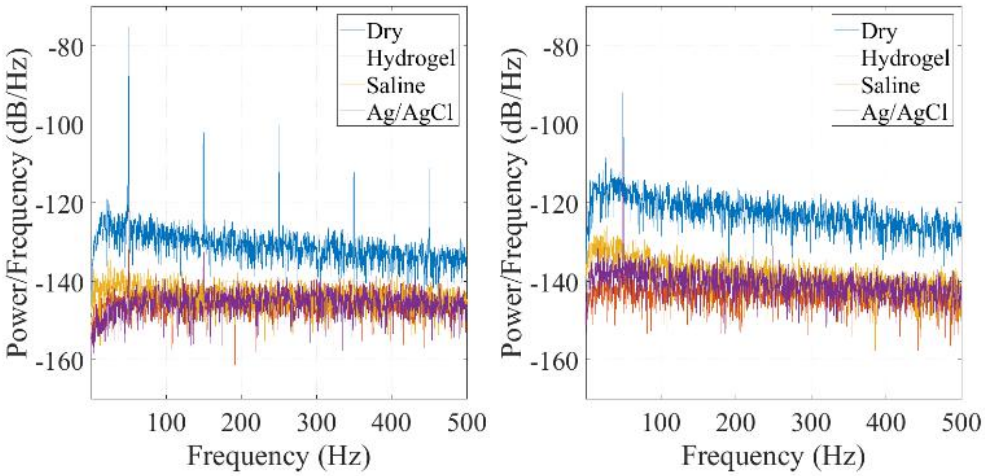

Figure 5.31 PSD of the noise for each electrode and condition (from left to right, for ∅24 and ∅10).

∅24 electrodes			∅10 electrodes		
NMSE %	Dry	3±2	NMSE %	Dry	4±3
	Saline	2.1±1.4		Saline	5±2
	Hydrogel	1.6±1.4		Hydrogel	4±3
SLOPE mV/mV	Dry	1.1±0.1	SLOPE mV/mV	Dry	1.0±0.1
	Saline	0.98±0.09		Saline	1.00±0.12
	Hydrogel	0.98±0.07		Hydrogel	1.09±0.08
R^2	Dry	0.98±0.01	R^2	Dry	0.98±0.01
	Saline	0.98±0.001		Saline	0.97±0.02
	Hydrogel	0.988±0.007		Hydrogel	0.98±0.01

Table 5.5 Comparison between textile and commercial electrodes in terms of linear regression parameters

5.6.1 EMG results with smart shirt

From an initial analysis of the signals acquired with the sensorized t-shirt, it was evident that not all the electrodes presented a good contact with the skin and, even in this case, this is confirmed from the skin contact impedance in Figure 5.34. As can be seen in Figure 5.34, the raw signals acquired during the dynamic tests by the left external abdominal oblique muscle reveal a significant abrupt baseline shift artifact with the same pacing of the contractions performed by the subject. This artifact, about 15 mV large, is larger than the interference

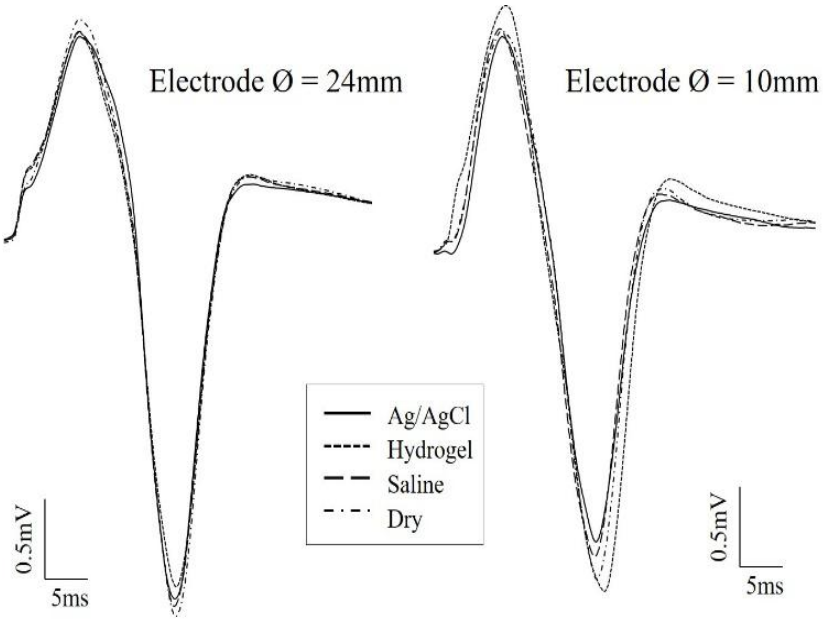

Figure 5.32 Average M-wave acquired on the same subject with the different electrodes in the different measurement conditions (from left to right, for ∅24 and ∅10).).

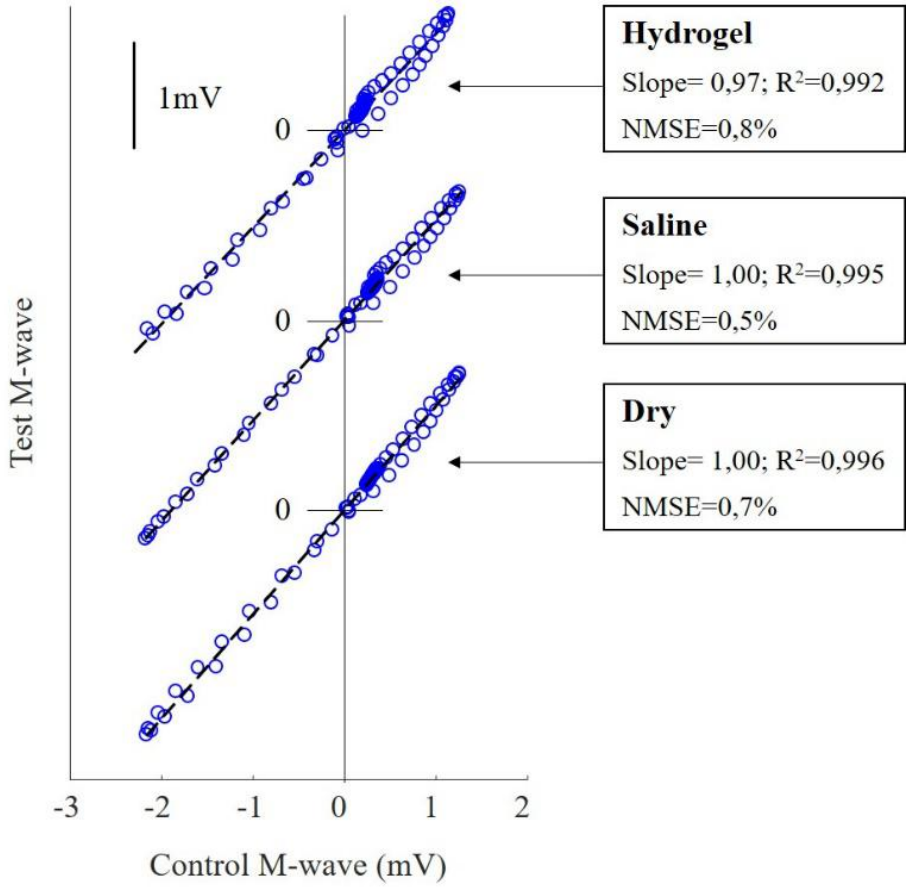

Figure 5.33 Linear regression between average M-waves recorded with ∅24 disposable gelled Ag/AgCl electrodes (control wave) and screen-printed textile electrodes (test wave).

pattern associated to the muscle contraction, that is also present and embedded in the signal and was highlighted in Figure 5.35 removing the artifact due to the movement applying to the signal a high-pass filter. This behavior was not present during the isometric contractions, and it is due to the movement of the electrodes on the skin because of the absence of any adhesive layer able to keep them in place. Because of the abnormally large amplitude of the artifact, special care should be reserved to the signal processing in real applications in order to take into account the step response of the filters evoked by the electrophysiological signal.

In general, the signals are affected by noise, which may be due to different causes (basic drift due to the movement of the cables or the subject during acquisition, ECG, network interference etc.), which manifests itself with unwanted changes in the signal. In the signals presented it was evaluated by averaging the RMS on a 10-second sliding window and the results are presented in Table 5.6.

	Left abdominal oblique muscle	**Right abdominal oblique muscle**
Gelled Ag/AgCl electrodes	0.90 μV	0.58 μV
Wet textile electrodes	1.51 μV	0.62 μV

Table 5.6 Noise estimated as the RMS of the signal at rest.

The results obtained with the smart shirt designed to acquire the EMG signal, according with the model developed for the ECG, demonstrate that screen-printed textile electrodes could represent an optimal solution to acquire these physiological signals in a comfortable and unobtrusive way.

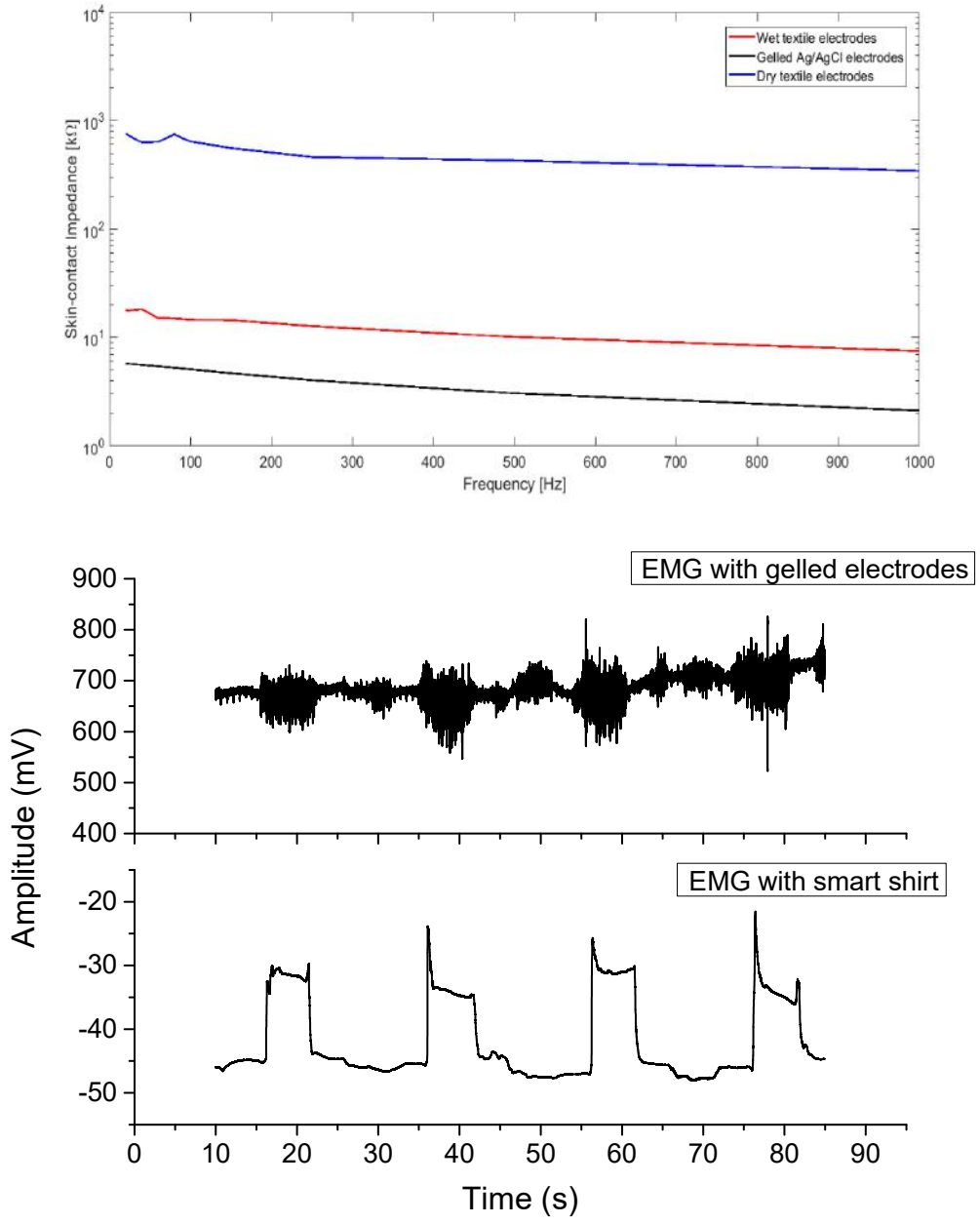

Figure 5.34 Skin-contact impedance (top) and EMG signal (bottom) recorded during the exercise for the left external abdominal oblique muscle with standard and wet textile electrodes.

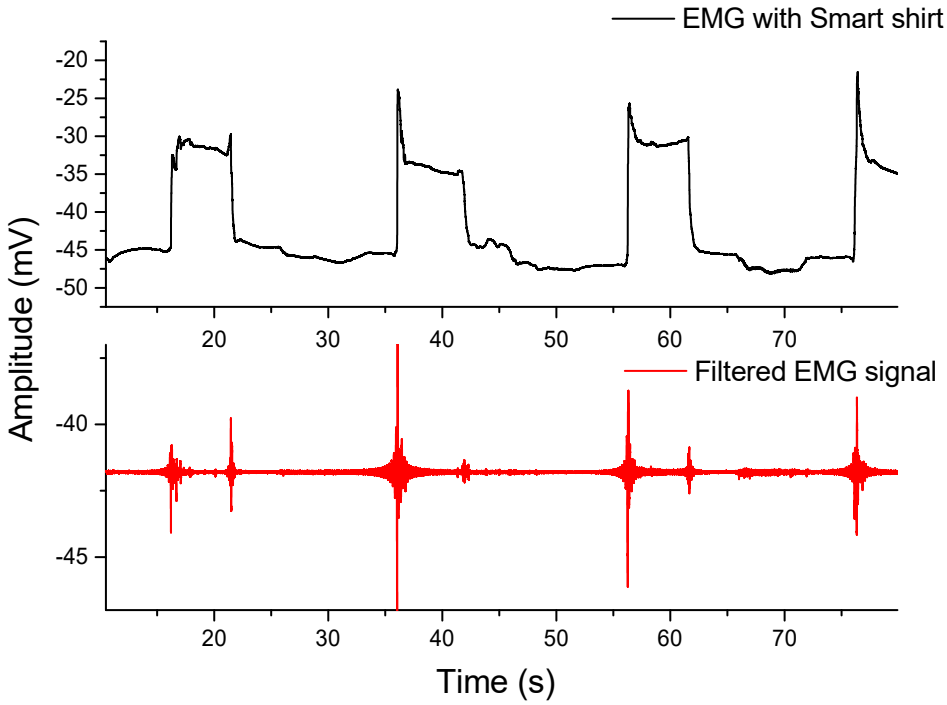

Figure 5.35 Raw and filtered EMG signal recorded with a smart shirt during dynamic exercises for external abdominal oblique muscles.

Chapter 6

Discussion

6.1 Preliminary testing results

6.1.1 Dip coating

The effect on the conductivity of the second dopant and different affinity to the PEDOT:PSS treatment of the substrate material has been measured and is presented in Table 2.1. It can be clearly seen that polyester performs sensibly better than cotton. In preliminary tests, we also observed that treated polyester fabrics were mechanically stronger and withstand better the sewing than cotton, which becomes more fragile after treatment. Given these results, only polyester electrodes treated with glycerol were selected for impedance and ECG recordings.

6.1.2 ink-jet printing

As we have seen in the previous chapters, the limited size of the drops in the ink-jet printing process and their reduced volume tend to create single layers with a high geometrical resolution, thanks to the limited amount of conductive ink deposited. For this reason, it is necessary to repeat the process several times and overprint a large number of layers to reach the desired value of sheet resistance. This is demonstrated in Figure 5.2 where it is possible to see the relationship between the sheet resistance and the number of printed layers. The images demonstrate also that the increment in the layers number does not affect the resolution because the drops are too small (both 10 and 15 microns) to spread over the fabric for capillarity. Otherwise, the fabrication of electrodes with 6, 7 and 8 layers is not the optimal solution because printing too many layers increase the possibility to incur in the

nozzles clogging. In fact, the cartridge with the heated plate tends to dry the drops in the nozzles interrupting the printing process not depositing on the fabric the desired amount of ink. In addition, this printing repetition in the fabrication process decreases dramatically the throughput because to print 8 layers with a limited area of 2 mm X 4 mm could last even 3 hours.

6.1.3 Screen printing

The screen-printing process at the same time is a faster procedure than the ink-jet printing but the amount of ink deposited is controlled by a high number of parameters involved in the process. A little variation in one of these parameters could change the amount of ink deposited and for this reason, even repeating the process with a high reproducibility, all the textile electrodes were tested after the fabrication with an optical microscope and 4-probe measurements to evaluate the geometrical resolution and the sheet resistance.

To optimize the printing process we developed two different inks based on PEDOT:PSS and the best results were obtained with the solution characterized by a high viscosity. This decision was taken because this ink, once dried after the deposition, remained on the fabric surface and did not penetrate through the fibers reaching the other surface. With this behavior is possible to obtain good results in terms of geometrical resolution and surface conductivity. With a lower viscosity, it was evident the percolation and the loss of resolution and in that case the dip coating remains the better solution for the deposition of a conductive ink.

In literature, there are works that, after printing, analyze the amount of ink deposited on the surface. The analysis of the morphology of the fabric before and after the screen printing was avoided after several considerations. First of all, the extreme roughness of the fabrics excludes any possibility to profile the surface with a microscopic scale and it is impossible to compare the profiles of treated fabrics with the untreated ones.

Usually, these measurements are performed to study the deposition on plastic substrates because dried drops could provide information about the ink or the surface included the conductivity. This is not possible with a textile substrate because the capillarity induces the penetration of the drops in relation to their viscosity. Even with the conductive ink developed from PEDOT:PSS with a high viscosity, the superficial layer is comparable with the ink penetrated in the fabric, as shown in Figure 5.6.

Another important limitation to the morphological analysis is the selected area, because these tests require a comparison between an image without the polymer and another one

with the ink. The fabric is composed of different fibers and it is almost impossible to find two microscopical images with identical fibers. This is evident in (Tsukada et al. (2012b)), where treated and untreated filaments are compared. They show a macroscopic image with PEDOTPSS silk bundled fibers and pristine silk thread (Figure 6.1A). A transmitted light observation of a cross-section of pristine silk and PEDOT:PSS silk thread (Figure 6.1B, Figure 6.1C) In the same figure (Figure 6.1D, Figure 6.1E, Figure 6.1F) the scanning electron microscope (SEM) images reveal a membranous covering of PEDOT:PSS over the entire surface of the silk fibers. From this example, it is possible to see the great difference between different fibers and it is difficult to compare fairly fibers with and without PEDOT:PSS. For this reason, the deposition was tested macroscopically and only in terms of sheet resistance to compare in a second moment the performance with the measured electrical properties.

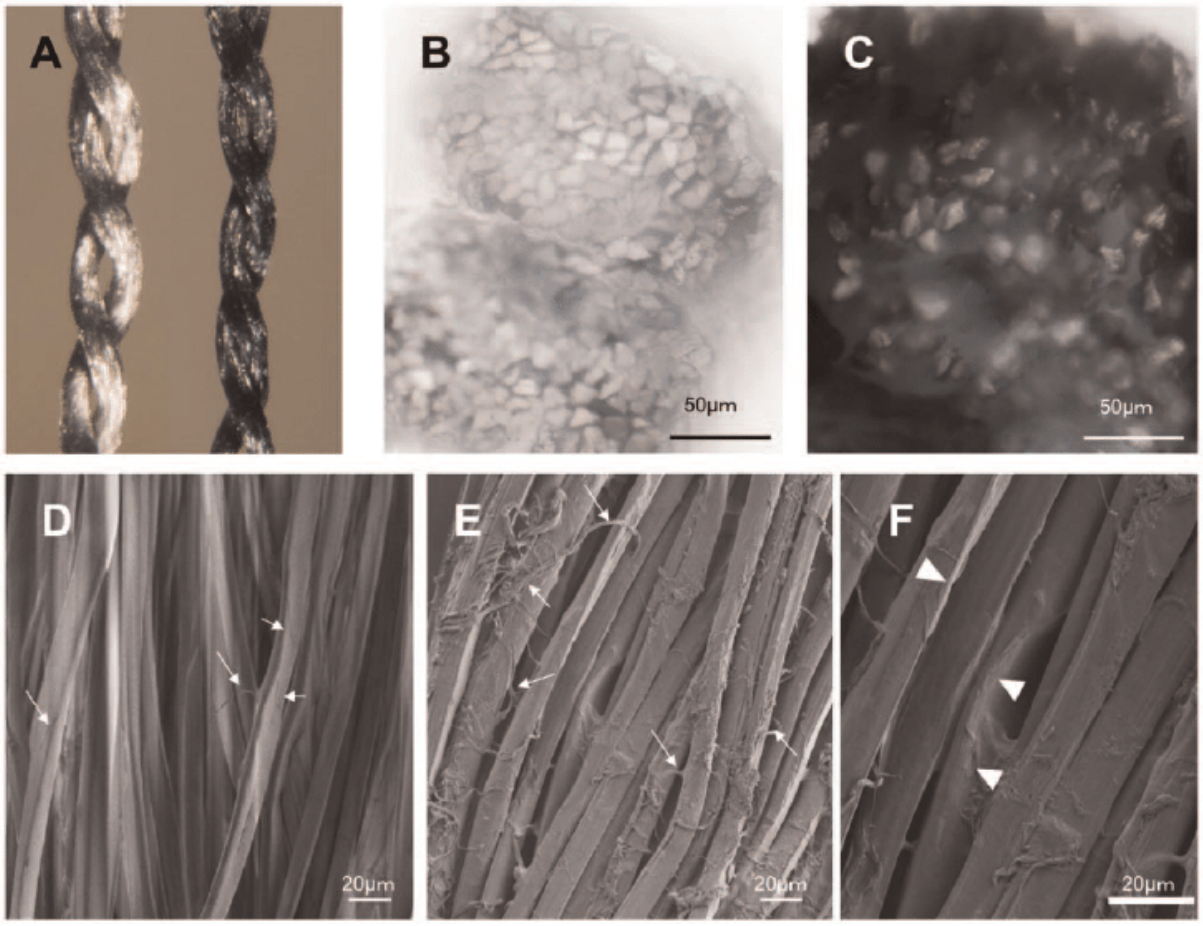

Figure 6.1 A. Macroscopic image of pristine silk thread (left) and PEDOT:PSS combined silk thread (right). B. C. Cross-section of pristine silk (B) and PEDOT:PSS silk thread (C) observed with a transmitted light optical microscope. D–F. Scanning electron micrograph of pristine silk (D) and PEDOT:PSS silk thread (E, F).

6.1.4 Washing resistance

Repeating the washing procedure 20 times, the fabric and the ink suffer a stress that affects the performance of the electrodes. This is visible in Figure 5.15, where it is evident the presence of spots where the ink was removed or cleaned from the surface. Another aspect less visible from the optical analysis is the increment of the roughness of the fabric due to the fibers degradation. The first aspect affects the sheet resistance as demonstrated in Figure 5.16 with 4-probes measurements, where this variation could be approximated by a linear trend with a 99% confidence. Again, this parameter (whose slope was evaluated as 4.0 ± 0.2 Ω/(sq·cycle)) cannot completely describe the electrode performance. In fact, both impedance and noise after 10 washing cycles were stabilized, reaching the respective values of about 0.9 kΩ and 230 μV. Remarkably, the dry washed electrodes showed a skin contact impedance compatible with the acquisition of an ECG signal, as clearly depicted in Figure 5.22. It is conceivable that this effect could be due to the changes in the morphology of the surface caused by the washing procedure. This process also tends to defibrate the conductive garment, increasing the effective area in contact with the skin. In dry conditions, a higher active area increases the skin contact impedance related to dry brand-new textile electrodes. Wetting the screen-printed electrodes with saline solution or adding a hydrogel layer, the fibers are smoothed and the performance is comparable or lower than the one obtained with brand-new electrodes. The results revealed also that these electrodes could be washed up to 20 times without compromising their ability to acquire the ECG signal, maintaining an acceptable signal quality comparable to that of commercial electrodes.

6.1.5 Stretching resistance

All the tested inks are somehow flexible, but this flexibility depends on two factors, the thickness of the printed layer and the selected substrate. This was demonstrated clearly by the optimal results obtained with the inks screen printed onto an unstretchable fabric as cotton. In fact, the screen-printed textile electrodes deposited on cotton presented enough flexibility to enable their everyday use without losing in terms of sheet conductivity.

Regardless of substrate, it was observed that conductive elements composed of a thin layer of ink, presented a high flexibility. The deposition of these elements was simplified by screen-printing, were the amount of ink was accurately controlled because it was noticed that in case of areas with wide variation in thickness the ink tends to produce fracturing. The same effect was noticed after stretching tests executed on stretchable fabrics. The results

demonstrated a high increment in the impedance and noise values compared to that with the brand-new electrodes, reaching 250% of their starting values. This is due to polymer film cracking on the electrode surface caused by the physical separation of the fibers shown in Figure 5.13.

In conclusion, it was observed that substrates which are flexible, but not stretchy (such as cotton or paper) work better than materials like Lycra which could be stretched in one or two directions. Furthermore, the screen-printed textile electrodes can be used to produce smart technical sportswear providing that special care should be taken to avoid excessive stretch forces that could irreparably damage the conductive surface.

6.2 ECG results

After the physical and electrical characterization, a series of tests was performed to evaluate the performance of the proposed electrodes as ECG sensors, in controlled conditions, i.e. by directly coupling the conductive surfaces of the two electrodes, getting rid of the variability introduced by the coupling with the skin. The results clearly show how the electrolyte increases both the impedance and the noise, doubling the values obtained under dry condition. It should be noted that these results are within the limits imposed by the standard, except for the noise level measured with the hydrogel. The effect of the electrolytes on the impedance is confirmed by the analysis over different frequencies in the typical ECG band, presented in Figure 5.20. In this figure, the fluctuation below 100 Hz is partially due to the lower electrical mobility of organic semiconductors at low frequencies (Rivnay et al. (2016). Moreover, the difference in the impedance can be explained by the increase in the capacitive component introduced by the addition of an electrolyte layer in between the two-faced electrodes. In both cases, the impedance is higher when the hydrogel layer is applied, mainly because of the physical separation between the electrode surfaces. This condition also influenced other parameters, such as the DC offset, since the hydrogel layer leads to an ionic charge distribution at the interface with the polymer (Baura (2012)), were interactions between the solid hydrogel polymer and the PEDOT:PSS can occur. This polarization was confirmed also from the DC offset bias recorded over a long period and the reduced current applied between the textile electrodes excludes the conducive polymer oxidation and confirms the contribution of the interface between the electrode and the electrolyte. Even though textile electrodes are aimed at the development of smart garments, and not for clinical use, we also performed the analyses related to the simulated defibrillation recovery. The obtained results agree with the

limits of the organic polymers, which present a threshold voltage of about 1.6 V for a non-reversible polarization (Wen and Xu (2017). In this case, the application of the defibrillation discharge irreparability polarizes the electrodes, making them unusable, so that the other limits imposed by the standard are no more respected. The reduced current applied to study the DC offset was not enough to polarize the textile electrodes. After benchtop measurement characterization, we evaluated the features of these screen-printed electrodes as ECG sensors on human subjects. The skin contact impedance results decreased with addition of different electrolytes, Figure 5.21a, because of the hydration of the skin and its better coupling with the functionalized fabric (Zhou et al. (2015)). Remarkably, the skin contact impedance without any electrolyte is strongly affected by the skin characteristics of the different subjects (Pani et al. (2016b), also considering that no skin preparation was performed to simulate a real application scenario. This aspect, along with the limited validity of the assumptions behind the skin contact impedance estimation model, hamper a detailed analysis of the curve shape that, conversely, could be easily performed in presence of electrolytes, Figure 5.21b. A decrease of up to two orders of magnitude between the values recorded with electrolytes and the values without electrolytes under the same measurement conditions was recorded, leading to a performance close to that achievable with commercial electrodes. Remarkably, this behavior is opposite to what was observed in benchtop measurements, where the effect of the signal conduction through the skin was not present. As shown in Table 5.2, a strong statistical correlation was observed between the skin contact impedance curves obtained with Ag/AgCl electrodes and textile electrodes with addition of hydrogel and saline. In addition to the aforementioned conditions, there are several other aspects related to the production process that can affect the skin contact impedance. This makes it unfair any detailed comparison with other studies in the scientific literature. First, the polymer-based ink could be composed of different PEDOT:PSS formulations commercially available (Heraeus CleviosTMPH500, CleviosTMPH1000, etc.), characterized by a different conductivity. Furthermore, to produce the ink, different secondary dopants and other surfactants are typically added to improve the conductivity and change the ink viscosity. This, in turn, also influences the amount of polymer that is effectively transferred to the fabric. Moreover, the deposition processes have a strong influence on this aspect. Nevertheless, the skin contact impedance results are comparable with those reported in (Bihar et al. (2017), where ink-jet printing on a commercially available pantyhose (100 wt % polyamide) was used, only when eight layers of PEDOT:PSS and five layers of liquid ionic gel were deposited on the fabric. Also direct patterning of PEDOT:PSS on fabric, with the same ionic gel, presents similar values for this parameter (Takamatsu et al. (2015). Compared to (Pani et al. (2016b), a worse impedance is achieved, as clearly

demonstrated by the acceptable performance of the dry electrodes in that work. However, in (Pani et al. (2016b) a mild skin treatment was performed, and the electrodes were produced by dip coating, leading to a significantly higher amount of polymer deposited on the fabric, compared to screen-printing. The importance of this aspect is evident when considering the number of layers that must be printed on the fabric to achieve a good conductivity, when using ink-jet printing (Bihar et al. (2017)). The results reported show the comparison between disposable gelled Ag/AgCl electrodes and the screen-printed electrodes with addition of electrolytes. These results confirm the possibility of using the proposed textile electrodes as ECG sensors, since the signal quality and the spectral analyses reveal high similarity with the commercial Ag/AgCl electrodes. From a spectral perspective, the PSD values obtained using the different electrodes overlap. This is reasonable in the light of the impedance behavior of the different electrodes (Figure 5.21b). Furthermore, the estimated PSD values are analogous to those obtained in other studies with textile electrodes realized by stainless steel threads twisted around a standard continuous viscose textile yarn, with addition of solid hydrogel (Scilingo et al. (2005)). Obviously, the quality of the signals recorded with the different electrodes is similar also when looking at the ECG morphology in the time domain (Figure 5.23). Baseline drift is comparable, even though this is a critical aspect for textile electrodes (Paul et al. (2014a)), and the primary waves and the complex of the ECG signal are clearly recognizable without significant distortion. The QRS morphological features (QRS amplitude and QRS duration) and the RR interval reveal a substantial coherence, with the variability depending on their physiological changes over time (60 s), across the different electrodes confirmed, respectively, by a 96 % ± 4% confidence level for saline solution and a 70% ± 8% confidence level for hydrogel compared with the results computed using disposable Ag/AgCl electrodes. Such results reveal how the best condition for ECG acquisition with screen-printed textile electrodes is represented by the addition of saline to the electrodes. In fact, even though the hydrogel addition could help in contrasting motion artifacts because of the better adhesion to the skin, the previously discussed higher noise of this solution hampers a correct delineation. The novelty of the proposed approach lies in the functionalization procedure used to develop textile ECG electrodes directly on the fabric, by screen-printing with a biocompatible conductive polymer. In fact, PEDOT:PSS-based textile electrodes can be fabricated in several ways, i.e. by coating single yarns (Tsukada et al. (2012b), by immersion of the whole fabric (Pani et al. (2016b) or by a controlled deposition of a polymer solution on the surface of a finished fabric (Bihar et al. (2017); Takamatsu et al. (2015)). Excluding the first approach, which cannot be applied to finished fabrics, a major difference exists between the other two. In fact, in the second process, the

complete encapsulation of all the fibers is achieved without any control on the polymer amount, whereas in the third approach, the amount of polymer deposited on the fabric surface is finely controlled. However, by treating only the fabric surface, the volume of PEDOT:PSS transferred to the fabric by screen printing is several times lower than the amount transferred by immersion, where a bulk of conductive material is obtained. This is why the skin contact impedance under dry condition for screen-printed electrodes is higher, thereby hampering the ECG acquisition (Pani et al. (2016b)). Nevertheless, by the controlled deposition of the ink, screen printing allows a good reproducibility, a high geometrical resolution and the possibility to functionalize components of finished garments, enabling the realization of seamless smart textiles. Using the polyester mesh applied in this study, with 43 lines/cm, it is possible to achieve a geometrical resolution of 0.3 mm. Previous works on SPEs adopted the same technique but with a different ink (such as carbon-based (Chlaihawi et al. (2015)) or silver-based (Rattfalt et al. (2007)) on a plastic substrate. Compared to the proposed approach, such inks present a higher conductivity. However, for wearable applications, SPEs cannot be directly realized on the garment, requiring an assembly procedure. Furthermore, the plastic substrate is less conformable and breathable than a fabric, leading to reduced comfort and potential skin irritation in long-term monitoring applications. ink-jet printing was also proposed for the realization of polymer-based textile ECG electrodes. In (Bihar et al. (2017)), a Dimatix DMP-2800 ink-jet printer was used to deposit a PEDOT:PSS ink on synthetic fabric. The same commercial polymeric solution adopted in this work was used, but with different additives to adapt the final ink viscosity to the printing process. In fact, viscosity influences the ink drops size, which in turn defines the geometrical resolution and the shape reproducibility. The best resolution achievable with that printer, by using 1 pL cartridges, is around 20 µm, whereas screen-printing, depending on the screen used, can reach only 200 µm. Despite the better resolution, ink-jet printing introduces huge limitations in terms of throughput since, even with cartridges by 10 pL, the drops deposition is a slow process. In fact, the reduced amount of ink deposited by each drop requires several layers (up to 10 in (Bihar et al. (2017)) to provide enough conductivity. Conversely, screen-printing allows producing at the same time, with a single ink layer, several electrodes, even though characterized by a lower resolution. Notably, such a high resolution is not required for textile ECG electrodes whereas the production costs, significantly higher for ink-jet printing because of the limited throughput, are of paramount importance. Finally, screen-printing is a well-known and widely used printing technique in fashion industry, and could be easily adapted to enable smart garments development by replacing the ink, compared to more custom printing procedures (Takamatsu et al. (2015)). The quality of screen-printed textile

electrodes as sensors for the ECG electrodes was evaluated also from a clinical perspective. For this purpose, the signals acquired with textile electrodes were visually inspected by the cardiologists to see the signatures typical of the different subjects' conditions and any statistical difference was noticed with the golden standard. This similarity in the performance was recorded comparing QRS_{Vi}, QRS_{M} and the main temporal features and this validation represent an optimal starting point to use these electrodes also for clinical acquisitions.

The quality of screen-printed textile electrodes as sensors for the ECG electrodes was evaluated also from a clinical perspective. For this purpose, the signals acquired with textile electrodes were visually inspected by the cardiologists to see the signatures typical of the different subjects' conditions and any statistical difference was noticed with the golden standard. This similarity in the performance was recorded comparing QRS_{Vi}, QRS_{M} and the main temporal features and this validation represent an optimal starting point to use these electrodes also for clinical acquisitions.

6.3 EMG results

Even in this case with textile electrodes developed in two different dimensions the results for the sheet resistance highlighted a high repeatability of the process used to fabricate them by screen-printing. This demonstrates the high reproducibility of the printing process, due to the controlled amount of ink deposited on the substrate (Achilli et al. (2018)).

However, as described before, the sheet resistance is not the only parameter involved in the electrodes performance in the detection of physiological signals (Pani et al. (2018)). Other aspects, such as the skin-contact impedance, affect the quality of conductive materials when used as biopotential electrodes.

The skin-contact impedance measured before each sEMG measurement could be used to describe how the electrolytes and the electrode size influence the performance (Zhou et al. (2015)). In the acquisition without any electrolyte, the impedance presented a high value even if a mild skin treatment, after shaving, was performed. The boxplots in Figure 5.29 clearly demonstrate that the presence of the electrolyte influenced this parameter both for ∅10 and ∅24 textile electrodes, it in both cases contributing to decreasing the skin-contact impedance of one order of magnitude. This led to no statistically significant difference between conventional and textile electrodes in presence of an electrolyte. According to the scientific literature (Li et al. (2017a)), there is also an inverse relationship between the electrode size and the skin-contact impedance, regardless of the measurement condition.

A similar analysis on the *rms* of the noise with ∅24 and ∅10 electrodes leads to similar conclusions. The first evident aspect is the noise level in dry conditions, which reaches respectively 3 ± 2 μV and 12 ± 5 μV for the two textile electrode sizes. The box-plot of the noise demonstrates that also in this case the electrolytes addition dramatically improves the electrode performance, leading to values comparable with conventional electrodes.

Overall, the addition of saline solution introduces a greater variability, compared to solid hydrogel, and this is reflected by the presence of outliers. This variability is probably due to transient instability of the contact caused by the limited adhesion of the electrodes on the skin. The statistical analysis again revealed the substantial similarity in terms of electrode performance when an electrolyte is used, at least when the electrodes are not small.

The comparative analysis of Figure 5.29 and Figure 5.30 shows a similarity that was quantified with the Pearson correlation coefficient (the average value obtained by considering the two sizes was computed). Average correlation for Ag/AgCl electrodes was 78.2%, whereas for textile electrodes the correlation was 88.2% and 93.3%, respectively for dry electrodes and in presence of solid hydrogel. Conversely, very low values of the correlation coefficient were observed for textile electrodes with saline solution (-28.7%), confirming the aforementioned problems associated to their use in this condition.

The analysis of the *rms* of the noise was confirmed by the PSD results, revealing how dry electrodes present a higher level of noise in general and, power-line interference harmonics. Furthermore, the PSD reveals how the largest part of the noise for the textile electrodes with saline solution is in the lowest part of the spectrum. Remarkably, the PSD at rest with the proposed textile electrodes composed of organic polymers is comparable, except in dry condition, with other works where the EMG was acquired with electrodes composed of metallic wires in contact with the skin (Linz et al. (2007).

The results of the M-wave analysis over the ten volunteers, reported in Table 5.5, demonstrates that the signal acquired in dry conditions is less similar to the one acquired with conventional electrodes or to those obtained by adding some electrolyte to the textile electrodes. The NMSE, R^2 and Slope values were computed from the linear correlations between the average M-waves recorded with conventional electrodes and those achievable with the scree-printed electrodes. The descriptive statistics in Table 5.5 reveal a similar behavior of the electrodes produced with the different technologies in every condition, independently from the electrode size. Remarkably, both the R^2 coefficient close to 1 and the average slope around 1 mV/mV indicate a high similarity between the M-waves curves detected with textile electrodes and gelled Ag/AgCl electrodes.

The results obtained with the smart shirt designed to acquire EMG signals during dynamic exercises demonstrated a high similarity between the signals acquired with standard electrodes and the ones recorded with textile electrodes. At the same time this configuration shows the limitations introduced by sensorized clothes. In fact, the EMG recorded with gelled electrodes, thanks to the gel adhesion, are not affected by baseline drift induced by shirt movements. This artifact was removed with a highpass filtering with a cutoff frequency imposed at 5 Hz and the resulting signal highlights a comparable behavior with gelled electrodes even with a reduced amplitude. This demonstrates that the 15 mV variation is not due to the muscular activation but is produced from the shirt movements and could be removed as artifact and in that case is evident the muscular activity that induce that movement. This artifact could be minimized adding as electrolyte a hydrogel layer to increase the adherence of the fabric to the skin but this will affect the comfort, reducing the wearability, and will increase the skin contact impedance reducing the signal quality.

Chapter 7

Conclusions

Smart textiles presented in the scientific literature offer the opportunity to detect important vital signs as ECG or EMG not only for diagnosis, but also for monitoring purposes. The research in this field produced several scientific works presenting optimized textile electrode technologies able to adequately acquire these signals, improving some specific features with respect to the typical Ag/AgCl disposable gelled electrodes commonly adopted in clinical practice.

In this work, a comparison between different technologies behind textile electrode fabrication was presented and the performance of textile electrodes composed of printed conductive polymers was demonstrated. Electrodes with Ag/AgCl on the surface present a high stability and can monitor signals with a good quality but textile electrodes can reach similar performance with higher comfort, preventing skin irritation in long-term monitoring, thanks to the absence of electrolytes and to the improved breathability and conformability. This study presented a novel approach for the development of textile electrodes for ECG and sEMG based on the conductive polymer PEDOT:PSS. To obtain the optimal deposition procedure we tested several ink recipes and printing processes and the final one used to fabricate the presented textile electrodes was the screen-printing. On screen-printed textile electrodes, a complete characterization was carried out, including benchtop measurements and human tests, comparing the electrode performance with that of disposable gelled Ag/AgCl commercial electrodes and taking into account the recommendations of the ANSI/AAMI EC12:2000/(R)2010 standard for disposable gelled ECG electrodes.

The first results revealed the possibility of using them as ECG sensors, except when defibrillation proof properties are required, even using parameters obtained by means of commercially available clinical tools and signal post-processing. Due to the limited amount of conductive polymer deposited onto the fabric surface, the exploitation under dry conditions

is also limited by the high skin contact impedance. Since smart garments must be able to resist to the typical stresses due to everyday use, including washing, the electrodes assessment through bench procedures and human tests were aimed at the evaluation of the textile electrodes fastness to the cleaning process. The results revealed how these textile electrodes could be washed up to 20 times without compromising their ability to acquire the ECG signal, maintaining an acceptable signal quality, comparable to that of commercial electrodes. With the purpose to develop sensorized shirts able to detect physiological signals with screen-printed textile electrodes, the performance of textile electrodes on a stretchable fabric was also assessed. We highlighted that a special care should be taken on substrates with this behavior to avoid damaging the electrodes by applying a significant level of stretch. The simplicity and high reproducibility, in terms of the geometry and electrical properties, of the proposed fabrication process pave the way to the possibility of exploiting this approach for the development of seamless smart garments without the limitations imposed by other approaches. In light of the results obtained with screen printed textile electrode, we developed and tested a sensorized smart-shirt able to detect the ECG signal. The soft touch of the material on the skin also enables a comfortable use, thereby avoiding the stress on the skin due to metallic elements or seams.

For EMG detection ability, the achieved results suggest that these electrodes can be used in static conditions to study the sEMG signal, in presence of a liquid or solid electrolyte (such as saline or solid hydrogel), without significant differences compared to conventional disposable gelled EMG electrodes. However, their use in dry conditions is limited by the higher level of noise, which slightly affects the M-wave morphology, but may be more problematic on lower-amplitude sEMG signals, such as those acquired in voluntary contractions. In the light of the results achieved both for large and small size electrodes, the adoption of this technology could be interesting for examinations requiring high electrode conformability, simple setup or high-density sEMG measurements. Even though the results obtained with stimulated signals could be generalized to different recording conditions, the case of dynamic use, where the motion artifacts could arise, was preliminarly investigated. To execute this analysis was used a smart shirt with EMG textile electrode embedded in the fabric and, as expected, during dynamic exercises the amount of artifacts due to the electrode-skin relative movement is larger than expected. For this reason, it is suggested a special care in the processing or the adoption of a manufacturing approach able to preserve the electrodes stability. This preliminary analysis included only measurements performed with the addition of saline solution, to avoid the limitation due to the high skin contact impedance typical of dry textile electrodes.

Further studies are in processing to evaluate the behavior of the electrodes in different working conditions. Further studies are currently in process to characterize the signals in dynamic conditions when a stable skin-electrode contact is unachievable, which is the typical situation in which the smart garments are called to operate.

References

Achilli, A., Bonfiglio, A., and Pani, D. (2018). Design and characterization of screen-printed textile electrodes for ECG monitoring. *IEEE Sensors Journal*, 18(10):4097–4107.

Akşit, A. C., Onar, N., Ebeoglugil, M. F., Birlik, I., Celik, E., and Ozdemir, I. (2009). Electromagnetic and electrical properties of coated cotton fabric with barium ferrite doped polyaniline film. *Journal of Applied Polymer Science*, 113(1):358–366.

Al-Zaiti, S. S., Shusterman, V., and Carey, M. G. (2013). Novel technical solutions for wireless ECG transmission & analysis in the age of the internet cloud. *Journal of Electrocardiology*, 46(6):540–545.

Aleksandrowicz, A. and Leonhardt, S. (2007). Wireless and non-contact ECG measurement system – the "aachen smartchair. *Integration The Vlsi Journal*, 47(4):5–8.

Alkhidir, T., Sluzek, A., and Yapici, M. K. (2015). Simple method for adaptive filtering of motion artifacts in e-textile wearable ECG sensors. *Proceedings of the Annual International Conference of the IEEE Engineering in Medicine and Biology Society, EMBS*, 2015-Novem:3807–3810.

Alvarez, N., Ochmann, T., Kienzle, N., Ruff, B., Haase, M., Hopkins, T., Pixley, S., Mast, D., Schulz, M., and Shanov, V. (2014). Polymer coating of carbon nanotube fibers for electric microcables. *Nanomaterials*, 4(4):879–893.

Alzaidi, A., Bajwa, H., Patra, P., and Zhang, L. (2013). Noncontact textile electrodes for wireless ECG system. *9th Annual Conference on Long Island Systems, Applications and Technology, LISAT 2013*, pages 2–6.

Alzaidi, A., Zhang, L., and Bajwa, H. (2012). Smart textiles based wireless ECG. *IEEE Long Island Systems, Applications and Technology Conference (LISAT)*, pages 1–5.

ANSI/AAMi (2000). Disposable ECG electrodes: American national standard, ANSI/AAMI EC12:2000.

Austin, M. B. (1970). Thick-film screen printing. *Microelectronics Reliability*, 9(3):231.

Baig, M. M., Gholamhosseini, H., and Connolly, M. J. (2013). A comprehensive survey of wearable and wireless ECG monitoring systems for older adults. *Medical and Biological Engineering and Computing*, 51(5):485–495.

Baig, M. M., GholamHosseini, H., Moqeem, A. A., Mirza, F., and Lindén, M. (2017). A systematic review of wearable patient monitoring systems – current challenges and opportunities for clinical adoption. *Journal of Medical Systems*, 41(7).

Baura, G. (2012). *Medical Device Technologies*.

Beckmann, L., Neuhaus, C., Medrano, G., Jungbecker, N., Walter, M., Gries, T., and Leonhardt, S. (2010). Characterization of textile electrodes and conductors using standardized measurement setups. *Physiological Measurement*, 31(2):233–247.

Berglin, L. (2013). Smart textiles and wearable technology – a study of smart textiles in fashion and clothing. *BalticFashion*.

Bifulco, P., Cesarelli, M., Fratini, A., Ruffo, M., Pasquariello, G., and Gargiulo, G. (2011). A wearable device for recording of biopotentials and body movements.

Bihar, E., Roberts, T., Ismailova, E., Saadaoui, M., Isik, M., Sanchez-Sanchez, A., Mecerreyes, D., Hervé, T., De Graaf, J. B., and Malliaras, G. G. (2017). Fully printed electrodes on stretchable textiles for long-term electrophysiology. *Advanced Materials Technologies*, page 1600251.

Boehm, A., Yu, X., Neu, W., Leonhardt, S., and Teichmann, D. (2016). A novel 12-lead ECG t-shirt with active electrodes. *Electronics*, 5(4):75.

Botter, A., Vieira, T. M. M., Loram, I. D., Merletti, R., and Hodson-Tole, E. F. (2013). A novel system of electrodes transparent to ultrasound for simultaneous detection of myoelectric activity and b-mode ultrasound images of skeletal muscles. *Journal of Applied Physiology*.

Bouwstra, S., Chen, W., and Feijs, L. (2009). Smart jacket desing for neonatal monitorin with wearable sensors. *IEEE computer society*, pages 162–169.

Bouwstra, S., Chen, W., Oetomo, S. B., Feijs, L. M. G., and Cluitmans, P. J. M. (2011). Designing for reliable textile neonatal ECG monitoring using multi-sensor recordings. *Proceedings of the Annual International Conference of the IEEE Engineering in Medicine and Biology Society, EMBS*, pages 2488–2491.

Burnham, K. and Anderson, D. (2002). *Model selection and multimodel inference: a practical information-theoretic ...*

Bystricky, T., Moravcova, D., Kaspar, P., Soukup, R., and Hamacek, A. (2016). A comparison of embroidered and woven textile electrodes for continuous measurement of ECG. *Proceedings of the International Spring Seminar on Electronics Technology*, 2016-Septe:7–11.

Carvalho, H., Catarino, A. P., Rocha, A., and Postolache, O. (2014). Health monitoring using textile sensors and electrodes: An overview and integration of technologies.

Chan, M.-S. (1996). Water-based silver-silver chloride compositions.

Chen, W., Bambang Oetomo, S., Feijs, L., Bouwstra, S., Ayoola, I., and Dols, S. (2010). Design of an integrated sensor platform for vital sign monitoring of newborn infants at neonatal intensive care units. *Journal of Healthcare Engineering*, 1(4):535–553.

Cheng, M. H., Chen, L. C., Hung, Y. C., Chang, M. Y., and Tzu, L. Y. (2008). A real-time heart-rate estimator from steel textile ECG sensors in a wireless vital wearing system. *2nd International Conference on Bioinformatics and Biomedical Engineering, iCBBE 2008*, pages 1339–1342.

Chi, Y. M., Jung, T. P., and Cauwenberghs, G. (2010). Dry-contact and noncontact biopotential electrodes: Methodological review. *IEEE Reviews in Biomedical Engineering*, 3:106–119.

Chlaihawi, A. A., Narakathu, B. B., Eshkeiti, A., Emamian, S., Avuthu, S. G., and Atashbar, M. Z. (2015). Screen printed mwcnt/pdms based dry electrode sensor for electrocardiogram (ECG) measurements. volume 2015-June, pages 526–529.

Cho, G., Jeong, K., Paik, M. J., Kwun, Y., and Sung, M. (2011). Performance evaluation of textile-based electrodes and motion sensors for smart clothing. *IEEE Sensors Journal*, 11(12):3183–3193.

Chowdhury, R. H., Reaz, M. B., Bin Mohd Ali, M. A., Bakar, A. A., Chellappan, K., and Chang, T. G. (2013). Surface electromyography signal processing and classification techniques. *Sensors (Switzerland)*.

Cisterna, T. (2000). Conductive hydrogels and physiological electrodes and electrode assemblies therefrom.

Clifford, G. D., Azuaje, F., and McSharry, P. E. (2006). *Advanced Methods and Tools for ECG Data Analysis*.

Clifford J. Anderson, J. T. G. (1976). Bio-medical electrode conductive gel pads.

Clippingdale, A. J., Prance, R. J., Clark, T. D., and Watkins, C. (1994). Ultrahigh impedance capacitively coupled heart imaging array. *Review of Scientific Instruments*, 65(1):269–270.

Cochrane, C., Koncar, V., Lewandowski, M., and Dufour, C. (2007). Design and development of a flexible strain sensor for textile structures based on a conductive polymer composite. *Sensors*, 7(4):473–492.

Colyer, S. L. and McGuigan, P. M. (2018). Textile electrodes embedded in clothing: A practical alternative to traditional surface electromyography when assessing muscle excitation during functional movements. *Journal of Sports Science and Medicine*.

Conover, W. J. and Iman, R. L. (1981). Rank transformations as a bridge between parametric and nonparametric statistics. *American Statistician*.

Copp-howland, Warren W. (Chicopee, M. U. (2010). Medical electrode containing a hydrophilic polymer.

Crawford, J. and Doherty, L. (2012). *Practical aspects of ECG recording*. UK.

Criswell Eleanor, C. J. R. (2011). Cram's introduction to surface electromyography.

David, R. M. and Portnoy, W. M. (1972). Insulated electrocardiogram electrodes. *Medical & Biological Engineering*, 10(6):742–751.

Deignan, J., Monedero, J., Coyle, S., O'Gorman, D., Diamond, D., and McBrearty, M. (2015). Wearable chemical sensors: Characterization of heart rate electrodes using electrochemical impedance spectroscopy. *2015 IEEE 12th International Conference on Wearable and Implantable Body Sensor Networks (BSN)*, pages 1–6.

Elschner, A., Kirchmeyer, S., Lövenich, W., Merker, U., and Reuter, K. (2010). *PEDOT*. CRC Press.

Erdmier, C., Hatcher, J., and Lee, M. (2016). Wearable device implications in the healthcare industry. *Journal of Medical Engineering and Technology*, 40(4):141–148.

Fernandez, M. and Pallas-Areny, R. (1996). A simple active electrode for power line interference reduction in high resolution biopotential measurements. *Proceedings of 18th Annual International Conference of the IEEE Engineering in Medicine and Biology Society*, 1:97–98.

Finni, T., Hu, M., Kettunen, P., Vilavuo, T., and Cheng, S. (2007). Measurement of emg activity with textile electrodes embedded into clothing. *Physiological Measurement*, 28(11):1405–1419.

Fletcher, S. (2016). Screen-printed carbon electrodes. In *Advances in Electrochemical Science and Engineering*.

Gadsby, P. M. a. P. (2004). Electrode chemistry of prolonged external pacing. *Proceedings of the IEEE 30th Annual Northeast Bioengineering Conference*.

Gaikwad, M. P. R. and Dekate, K. N. (2017). Review on design and development of remote cardiac analysis. *International Journal of Science, Engineering and Technology Research*, 6(2):249–252.

Ghahremani Honarvar, M. and Latifi, M. (2017). Overview of wearable electronics and smart textiles. *The Journal of The Textile Institute*, 108(4):631–652.

Gonçalves, C., Ferreira da Silva, A., Gomes, J., and Simoes, R. (2018). Wearable e-textile technologies: A review on sensors, actuators and control elements. *Inventions*.

Gopalsamy, C., Park, S., Rajamanickam, R., and Jayaraman, S. (1999). The wearable motherboard™: The first generation of adaptive and responsive textile structures (arts) for medical applications. *Virtual Reality*, 4(3):152–168.

Gordon Paul, Russel Torah, S. B. and Tudor, J. (2017). A printed, dry electrode frank configuration vest for ambulatory vectorcardiographic monitoring. *Smart Materials and Structures*, 26(025029).

Griffith, M. E., Portnoy, W. M., Stotts, L. J., and Day, J. L. (1979). Improved capacitive electrocardiogram electrodes for burn applications. *Medical & Biological Engineering & Computing*, 17(5):641–646.

Gualandi, I., Marzocchi, M., Achilli, A., Cavedale, D., Bonfiglio, A., and Fraboni, B. (2016). Textile organic electrochemical transistors as a platform for wearable biosensors. *Scientific Reports*, 6(1):33637.

Hakyung, Cho; Hosun Lim, S. C. (2016). Efficacy research of electrocardiogram and heart rate measurement in accordance with the structure of the textile electrodes. *Fibers and Polymers*, 17(12):2069–2077.

Hayward, M. J., Chansin, D. G., and Zervos, D. H. (2017). Wearable technology 2017-2027: Markets, players, forecasts. *IDTechEx*.

Hertleer, C., Grabowska, M., Van Langenhove, L., Hermans, B., Puers, R., Kalmar, A., van Egmond, H., and Matthys, D. (2004). The use of electroconductive textile material for the development of a smart suit. *World Textile Conference - 4th AUTEX Conference*, (June).

Hoof, v. H.-J. Y. C. (2013). *Bio-Medical CMOS ICs*, volume 53.

Horwood, R. J. (1974). Towards a Better Understanding of Screen Print Thickness Control. *ElectroComponent Science and Technology*.

Jayoung, C., Jihye, M., Keesam, J., and Gilsoo, C. (2005). An exploration of electrolessly cu/ni plated polyester fabrics as e-textiles. *Proceedings - International Symposium on Wearable Computers, ISWC*, 2005:206–207.

Jung, H.-c., Moon, J.-h., Baek, D.-h., Lee, J.-h., Choi, Y.-y., and Hong, J.-s. (2012). Cnt / pdms composite flexible dry electrodes for long-term ECG monitoring. *IEEE Trans Biomed Eng.*, 59(5):1472–1479.

Kang, T. H., Merritt, C. R., Grant, E., Pourdeyhimi, B., and Nagle, H. T. (2008). Nonwoven fabric active electrodes for biopotential measurement during normal daily activity. *IEEE Transactions on Biomedical Engineering*, 55(1):188–195.

Kato, T., Ueno, A., Kataoka, S., Hoshino, H., and Ishiyama, Y. (2006). An application of capacitive electrode for detecting electrocardiogram of neonates and infants. pages 916–919.

Kellomäki, T., Virkki, J., Merilampi, S., and Ukkonen, L. (2012). Towards washable wearable antennas: A comparison of coating materials for screen-printed textile-based uhf rfid tags. *International Journal of Antennas and Propagation*, 2012.

Kim, J., Kumar, R., Bandodkar, A. J., and Wang, J. (2017). Advanced materials for printed wearable electrochemical devices: A review. *Advanced Electronic Materials*, 3(1):1–15.

Kim, J. Y., Jung, J. H., Lee, D. E., and Joo, J. (2002). Enhancement of electrical conductivity of poly(3, 4-ethylenedioxythiophene)/poly(4-styrenesulfonate) by a change of solvents. *Synthetic Metals*.

Kirstein, T., Lawrence, M., and Tröster, G. (0). Functional electrical stimulation (fes) with smart textile. pages 1–5.

Kligfield, P., Gettes, L. S., Bailey, J. J., Childers, R., Deal, B. J., Hancock, E. W., Van Herpen, G., Kors, J. A., Macfarlane, P., Mirvis, D. M., Pahlm, O., Rautaharju, P., and Wagner, G. S. (2007). Recommendations for the standardization and interpretation of the electrocardiogram: Part i: The electrocardiogram and its technology: A scientific statement from the american heart association electrocardiography and arrhythmias committee, council on cli. *Circulation*, 115(10):1306–1324.

Kumari, P., Mathew, L., and Syal, P. (2017). Increasing trend of wearables and multimodal interface for human activity monitoring: A review. *Biosensors and Bioelectronics*, 90(September 2016):298–307.

Lam, C. L., Nur, N., Mohd, Z., and Wicaksono, D. H. B. (2013). Mwcnt / cotton-based flexible electrode for electrocardiography. pages 3–6.

Lee, E., Kim, I., Liu, H., and Cho, G. (2017). Exploration of agnw/pu nanoweb as ECG textile electrodes and comparison with ag/agcl electrodes. *Fibers and Polymers*, 18(9):1749–1753.

Lewy, H. (2015). Wearable technologies – future challenges for implementation in healthcare services. *Healthcare Technology Letters*, 2(1):2–5.

Li, G., Geng, Y., Tao, D., and Zhou, P. (2011). Performance of electromyography recorded using textile electrodes in classifying arm movements. pages 4243–4246.

Li, G., Wang, S., and Duan, Y. Y. (2017a). Towards gel-free electrodes: A systematic study of electrode-skin impedance. *Sensors and Actuators, B: Chemical*.

Li, M., Li, Y. T., Li, D. W., and Long, Y. T. (2012). Recent developments and applications of screen-printed electrodes in environmental assays-a review. *Analytica Chimica Acta*, 734:31–44.

Li, X., Member, S., Sun, Y., and Architecture, A. S. (2017b). Design and evaluation of a non-contact wireless biopotential monitoring system with motion artifacts. (906):69–72.

Li, Y., Li, Y., Su, M., Li, W., Li, Y., Li, H., Qian, X., Zhang, X., Li, F., and Song, Y. (2017c). Electronic textile by dyeing method for multiresolution physical kineses monitoring. *Advanced Electronic Materials*, 1700253:1700253.

Liao, D. L., Wang, I. J., Chen, S. F., Chang, J. Y., and Lin, C. T. (2011). Design, fabrication and experimental validation of a novel dry-contact sensor for measuring electroencephalography signals without skin preparation. *Sensors*.

Linz, T., Gourmelon, L., and Langereis, G. (2007). Contactless emg sensors embroidered onto textile. *4th International Workshop on Wearable and Implantable Body Sensor Networks (BSN 2007)*, pages 29–34.

Liu, Z. and Liu, X. (2015). Progress on fabric electrodes used in biological signal acquisition. *Journal of Minerals and Materials Characterization and Engineering*, 3(May):204–214.

Lou, C., Li, R., Li, Z., Liang, T., Wei, Z., Run, M., Yan, X., and Liu, X. (2016). Flexible graphene electrodes for prolonged dynamic ECG monitoring. *Sensors (Switzerland)*, 16(11):1–12.

Lymberis, A. and Olsson, S. (2003). Intelligent biomedical clothing for personal health and disease management: State of the art and future vision. *Telemedicine Journal and E-Health*, 9(4):379–386.

Löfhede, J., Seoane, F., and Thordstein, M. (2012). Textile electrodes for eeg recording–a pilot study. *Sensors (Basel, Switzerland)*, 12(12):16907–19.

M. Inoue, Y. A. and Tada, Y. (2017). Design of printed e-textile probers to supress electrocardiograpy noise. *International Conference on Electronics Packaging (ICEP)*, pages 464–465.

MacLeod, R. S., Shome, S., Stinstra, J., Punske, B. B., and Hopenfeld, B. (2005). Mechanisms of ischemia-induced st-segment changes. volume 38, pages 8–13.

Malmivuo, J. and Plonsey, R. (2012). *Bioelectromagnetism: Principles and Applications of Bioelectric and Biomagnetic Fields*.

Mangezi, A., Rosendo, A., Howard, M., and Stopforth, R. (2017). Embroidered archimedean spiral electrodes for contactless prosthetic control. pages 1343–1348.

Marozas, V., Petrenas, A., Daukantas, S., and Lukosevicius, A. (2011). A comparison of conductive textile-based and silver/silver chloride gel electrodes in exercise electrocardiogram recordings. *Journal of Electrocardiology*, 44(2):189–194.

Martinez, J. P., Almeida, R., Olmos, S., Rocha, A. P., and Laguna, P. (2004). A wavelet-based ECG delineator evaluation on standard databases. *IEEE Transactions on Biomedical Engineering*, 51(4):570–581.

Martins, Fernanda (São Paulo, B. S. R. K. S. P. B. O. J. D. S. P. B. (2017). Biomedical electrode comprising discontinuous primer layer.

Mason, J. W., Hancock, E. W., and Gettes, L. S. (2007). Recommendations for the standardization and interpretation of the electrocardiogram. *Journal of the American College of Cardiology*, 49(10):1128–1135.

Mason, R. E. and Likar, I. (1966). A new system of multiple-lead exercise electrocardiography. *American Heart Journal*, 71(2):196–205.

Matthews, R., Mcdonald, N. J., Fridman, I., Hervieux, P., and Nielsen, T. (2005). The invisible electrode – zero prep time, ultra low capacitive sensing. *11th International Conference on Human-Computer Interaction*.

Mattila, H. R. (2006). *Intelligent Textiles and Clothing*.

Merletti, R., Knaflitz, M., and DeLuca, C. J. (1992). Electrically evoked myoelectric signals. *Critical reviews in biomedical engineering*, 19(4):293–340.

Mewett, D. T., Reynolds, K. J., and Nazeran, H. (2004). Reducing power line interference in digitised electromyogram recordings by spectrum interpolation. *Medical and Biological Engineering and Computing*.

Mihajlovi, V. and Grundlehner, B. (2012). The effect of force and electrode material on electrode-to-skin impedance. (1):57–60.

Miller, L. F. (1968). Paste transfer in the screening process.

Murnaghan, D. P. (1949). *Clinical electrocardiography.*, volume 26.

Müller, C., Hamedi, M., Karlsson, R., Jansson, R., Marcilla, R., and Hedhammar, M. (2011). Woven electrochemical transistors on silk fibers. *Advanced Materials*, 23(7):898–901.

Nayak, R., Wang, L., and Padhye, R. (2015). Electronic textiles for military personnel. In *Electronic Textiles: Smart Fabrics and Wearable Technology*, pages 239–256.

Neves, A. I. S., Rodrigues, D. P., De Sanctis, A., Alonso, E. T., Pereira, M. S., Amaral, V. S., Melo, V. L., Russo, S., de Schrijver, I., Alves, H., and Craciun, M. F. (2017). Towards conductive textiles: coating polymeric fibres with graphene. *Scientific Reports*, 7(1):4250.

Niijima, A., Isezaki, T., Aoki, R., Watanabe, T., and Yamada, T. (2017). hitoecap : Wearable emg sensor for monitoring masticatory muscles with PEDOT:PSS textile electrodes. *Proceedings of the 2017 ACM International Symposium on Wearable Computers*, Part F1305:215–220.

Ottenbacher, J., Romer, S., Kunze, C., Grosmann, U., and Stork, W. (2004). Integration of a bluetooth based ECG system into clothing. *Eighth International Symposium on Wearable Computers*, (1):186–187.

Ouyang, J., Xu, Q., Chu, C. W., Yang, Y., Li, G., and Shinar, J. (2004). On the mechanism of conductivity enhancement in poly(3,4- ethylenedioxythiophene):poly(styrene sulfonate) film through solvent treatment. *Polymer*.

Owczarek, J. A. and Howland, F. L. (1990). A study of the off-contact screen printing process—part ii: Analysis of the model of the printing process. *IEEE Transactions on Components, Hybrids, and Manufacturing Technology*.

Page, T. (2015). A forecast of the adoption of wearable technology. *International Journal of Technology Diffusion*, 6(2):12–29.

Pan, J., Tonkay, G. L., Quintero, A., and Ave, W. P. (1999). Screen printing process design of experiments for fine line printing of thick film ceramic substrates. *Journal of Electronics Manufacturing*.

Pani, D., Achilli, A., Bassareo, P., Cugusi, L., Mercuro, G., Fraboni, B., and Bonfiglio, A. (2016a). Fully-textile polymer-based ECG electrodes: Overcoming the limits of metal-based textiles. *Computing in Cardiology*, 43:373–376.

Pani, D., Achilli, A., and Bonfiglio, A. (2018). Survey on textile electrode technologies for electrocardiographic (ECG) monitoring, from metal wires to polymers. *Advanced Materials Technologies*, 0(0):1800008.

Pani, D., Dessi, A., Saenz-Cogollo, J. F., Barabino, G., Fraboni, B., and Bonfiglio, A. (2016b). Fully textile, PEDOT:PSS based electrodes for wearable ECG monitoring systems. *IEEE Transactions on Biomedical Engineering*, 63(3):540–549.

Pani, D., Dessì, A., Gusai, E., Saenz-cogollo, J. F., Barabino, G., Fraboni, B., and Bonfiglio, A. (2015). Evaluation of novel textile electrodes for ECG signals monitoring based on PEDOT:PSS-treated woven fabrics. pages 3197–3200.

Paradiso, R., Loriga, G., and Taccini, N. (2005). Wealthy, a wearable healthcare system: new frontier on e-textile. *Journal of Telecomunications and Information Technology*, 4:105–113.

Paradiso, R. and Pacelli, M. (2011). Textile electrodes and integrated smart textile for reliable biomonitoring.

Park, J. A., Han, H. J., Heo, J. C., and Lee, J. H. (2017). Computer aided diagnosis sensor integrated outdoor shirts for real time heart disease monitoring. *Computer Assisted Surgery*.

Park, S. and Jayaraman, S. (2003). Enhancing the quality of life through wearable technology. *IEEE Engineering in Medicine and Biology Magazine*, 22(3):41–48.

Park, S. and Jayaraman, S. (2010). Smart textile-based wearable biomedical systems: A transition plan for research to reality. volume 14, pages 86–92.

Park, S. and Jayaraman, S. (2017). The wearables revolution and big data: the textile lineage. *The Journal of The Textile Institute*, 108(4):605–614.

Paul, G., Torah, R., Beeby, S., and Tudor, J. (2014a). The development of screen printed conductive networks on textiles for biopotential monitoring applications. *Sensors and Actuators, A: Physical*, 206:35–41.

Paul, G. M., Cao, F., Torah, R., Yang, K., Beeby, S., and Tudor, J. (2014b). A smart textile based facial emg and eog computer interface. *IEEE Sensors Journal*, 14(2):393–400.

Ping, J., Wu, J., Wang, Y., and Ying, Y. (2012). Simultaneous determination of ascorbic acid, dopamine and uric acid using high-performance screen-printed graphene electrode. *Biosensors and Bioelectronics*.

Piwek, L., Ellis, D. A., Andrews, S., and Joinson, A. (2016). The rise of consumer health wearables: Promises and barriers. *PLoS Medicine*, 13(2).

Pola, T. and Vanhala, J. (2007). Textile electrodes in ECG measurement. *Proceedings of the 2007 International Conference on Intelligent Sensors, Sensor Networks and Information Processing, ISSNIP*, (Figure 1):635–639.

Puurtinen, M. M., Komulainen, S. M., Kauppinen, P. K., Malmivuo, J. A., and Hyttinen, J. A. (2006). Measurement of noise and impedance of dry and wet textile electrodes, and textile electrodes with hydrogel.

Pylatiuk, C., Müller-Riederer, M., Kargov, A., Schulz, S., Schill, O., Reischl, M., and Bretthauer, G. (2009). Comparison of surface emg monitoring electrodes for long-term use in rehabilitation device control.

Rattfalt, L., Lindén, M., Hult, P., Berglin, L., and Ask, P. (2007). Electrical characteristics of conductive yarns and textile electrodes for medical applications. *Medical and Biological Engineering and Computing*, 45(12):1251–1257.

Renedo, O. D., Alonso-Lomillo, M. A., and Martínez, M. J. A. (2007). Recent developments in the field of screen-printed electrodes and their related applications. *Talanta*, 73(2):202–219.

Riemer, D. (1988). Analytical engineering model of the screen printing process: Part i. pages 107–111.

Rijnbeek, P. R., Kors, J. A., and Witsenburg, M. (2001). Minimum bandwidth requirements for recording of pediatric electrocardiograms. *Circulation*, 104(25):3087–3090.

Rivnay, J., Inal, S., Collins, B. A., Sessolo, M., Stavrinidou, E., Strakosas, X., Tassone, C., Delongchamp, D. M., and Malliaras, G. G. (2016). Structural control of mixed ionic and electronic transport in conducting polymers. *Nature Communications*, 7:11287.

Rosell, J., Colominas, J., Riu, P., Pallas-Areny, R., and Webster, J. (1988). Skin impedance from 1 hz to 1 mhz. *IEEE Transactions on Biomedical Engineering*, 35(8):649–651.

Scilingo, E. and Valenza, G. (2017). Recent advances on wearable electronics and embedded computing systems for biomedical applications. *Electronics*, 6(1):12.

Scilingo, E. P., Gemignani, A., Paradiso, R., Taccini, N., Ghelarducci, B., and De Rossi, D. (2005). Performance evaluation of sensing fabrics for monitoring physiological and biomechanical variables. *IEEE Transactions on Information Technology in Biomedicine*, 9(3):345–352.

Searle, A. and Kirkup, L. (2000). A direct comparison of wet, dry and insulating bioelectric recording electrodes. *Physiological Measurement*, 21(2):271–283.

Shafti, A., Manero, R. B., Borg, A. M., Althoefer, K., and Howard, M. J. (2016). Designing embroidered electrodes for wearable surface electromyography. volume 2016-June, pages 172–177.

Shyamkumar, P., Rai, P., Oh, S., Ramasamy, M., Harbaugh, R., and Varadan, V. (2014). Wearable wireless cardiovascular monitoring using textile-based nanosensor and nanomaterial systems. *Electronics*, 3(3):504–520.

Smits, F. M. (1958). Measurement of sheet resistivities with the four-point probe. *Bell System Technical Journal*.

Standards, B. (2010). Textiles — tests for colour fastness. *Calculation of colour differences (ISO*.

Stern, S. (2006). Electrocardiogram: Still the cardiologist's best friend. *Circulation*, 113(19):e753–e756.

Stoppa, M. and Chiolerio, A. (2014). Wearable electronics and smart textiles: A critical review. *Sensors (Switzerland)*, 14(7):11957–11992.

Suganuma, K. (2014). Printing technology. In *Introduction to Printed ELectronics*.

Sun, Z., Zussman, E., Yarin, A. L., Wendorff, J. H., and Greiner, A. (2003). Compound core-shell polymer nanofibers by co-electrospinning. *Advanced Materials*, 15(22):1929–1932.

Sunaga, T., Ikehira, H., Furukawa, S., Shinkai, H., Kobayashi, H., Matsumoto, Y., Yoshitome, E., Obata, T., Tanada, S., Murata, H., and Sasaki, Y. (2002). Measurement of the electrical properties of human skin and the variation among subjects with certain skin conditions. *Physics in Medicine and Biology*, 47(1).

Taelman, J., Adriaensen, T., Van Der Horst, C., Linz, T., and Spaepen, A. (2007). Textile integrated contactless emg sensing for stress analysis. pages 3966–3969.

Taheri, B. A., Knight, R. T., and Smith, R. L. (1994). A dry electrode for eeg recording. *Electroencephalography and Clinical Neurophysiology*, 90(5):376–383.

Taji, B., Shirmohammadi, S., Groza, V., and Batkin, I. (2014). Impact of skin–electrode interface on electrocardiogram measurements using conductive textile electrodes. *IEEE Transactions on Instrumentation and Measurement*, 63(6):1412–1422.

Takagahara, K., Ono, K., and Oda, N. (2013). " hitoe "— a wearable sensor developed through cross-industrial collaboration.

Takamatsu, S., Lonjaret, T., Crisp, D., Badier, J.-M., Malliaras, G. G., and Ismailova, E. (2015). Direct patterning of organic conductors on knitted textiles for long-term electrocardiography. *Scientific Reports*, 5:15003.

Taleat, Z., Khoshroo, A., and Mazloum-Ardakani, M. (2014). Screen-printed electrodes for biosensing: A review (2008-2013). *Microchimica Acta*, 181(9-10):865–891.

Thomas, J. P., Zhao, L., McGillivray, D., and Leung, K. T. (2014). High-efficiency hybrid solar cells by nanostructural modification in PEDOT:PSS with co-solvent addition. *Journal of Materials Chemistry A*.

Tsukada, S., Kasai, N., Kawano, R., Takagahara, K., Fujii, K., and Sumitomo, K. (2012a). Electrocardiogram monitoring simply by wearing a shirt– for medical, healthcare, sports, and entertainment.

Tsukada, S., Nakashima, H., and Torimitsu, K. (2012b). Conductive polymer combined silk fiber bundle for bioelectrical signal recording. *PLoS ONE*, 7(4).

Tuohimäki, K., Mahdiani, S., Jeyhani, V., Vehkaoja, A., Iso-Ketola, P., Vanhala, J., Viik, J., and Mäntysalo, M. (2017). Electrode comparison for textile-integrated electrocardiogram and impedance pneumography measurement. *IFMBE Proceedings*, 65:302–305.

Ueno, A., Akabane, Y., Kato, T., Hoshino, H., Kataoka, S., and Ishiyama, Y. (2007). Capacitive sensing of electrocardiographic potential through cloth from the dorsal surface of the body in a supine position: A preliminary study. *IEEE Transactions on Biomedical Engineering*, 54(4):759–766.

Uy, Rosa (St. Paul, M. D. T. M. S. P. M. (1995). Solid state conductive polymer compositions, biomedical electrodes containing such compositions, and method of preparing same.

Van der Pauw, L. J. (1958). A method of measuring specific resistivity and hall effect of discs of arbitrary shape. *Philips Research Reports*, 13(1):1–11.

Viswanath, D. S., Ghosh, T. K., Prasad, D. H., Dutt, N. V., and Rani, K. Y. (2007). *Viscosity of liquids: Theory, estimation, experiment, and data*.

Wang, J., Lin, C. C., Yu, Y. S., and Yu, T. C. (2015). Wireless sensor-based smart-clothing platform for ECG monitoring. *Computational and Mathematical Methods in Medicine*.

Wang, Z., Yang, Z., and Dong, T. (2017). A review of wearable technologies for elderly care that can accurately track indoor position, recognize physical activities and monitor vital signs in real time. *Sensors (Switzerland)*, 17(2).

Warren, G. L. and Patel, S. (2008). Electrostatic properties of aqueous salt solution interfaces: A comparison of polarizable and nonpolarizable ion models. *Journal of Physical Chemistry B*, 112(37):11679–11693.

Weber, J. L., Blanc, D., Dittmar, A., Comet, B., Corroy, C., Noury, N., Baghai, R., Vaysse, S., and Blinowska, A. (2003). Vtam-a new "biocloth" for ambulatory telemonitoring. *Proceedings of the IEEE/EMBS Region 8 International Conference on Information Technology Applications in Biomedicine, ITAB*, 2003-Janua:299–301.

Webster, J. (2009). *Medical Instrumentation: Application and Design, 4th ed.*

Wen, Y. and Xu, J. (2017). Scientific importance of water-processable PEDOT:PSS and preparation, challenge and new application in sensors of its film electrode: A review. *Journal of Polymer Science, Part A: Polymer Chemistry*, 55(7):1121–1150.

Wieringa, F. P., Broers, N. J. H., Kooman, J. P., Van Der Sande, F. M., and Van Hoof, C. (2017). Wearable sensors: can they benefit patients with chronic kidney disease? *Expert Review of Medical Devices*, 14(7):505–519.

Xu, P. J., Zhang, H., and Tao, X. M. (2008). Textile-structured electrodes for electrocardiogram. *Textile Progress*, 40(4):183–213.

Yamanaka, K., Vestergaard, M. C., and Tamiya, E. (2016). Printable electrochemical biosensors: A focus on screen-printed electrodes and their application. *Sensors (Switzerland)*, 16(10):1–16.

Yapici, M. K. and Alkhidir, T. E. (2017). Intelligent medical garments with graphene-functionalized smart-cloth ECG sensors. *Sensors (Switzerland)*, 17(4):1–12.

Yokus, M. A. and Jur, J. S. (2016). Fabric-based wearable dry electrodes for body surface biopotential recording. *IEEE Transactions on Biomedical Engineering*, 63(2):423–430.

Yucelbas, C., Ozsen, S., Gunes, S., and Yosunkaya, S. (2013). Effect of some power spectral density estimation methods on automatic sleep stage scoring using artificial neural networks. *Proceedings of the IADIS International Conference Intelligent Systems and Agents 2013, ISA 2013, Proceedings of the IADIS European Conference on Data Mining 2013, ECDM 2013*.

Zhang, H., Tian, L., Zhang, L., and Li, G. (2013). Using textile electrode emg for prosthetic movement identification in transradial amputees.

Zhou, H., Lu, Y., Chen, W., Wu, Z., Zou, H., Krundel, L., and Li, G. (2015). Stimulating the comfort of textile electrodes in wearable neuromuscular electrical stimulation. *Sensors (Switzerland)*, 15(7):17241–17257.

Zhou, Y., Ding, X., Zhang, J., Duan, Y., Hu, J., and Yang, X. (2014). Fabrication of conductive fabric as textile electrode for ECG monitoring. *Fibers and Polymers*, 15(11):2260–2264.

Zhu, Z., Liu, T., Li, G., Li, T., and Inoue, Y. (2015). Wearable sensor systems for infants. *Sensors*, 15(2):3721–3749.

List of Publications

Journal papers

Design and Characterization of Screen-Printed Textile Electrodes for ECG Monitoring
by: **A. Achilli**, A. Bonfiglio and D. Pani
published in: IEEE Sensors Journal, vol. 18, no. 10, pp. 4097-4107, 15 May, 2018

Survey on Textile Electrode Technologies for Electrocardiographic (ECG) Monitoring, from Metal Wires to Polymers
by: D. Pani, A. Achilli, and A. Bonfiglio
published in: Adv. Mater. Technol., vol. 0, no. 0, p. 1800008, Jun. 2018.

Textile Organic Electrochemical Transistors as a Platform for Wearable Biosensors
by: I. Gualandi, M. Marzocchi, A. Achilli, D. Cavedale, A. Bonfiglio, B.Fraboni,
published in: Scientific Reports, 6, 33637, 2016, 10.1038/srep33637.

Validation of polymer-based screen-printed textile electrodes for surface EMG detection
by: D. Pani, A. Achilli, A. Bonfiglio, M. Gazzoni, A. Botter
submitted in: Transactions on Neural Systems & Rehabilitation Engineering

International Conference proceedings

Fully-textile polymer-based ECG electrodes: Overcoming the limits of metal-based textiles
by: Pani D., Achilli A., Bassareo P. P., Cugusi L., Mercuro G., Fraboni B., & Bonfiglio A.
published in: Computing in Cardiology Conference (CinC), 2016. IEEE.

Characterization of screen-printed textile electrodes based on conductive polymer for ECG acquisition
By: Achilli, A., Pani, D., Bonfiglio, A.,
Published in: Computing in Cardiology Conference (CinC) 2017

Screen-printed textile electrodes based on PEDOT:PSS for biopotential recording
By: A. Achilli, D. Pani, I. Gualandi, B. Fraboni, A. Bonfiglio,
10th International Symposium on Flexible Organic Electronics (ISFOE17) 3-6 July 2017, Thessaloniki, Greece

Objective Human Gustatory Sensitivity Assessment Through a Portable Electronic Device
By: Eleonora Sulas, Alice Evelina Martis, Piero Cosseddu, Andrea Achilli, Giorgia Sollai, Iole Tomassini Barbarossa, Luigi Raffo, Annalisa Bonfiglio, Danilo Pani,
BIOCAS 2018

Wearable Sensor For The Detection Of Redox-Active Biomolecules
By: I, Gualandi, M. Marzocchi, A. Achilli,J. F. Saenz-Cogollo, A. Bonfiglio, B. Fraboni
MRS Fall Meeting and Exhibit, Symposium B— Stretchable and Active Polymers and Composites for Electronics and Medicine, 2015, pp. 1 - 1, 29/11/2015-4/12/2015, Boston

National Conference proceedings

Fully textile electrodes for wearable electrophysiological signal monitoring systems
By: Danilo Pani, Gianluca Barabino, Andrea Achilli, Beatrice Fraboni, Annalisa Bonfiglio,
V Annual Congress for the Italian National Bioengineering Group, 20 - 22 June 2016, Naples, Italy

Characterization of screen-printed textile electrodes for EMG signal acquisition
By: A Achilli, A Zedda, E Sulas, A Botter, M Gazzoni, A Bonfiglio, D Pani,
VI Annual Congress for the Italian National Bioengineering Group, 25 - 27 June 2018, Milan, Italy